Theses and Dissertations

Spring 2012

Role of neck angulation and endograft oversizing in folding and its impact on device fixation strength

Kathleen Kei Lin
University of Iowa

ROLE OF NECK ANGULATION AND ENDOGRAFT OVERSIZING IN FOLDING

AND ITS IMPACT ON DEVICE FIXATION STRENGTH

by

Kathleen Kei Lin

An Abstract

Of a thesis submitted in partial fulfillment
of the requirements for the Doctor of
Philosophy degree in Biomedical Engineering
in the Graduate College of
The University of Iowa

May 2012

Thesis Supervisor: Associate Professor Madhavan L. Raghavan

ABSTRACT

Objective: To assess neck angulation and endograft oversizing as factors contributing to folding. Endograft folding will then be assessed on its role in endograft fixation strength.

Methods: Bench top flow loop experiments were performed with barbless Gore Excluder endovascular grafts (EVG) that were deployed into silicone aorta-AAA models with neck angles of 0, 30, and 60. A total of five oversizings were tested: -7%, 2%, 12%, 24%, and 38% with N= 3 for each oversizing at each neck angle for a total of 45 experiments. Photographs of the stent apex to apex distances were taken for the entire circumference of the device for a total of 8 photos per experiment. Measurements of the apex to apex distance were taken for the top three stent layers and variance for each stent layer was calculated. Variances for all three stent layers were summed to represent the folding metric. The silicone model was then removed from the flow loop and placed on the uniaxial extension tester to for pull out testing to assess impact on attachment strength.

Results: Neck angle and oversizing increases folding risk at oversizing ≥12% for 0° and 30° neck angles, and ≥ 2% oversizing for a 60° neck angle. Folding metric comparison between 0° vs. 30° and 0° vs. 60° across all oversizings had statistical significance (Mann-Whitney U, $p<0.05$). Folding decreases fixation strength at lower neck angles for oversizing ≥24%. As oversizing is increased, pull out forces increase as well. At higher neck angles, oversizing and folding has little effect on migration risk. There was no statistical difference in pull out forces across all neck angles.

Conclusion: Oversizing and neck angulation contributors to folding. Folding increases migration risk for at oversizing ≥24% and lower neck angles. At higher neck angles, folding and oversizing has no impact on attachment strength.

Abstract Approved: _____
                                                   Thesis Supervisor

                                                   _____
                                                   Title and Department

                                                   _____
                                                   Date

ROLE OF NECK ANGULATION AND ENDOGRAFT OVERSIZING IN FOLDING

AND ITS IMPACT ON DEVICE FIXATION STRENGTH

by

Kathleen Kei Lin

A thesis submitted in partial fulfillment
of the requirements for the Doctor of
Philosophy degree in Biomedical Engineering
in the Graduate College of
The University of Iowa

May 2012

Thesis Supervisor: Associate Professor Madhavan L. Raghavan

Graduate College
The University of Iowa
Iowa City, Iowa

CERTIFICATE OF APPROVAL

_____

PH.D. THESIS

_____

This is to certify that the Ph.D. thesis of

Kathleen Kei Lin

has been approved by the Examining Committee
for the thesis requirement for the Doctor of Philosophy
degree in Biomedical Engineering at the May 2012 graduation.

Thesis Committee: _____
Madhavan L. Raghavan, Thesis Supervisor

_____
Krishnan B. Chandran

_____
Sarah Vigmostad

_____
Jia Lu

_____
Jafar Golzarian

ACKNOWLEDGMENTS

I owe the completion of my dissertation to my adviser, committee members, family, and friends. Without their support and guidance, I would not be at the stage of my graduate career that I am at today.

I would like to express my deepest gratitude to my adviser Dr. Madhavan L Raghavan for all of his support and guidance throughout my PhD, as well as for the excellent research environment. I would also like to thank my other committee members who provided valuable input to shape my dissertation project.

Thank you to my fellow labmates for all of their help and input during my research, especially Ben Dickerhoff , Ben Berkowitz, Chaid Schwarz, and Andrew Jennings. A special thanks to Steve Struckman in the machine shop who patiently worked with me in creating all of my silicone molds and any other fixtures I needed for my experiments.

I would like to thank my best friend Manasi Ramachandran for keeping my sanity throughout this process. Without her friendship, I would've enjoyed this experience far less. She always calmed my nerves and gave advice whenever I would get frustrated with my research or with my personal life. I am grateful to have her in my life and to have developed a life-long friendship with her.

I would also like to thank my parents and brother for their constant encouragement and best wishes during my graduate career. They have always cheered me on and trusted me in all my endeavors.

Finally, I would like to thank my boyfriend Rich Peters for the patience he's had, especially during the past few weeks. He did everything in his power to make sure I was stress free to fully concentrate on my research and dissertation. Thank you for walking the dogs during all the Iowa winters!

ABSTRACT

Objective: To assess neck angulation and endograft oversizing as factors contributing to folding. Endograft folding will then be assessed on its role in endograft fixation strength.

Methods: Bench top flow loop experiments were performed with barbless Gore Excluder endovascular grafts (EVG) that were deployed into silicone aorta-AAA models with neck angles of 0, 30, and 60. A total of five oversizings were tested: -7%, 2%, 12%, 24%, and 38% with N= 3 for each oversizing at each neck angle for a total of 45 experiments. Photographs of the stent apex to apex distances were taken for the entire circumference of the device for a total of 8 photos per experiment. Measurements of the apex to apex distance were taken for the top three stent layers and variance for each stent layer was calculated. Variances for all three stent layers were summed to represent the folding metric. The silicone model was then removed from the flow loop and placed on the uniaxial extension tester to for pull out testing to assess impact on attachment strength.

Results: Neck angle and oversizing increases folding risk at oversizing $\geq$12% for 0° and 30° neck angles, and $\geq 2\%$ oversizing for a 60° neck angle. Folding metric comparison between 0° vs. 30° and 0° vs. 60° across all oversizings had statistical significance (Mann-Whitney U, $p<0.05$). Folding decreases fixation strength at lower neck angles for oversizing $\geq$24%. As oversizing is increased, pull out forces increase as well. At higher neck angles, oversizing and folding has little effect on migration risk. There was no statistical difference in pull out forces across all neck angles.

Conclusion: Oversizing and neck angulation contributors to folding. Folding increases migration risk for at oversizing $\geq$24% and lower neck angles. At higher neck angles, folding and oversizing has no impact on attachment strength.

TABLE OF CONTENTS

LIST OF TABLES

LIST OF FIGURES

CHAPTER 1: INTRODUCTION

<u>Abdominal Aortic Aneurysms</u>

Abdominal aortic aneurysms (AAA) are local dilations of the abdominal aorta by 3 cm or greater (Figure 1) [1]. This condition claims over 200,000 new patients a year with roughly 15,000 resulting in death. Often, AAAs are asymptomatic and undetected until rupture where immediate treatment is required to prevent death. If the patient has a family history of AAAs, physicians may perform a palpation exam of the abdominal cavity to detect the presence of an aneurysm. Unfortunately, this method is only effective 26% of the time for smaller aneurysms in the 3-3.9 cm range with effectiveness increasing to 76% for aneurysms greater than 5 cm [2]. Physical examination is not sensitive enough to catch aneurysm growth or formation so ultrasound is the preferred detection method. When symptoms do present themselves, they are often associated with abdominal, back, or groin pain. Symptomatic aneurysms are at a higher risk of rupture and require immediate attention. Causes of AAA remain unclear but risk factors are male patients over the age of 65 who smoke and have high cholesterol with a family history of the condition [3]. Physicians must know which patients are at higher risk of AAA formation and monitor them regularly.

Rupture of an aneurysm indicates mechanical failure of the wall to withstand biomechanical stresses exerted on the tissue. Larger aneurysms tend to have a higher rupture rate due to the higher degree of aortic ballooning. Aneurysms 5.5-6 cm in diameter have a one year incidence of rupture rate of 9%. This rate increases to 10% for aneurysms 6.0-6.9 cm in diameter and 33% for aneurysms ≥7.0 cm [4]. Currently, intervention for AAA is recommended for aneurysms with diameter ≥5.5 cm, or if there is growth of the aneurysm by 0.6mm-0.8mm within a year. Size has clearly been the main criteria in assessing aneurysm rupture but is unreliable when used alone. Rupture in

aneurysms <5.5 cm have been reported with rates of 12.8- 23% [5, 6]. This suggests a need for a more reliable criterion in determining rupture susceptibility.

Researchers have proposed using stress analysis to assess rupture risk in AAA. Raghavan et al [7] hypothesized that ruptured aneurysms had globally higher stresses. Results from this study showed that the global wall stresses for ruptured vs. un-ruptured aneurysms were not statistically significant (95±28 vs. 98±23 N/cm^2. Although the global stresses of ruptured vs. un-ruptured aneurysms are not different, groups have reported that peak stress may be a reliable indicator of rupture risk. Venkatasubramaniam et al [8] studied peak wall stresses between ruptured and un-ruptured patients using CT scans from 12 ruptured and 15 un-ruptured patients aneurysms. 3D geometries were generated from the CT scans and finite element analysis was performed to calculate peak wall stresses. Venkatasubramaniam et al reported that ruptured aneurysms had an average peak wall stress of 1.02 MPa versus 0.62 MPa, with statistical significance. Peak wall stresses also correlated with the rupture location.

<div align="center">AAA Treatment</div>

Rupture risk has been associated with elevated wall stresses so treatment methods should alleviate and redistribute these stresses throughout the aneurysm. Currently there are two treatment methods for management of AAA: open surgical repair and endovascular repair.

Open surgical repair is a highly invasive procedure requiring access into the abdominal cavity. The healthy proximal and distal portions of the aorta are then clipped and the aneurysm excised. A synthetic cylindrical graft is sutured in its place, onto the healthy ends of the cut aorta. An alternative method in open repair is to cut the aneurysm open, suture the graft into the lumen, and re-suture the AAA (Figure 2a). With both methods, the abdominal aorta is no longer exposed to peak wall stresses that may lead to

rupture. Open repair remains the gold standard for effective treatment of AAA and has very low risk for late re-intervention due to device related complications (0.4-2.3% incidence rate) [9]. Although re-intervention due to device failure is avoided, this method is associated with higher recovery times and risks of complications including extensive blood loss, renal failure, infection, lower limb ischemia, and death [10-13]. The highly invasive nature and complications make it an unsuitable treatment method for patients with co-morbidities.

Endovascular repair (EVAR) is an alternative method of treatment that is minimally invasive and favorable for patients with co-morbidities or contraindications to open surgical repair. In this procedure, small incisions in the femoral arteries are made so that the vasculature creates a pathway to access the abdominal aorta. A delivery sheath containing a collapsed endovascular graft (cylindrical graft with a metal stent exoskeleton) is inserted into the body via the iliac artery and guided through the vasculature into the healthy portion of the abdominal aorta. The endograft is then deployed into health aortic tissue directly below the renal arteries and at least 1.5 cm above the dilation and (Figure 2b). Once deployed, the endograft relieves stresses on the aortic wall by diverting blood flow through its lumen. Over time, the aneurysm can shrink, further reducing rupture risk.

Endografts rely heavily on passive fixation forces to secure the device in the aorta. These are radial and frictional forces induced by oversizing the endovascular graft (EVG) with respect to the host vessel. Clinically, oversizing is calculated from the outer diameter of the stent graft and outer diameter of the abdominal aorta using the following equation:

$$Oversizing = \left(\frac{D_{evg}}{D_{aorta}} - 1 \right) \qquad \text{Equation 1}$$

The outer diameter of the abdominal aorta is used because CT scans do not allow physicians to assess the true inner diameter of the aorta with much confidence. The true oversizing is therefore slightly higher than the calculated oversizing.

EVAR is an attractive alternative treatment to open surgical repair because of its lower surgical risks. Immediate post surgical mortality rates for open repair is 3.8% versus 1.2% for EVAR [14]. One month post surgical mortality rates range from 1.1 to 2.7% for open repair and 0-1.7% for EVAR [15, 16]. Endovascular repair is still a relatively new treatment method but 5 year follow up studies found no difference in mortality rates when compared to open surgical repair [17].

<div align="center">Endovascular Repair</div>

Parodi et al [18] first introduced endovascular repair as an alternative treatment method for AAA in 1991, drastically changing the field. In his study, Parodi excluded an aneurysm sac in an animal study using a Dacron supported by a stent endoskeleton. Experimental results showed that balloon-expanding the stent graft at the proximal and distal end created a frictional seal that anchored the device in place, successfully serving as a bypass. The device excluded the aneurysm from re-pressurization and potential rupture. Results from this study were very promising for the treatment method but it also signified the need for further research and development to improve the method.

Since then, the market for endovascular stent grafts has gained momentum, receiving FDA approval for use in 1991. In the past two decades, many medical device companies have developed devices servicing EVAR. As more data and experience with endografts was obtained, design changes were implemented to address complications that arose. Endoskeleton stent designs eventually progressed to exoskeleton stent design due to thrombus formation in the lumen of the device occluding flow. Simple tubular designs evolved to include bifurcations and modular components to increase fixation strength and

ease of delivery. Addition of more flexible designs to treat patients with tortuous anatomy was also introduced into the field. Original designs had high columnar strength that would make it difficult to conform to tortuous anatomy, limiting the treatment population. The large variation of patient anatomies pushed manufacturers to design endografts that would be more patient specific, increasing the pool of patients suitable for EVAR. The numerous endograft designs available allow the physician to choose the best device given a patient's condition. For example, a device with high columnar and radial A device that offers less columnar strength but more flexibility so that it can conform closely to the anatomy is more suitable for a patient with very tortuous anatomy to improve the proximal and distal seals.

Currently, five companies have endograft devices approved for use in the United States by the FDA: Cook Medical, Gore & Associates, Medtronic, Endologix, and TriVascular. A few of the companies have more than one EVG design, giving patients a total of 8 devices to choose from with TriVascular's Ovation device only approved for use under a Humanitarian Device Exemption at this time. A summary of device characteristics is shown in Table 1 with pictures of each device shown in Figure 3. As seen in Figure 3, all of the EVGs have a bifurcated design and with either ePTFE, PTFE, or woven polyester as the graft material supported by a nitinol, steel, or cobalt chromium stent. All devices are also modular with a main body and iliac leg attachments except for Endolgix endograft where it is all one unit.

Cook's Zenith, Medtronic's Talent and Endurant, TriVascular's Ovation, and Endologix's AFX and Powerlink devices are designed for suprarenal fixation while Gore's Excluder and Medtronic's AneuRx relies on infrarenal fixation. Suprarenal fixation is often suitable for patients with short aortic necks or severely diseased tissue near the aneurysm neck because of more landing site options. If the tissue immediately proximal to the dilation is too diseased, the device can attach above the renal arteries due

to the graft-less stent layer at the proximal end of the device that doesn't interfere with blood flow from the renal arteries. The Zenith, Endurant, Excluder, and Ovation have barbs on the proximal sealing site to provide active fixation and improve migration. The open cell design of the Talent, Endurant, Zenith, Ovation, and Excluder allows for better conformity of the device to tortuous patient anatomy because of decreased columnar rigidity. The gaps of where only graft material is present allows for bending of the device to conform closely to complicated patient anatomy.

The current trend for endograft manufacturers is development of lower profiled devices. A low profile device reduces delivery catheter sizes, enabling patients with smaller vasculature to be eligible for EVAR as a treatment option. Delivery systems available now range from 14 to 26 F accommodating device diameters of 20-36 mm.

Complications

Although EVAR avoids complications commonly associated with open repair, it is not without its own unique set of complications. EVAR has complications related to surgical access site, delivery system insertion, proper proximal attachment site, device related, and sizing errors [19]. Complications with the attachment site of the device are the most common and serious problem with endovascular repair. A compromised proximal attachment site may lead to migration and endoleak. Migration is clinically defined as caudal movement of the stent graft by ≥10 mm post-deployment and is the leading cause for late EVAR failure (Figure 4) [20]. A poor proximal seal is caused as the length of the sealing area is decreased. If the endograft migrates too far, blood can flow back into the aneurysm sack, developing a late type I endoleak [21, 22]. Endoleak occurs when blood flows back into the excluded aneurysm sac post treatment. There are four types of endoleaks, type I-IV, that characterize blood flow back into the aneurysm sac. Type I endoleak is due to a poor seal between the stent graft and vessel wall. This is

the most serious type of endoleak as it is not self sealing and requires secondary intervention. Type II endoleak is due to backflow from collateral vessels. Type III endoleak is due to leaks at the connection points for modular components of the device, or fabric tears. Type IV is leakage due to from porosity of the graft material. Types II-IV endoleaks are not as serious as type I endoleak and may not require immediate treatment or secondary intervention. Endoleaks have been associated with late term complications and do require close observation.

Migration is a long term complication reported by numerous researchers. Conners et. al [23] reported migration rates of 7.2% at 1 year, 20.4% at 2 years, 42.1% at 3 years, and 66.7% at 4 years post deployment for the AneuRx device after follow up of up to 4 years. Cao et al [24] reported migration rates of 15% after a mean follow up period of 2 years with a predicted 27% migration rate at 3 years. These findings are higher than those from Zarins et al [25]who reported a migration rate of 1.4% at 1 year, 6.6% at 2 years, and 18.8% at 3 years. Despite the different findings, migration is a problem associated with EVAR that is recognized in the field.

Migration is thought to be caused by biomechanical and drag forces due to pulsatile motion of the vessel wall as well as due to blood flow through the device. Typical drag forces in the abdominal aorta are roughly 3-4.5N but it can be as high as 10 N depending on patient anatomy [26]. Resch et.al reported median fixation forces for the Talent and Vanguard devices, both barbless, to be 4.5N and 9N respectively. These values are within the range of drag forces that could be experienced in the body and may cause migration and require intervention [27]. Endografts rely heavily on radial and frictional forces caused by oversizing the device. Manufacturers typically recommend an oversizing range of 10-20% but physicians have used devices off label and oversized up to 60% depending on the patient's condition [28, 29]. When the radial and frictional forces caused by oversizing are less than the drag forces encountered during normal

cardiac cycle functions, the device will migrate caudally. To address this issue, barbs were introduced to endograft design to increase attachment strength.

Malina et. al [27] compared fixation strengths of Dacron grafts sewn onto Gianturco stents with no barbs, 4 barbs/hooks, and 8 barbs/hooks. The forces were reported to be 2.5N, 7.8N, and 22.5N respectively [30]. Resch et. al also compared median fixation forces for both barbed and barbless endografts. He reported fixation forces of 4.5N, 9.0N, 12.5, 24N, and 25N for the Talent (barbless), Vanguard (barbless), Ancure, Zenith, and Palmaz stent-grafts, respectively. There is a clear increase in fixation strength with the addition of barbs.

From this, logic would dictate that addition of barbs and increased oversizing would also increase the radial and frictional forces, decreasing migration risk. Experimental studies also support this line of thinking as increased radial and frictional forces were reported as oversizing increased [30-32]. There is conflicting data that indicates no consensus in the field regarding the relationship between oversizing and pull out forces [33]. A recent study from Kratzberg et. al.[34] (Figure 5) investigating the role of oversizing on fixation strength of barbed endografts also reported decreased fixation strengths for stent grafts oversized >30%. Sternbergh et al [28] reported similar findings in patients treated with the Zenith device where a 14% migration rate was reported for oversizing >30% versus 0.9% for oversizing <30%. Other researchers [23-25, 35] have reported no correlation between oversizing and migration

The endografts mentioned in Kratzberg et al's [34] and Sternbergh et al's [28] studies were barbed devices while the devices mentioned in contradicting reports were barbless AneuRx devices. The presence of barbs may explain the lower attachment strengths observed by Kratzberg et al and Sternbergh et al. Although barbs were added to increase fixation strength, they may begin to interfere with proper apposition of the endograft with the aortic wall at higher oversizings. Kratzberg et. al conducted another

study [36] investigating the impact of barb length and angle on fixation strength in the 11-20% oversizing range. In this study, oversizing was maintained at 10-20% while barb length varied from 2-7mm (barb angle held constant at 20°) and barb angle varied from 0-90° (barb length held constant at 2mm). Results from this study found that lower barb lengths and angles resulted in higher fixation strengths.

There is poor understanding of the relationship between oversizing, barb length, and attachment strength. As mentioned before, high oversizing should result in higher frictional and radial forces. This is not the observation made in studies where barbed endografts were used. Inspection of CT scans from Kratzberg et al's body of work on the effect of oversizing and barb characteristics on attachment strength showed that some devices were folding or collapsing in or over itself (Figure 6). This phenomenon, termed folding, was hypothesized as the explanation for the lower fixation strengths observed at oversizings >30%. In Figure 6, poor apposition of the device is observed as a portion of the stent and graft is not in contact with the aortic wall, decreasing the frictional force and compromising the radial force of the endograft. A study from Wolf et al [37] also suggested that endograft folding, or eccentric compression as they termed it, may be linked to poor proximal fixation. In 100 patients treated with the AneuRx device, 5 (5%) patients had cases of folding and 4 of the 5 (80%) reported incidence of migration. Aside from Wolf et al's study, there is little literature on the phenomenon of folding in abdominal aortic aneurysm repair and its impact on migration. The causes or factors that increase endograft folding risk are also poorly understood.

In the thoracic endovascular field (TEVAR) however, numerous cases of folding have been reported. Reports in TEVAR field have suggested that high neck angulation and extreme oversizing increase folding risk that may result in poor device performance [38-42]. In a review of published cases by Jonker et al [43], 60 individuals with incidences of folding after TEVAR (range, 1 day -79 months) were identified. Median

oversizing of the endografts was $26.7 \pm 12\%$ (range 8.3% - 60%), with excessive oversizing the cause for 20% of folding cases observed. Canaud et. al [44] also observed folding after TEVAR that contributed to poor apposition of stent grafts oversized >20% in the aorta. In 285 patients, 4 (1.4%) experienced stent graft collapse. Of the four patients, all (100%) had extremely high neck angulation and three of the four (75%) were oversized >20%. Folding often occurs a few weeks after surgery with long term implications. Patients with endograft collapse were 10.4% more likely to develop complications than devices without folding [45]. Although the anatomy of the ascending aorta is different than the descending aorta, findings from the TEVAR reports still provide observations knowledge that can be reasonably applied to EVAR. Folding has been cited to clinically occur and impact attachment strength of the device in both EVAR and TEVAR.

<div align="center">Current Research on EVAR</div>

Endovascular repair has been of great research interest since its introduction to the medical field. Experimental research is of extreme value because of the insight that it brings. Computational research often requires a fairly comprehensive understanding of a problem before justice can be done to assure accurate computational modeling. Experimental research often provides a base understanding of the issue that facilitates in the computational modeling process. There are numerous clinical studies reporting on the performance of stent grafts as well as other patient and surgical variables that may affect the success of the treatment method. The reports are extremely valuable and provide the research community with clinically relevant information on the device. Device complications or failures provide research motivation to understanding the problem so that a solution can be formulated.

Significant research efforts are conducted to understand the complications associated with EVAR: endoleak and migration. Factors that affect endoleak or migration are of great interest to both manufacturers and clinicians. Many studies utilize experimental setup allows that enable the researcher to vary parameters and isolate the most relevant factors that may largely impact endoleak or migration in a clinically representative setting. The experimental approach in research is difficult because of the numerous variables that are unavoidable during testing. Because of this, development of a represented flow loop is critical in validating any results obtained from a study. An important component of the flow loop is an appropriate deployment substrate and abdominal aortic aneurysm flow phantom. Numerous groups have proposed methods for creating compliant AAA flow phantoms. Researchers such as Chong et al [46] and Berry et al [47] published methodology papers on flexible models using silicone to create patient specific abdominal aortic aneurysm for in vitro studies. Doyle et al [48] and Corbett et al [49] improved on this idea by incorporating intraluminal thrombus in the aneurysm model, further increasing the realism of the phantom by simulating the mechanical behavior of the AAA and intraluminal thrombus. Although flexible models are more difficult to create and more time consuming initially, they can be compliance matched with the human aorta/AAA and they provide a viable alternative to ex vivo tissues. The hemodynamic and deployment realism for the study is also present.

As previously mentioned, experimental studies are largely interested in understanding complications associated with EVAR. Xenos et al [50] conducted an experimental study investigating the effect of Type 1 and Type II endoleak on pressure distribution. A fusiform aneurysm was created using Gore-Tex grafts and patch material. Strain transducers were placed throughout the aneurysm wall and the model was placed into the flow loop with a pulsatile pump circulated citrated horse blood at 38° C. A stent graft was deployed into the fusiform aneurysm and Type 1 and Type II endoleaks were

created using shunts and a fusiform aneurysm with side branches, respectively. Strain measurements were taken at 80, 110 and 150 mmHg. The study found type I endoleak resulted in significantly higher pressures in the proximal neck region and was not statistically different than pressures experienced in the aneurysm sac prior to treatment. Such insight would be much more difficult to obtain from clinical patients as opposed to an experimental setting where factors are easily controlled.

Numerous studies on migration have also been reported in the research field. Corbett et al [51] experimentally investigated the role of neck fixation length and system pressures on proximal fixation strength but highlighted the need for test setup that account for the device's longitudinal rigidity. An AneuRx and homemade device with little longitudinal rigidity was deployed in an idealized silicone aneurysm model under pulsatile flow at 37°C. The AneuRx device had higher fixation strengths compared to the homemade device (6.95±0.49 to 8.52±0.5N vs. 2.57±0.11 to 4.62±0.25N). However, testing methods did not appropriately account for longitudinal rigidity of the device. Although proximal fixation may have decreased, iliac fixation may have increased to compensate. Corbett et al also investigated the role of pulsatile motion and vessel material properties on device migration. A commercially available stent graft was deployed in silicone AAAs of varying neck stiffness under pulsatile and no flow conditions. Displacement forces were found to be lower in more compliant vessels under pulsatile flow. Pressure variation did not cause a statistically significant result in fixation strength.

Corbett conducted another study in collaboration with Doyle et al [52] to experimentally and computationally evaluate rupture biomechanics in AAA. Synthetic AAA models were created from silicone with comparable mechanical properties as human aneurysms. Rupture tests were performed and confirmed with computational

results. The group reported that rupture often occurred at regions of inflection rather than at the maximum diameter.

Experimental test set ups have become a useful tool for researchers to further understand factors that contribute to complications with EVAR. Experimental research provides valuable insight on general trends in endograft behavior under specific conditions. Various test parameters are easily varied and executed in a physiologically representative manner that bornes out relationships between the parameters and device performance. These types of results may not be easily modeled computationally without a general grasp of endograft behavior phenomenon.

This project intends to investigate the relationship between, oversizing, neck angulation and freedom from migration. To my knowledge, there is no body of work that investigates factors that induce folding and the impact that it has on device fixation strength. A well controlled test plan was designed to systematically evaluate the inter-relationship between oversizing, folding, and fixation strength.
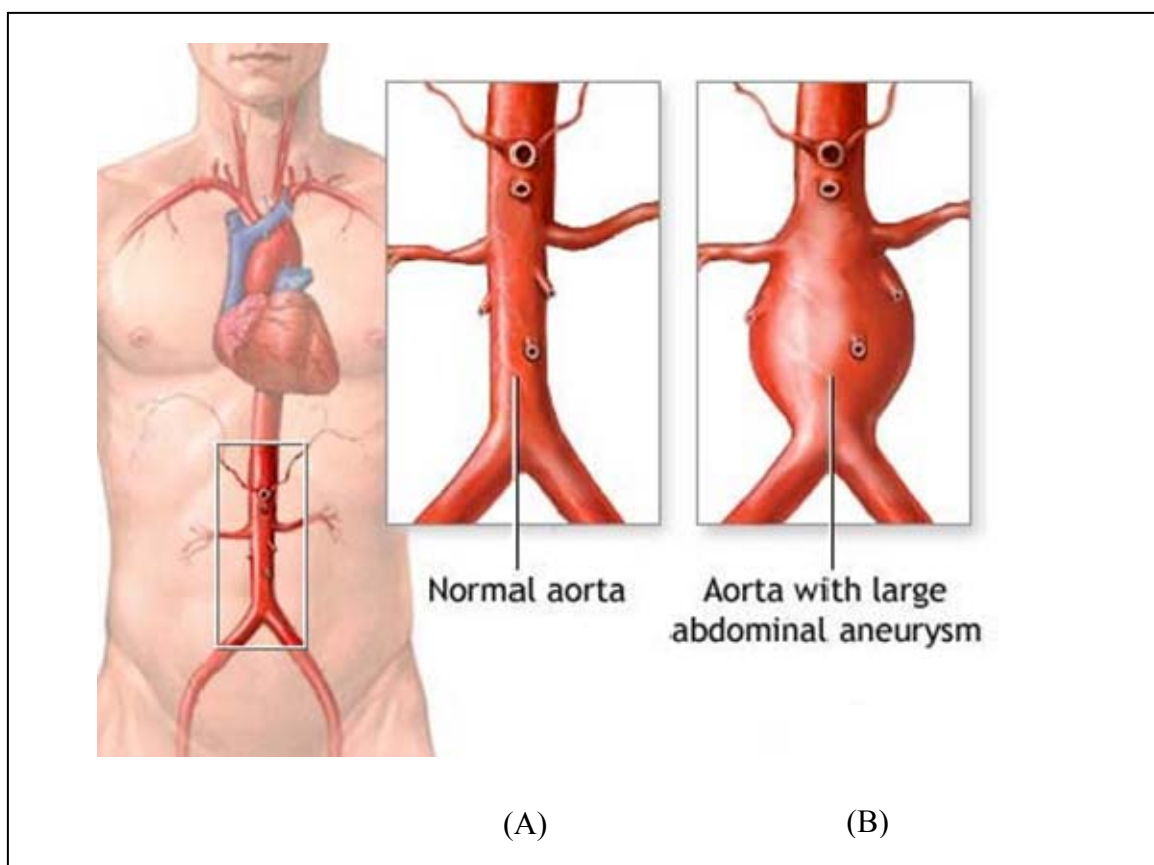
Figure 1: Cartoon of healthy (A) abdominal aorta and (b) aorta with aneurysm formation.
Img source: http://www.nlm.nih.gov/medlineplus/ency/images/ency/

(A)

(B)
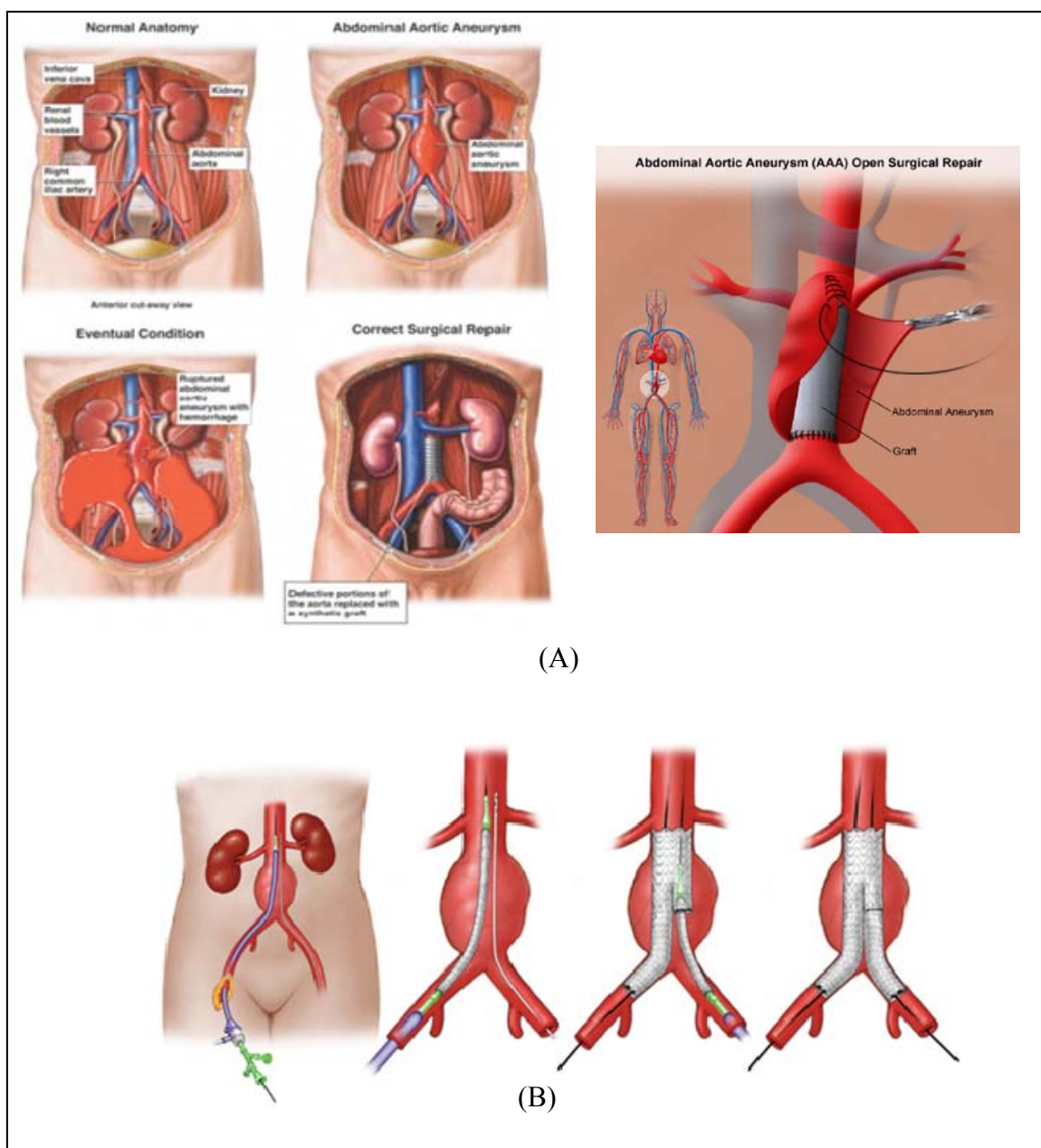
Figure 2: Cartoon depiction of current treatment methods available for abdominal aortic aneurysms. (A) Open surgical repair of abdominal aortic aneurysm. A graft material is sutured onto the healthy ends of the aorta. *Img source: http://www.cvtsa.com/MediaServer/MediaItems/MediaItem_237.jpg & http://www.jeffersonhospital.org/images/staywell/126159.GIF.* (B) Endovascular repair (EVAR) of abdominal aortic aneurysm. The physician makes a small incision in the femoral artery and the endograft is deployed in the aneurysm, excluding the sac from blood flow. *Img source: http://www.mayoclinic.org/medicalprofs/enlargeimage5675.html*

Table 1: Table of all commercially available devices and their design characteristics.

Company	Product	Fixation Location	Barbs	Closed vs. Opened Cell	Stent Material	Graft material
Cook Medical	Zenith Flex w/ Z-Trak	Suprarenal	Yes	Open	Stainless steel and nitinol	Woven polyester
Endologix	AFX Endovascular AAA System	Fixation at bifurcation, infrarenal or suprarenal configurations for seal	No	Closed	Cobalt-chromium alloy	Strata multilayer ePTFE
	IntuiTrak w/ Powerlink Stent Graft		No	Closed		High-density ePTFE
Gore & Associates	Gore Excluder AAA Endoprosthesis w/ C3 Delivery System	Infrarenal	Yes	Open	Nitinol	ePTFE
Medtronic, Inc.	AneuRx AAAdvantage	Infrarenal	No	Closed	Nitinol	Woven multifilament polyester
	Talent Abdominal	Suprarenal	Yes	Open		
	Endurant AAA Stent Graft		Yes	Open		
TriVascular	Ovation Abdominal Stent Graft System	Suprarenal	Yes	Open	Nitinol	PTFE
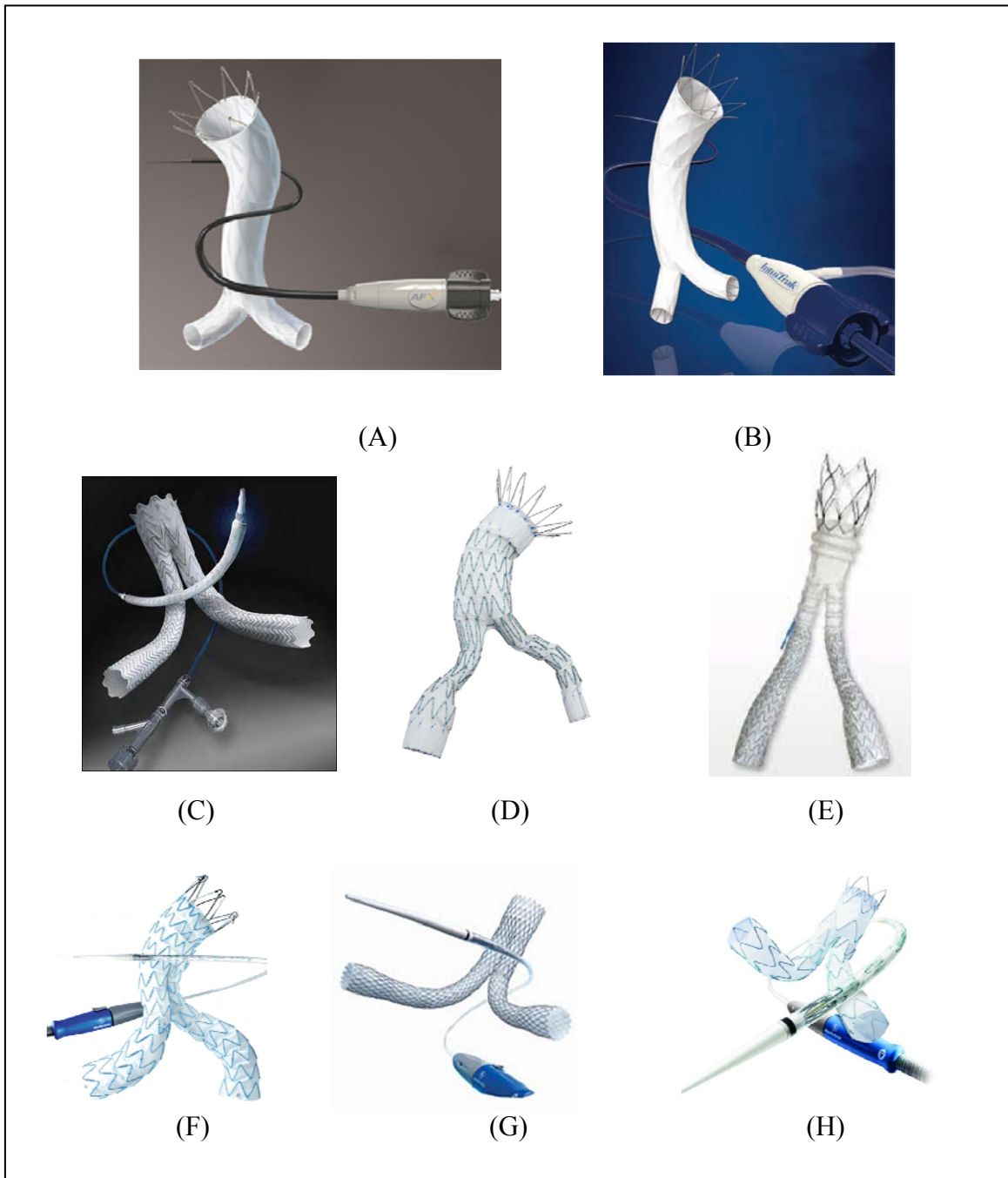
Figure 3: Currently available endovascular grafts from various manufacturers in the United States. (A) Endologix AFX (B) Endologix Powerlink, (C) Gore Excluder, (D) Cook Zenith, (E) TriVascular Ovation, (F) Medtronic Endurant, (G) Medtronic AneuRx, (F) Medtronic Talent. Img source: A, B: www.endologix.com; C: www.goremedical.com, D: www.cookmedical.com; E, www.trivscular.com; F, G, H: www.medtronic.com.
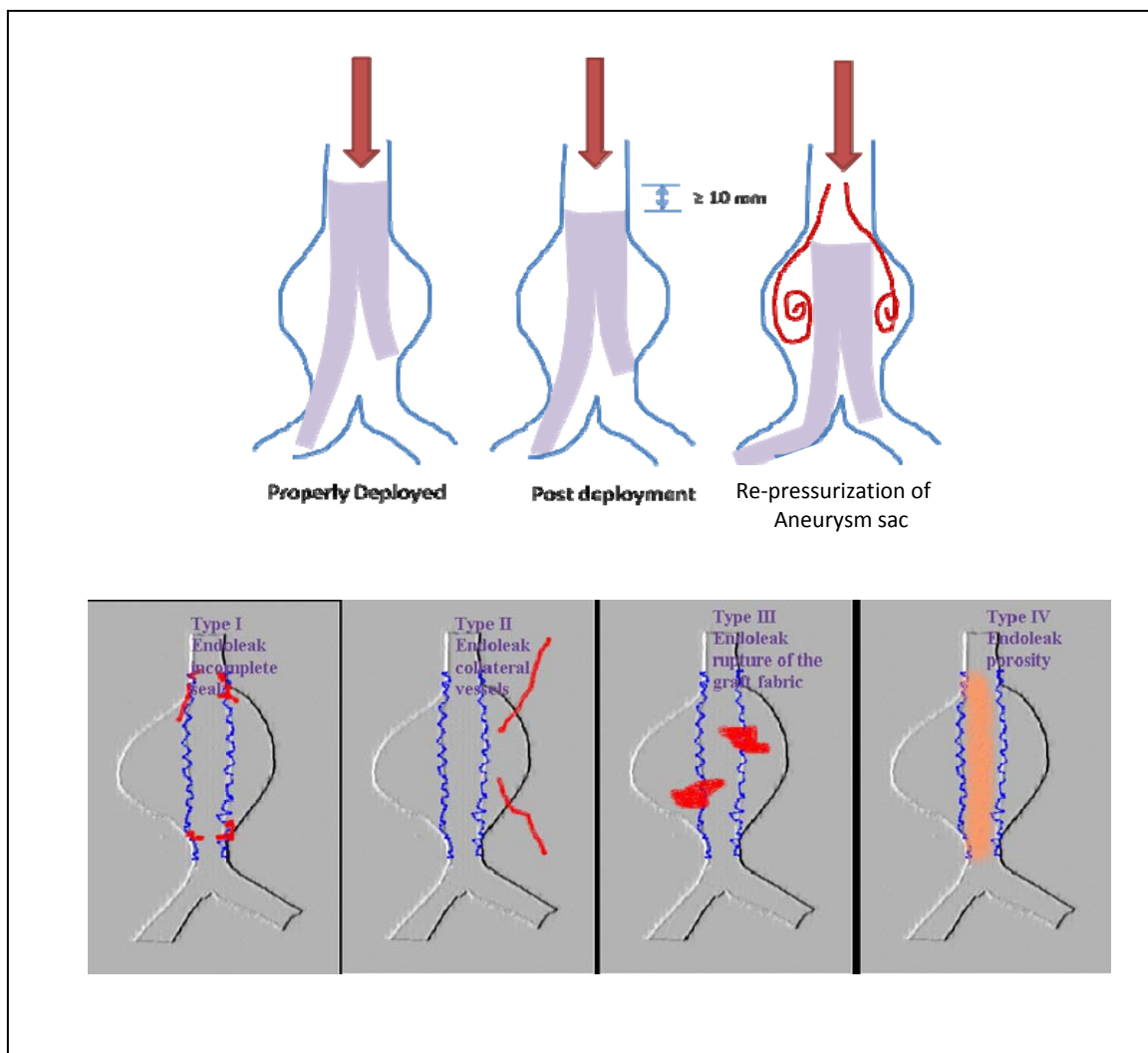
Figure 4: Schematic depiction of EVAR complications. (Top) Schematic of blood leakage into the aneurysm sac due to migration. (Bottom) Schematic of Type I-IV endoleak. Type I is most commonly associated with migration and requires immediate intervention. Img source: Rofo Fortschr Geb Rontgenstr Neuen Bildgeb Verfahr. 2003 Oct;175(10) :1392-402).
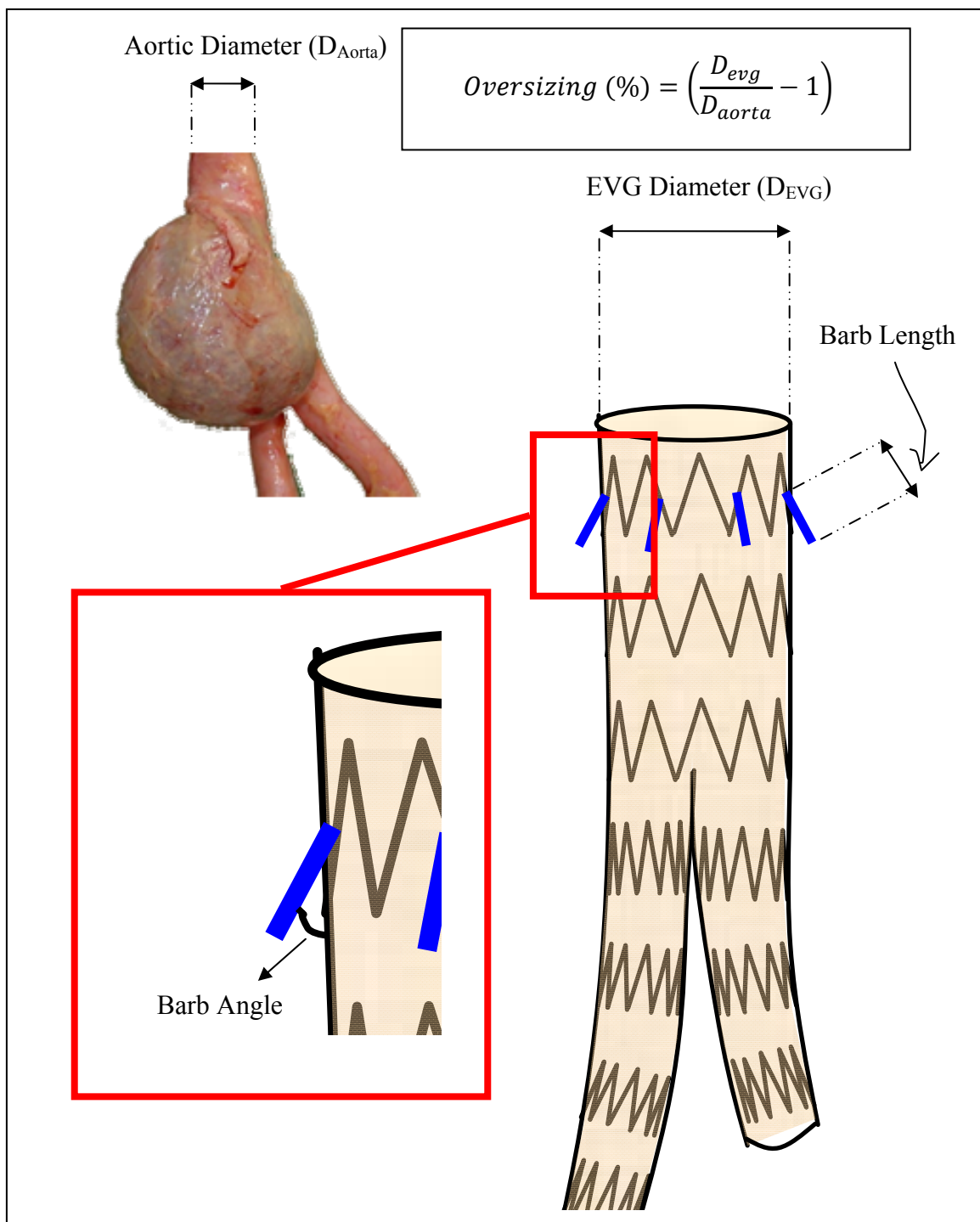
Figure 5: Schematic drawing of barb length, barb angle, and oversizing parameters that were varied in Kratzberg et al's study.
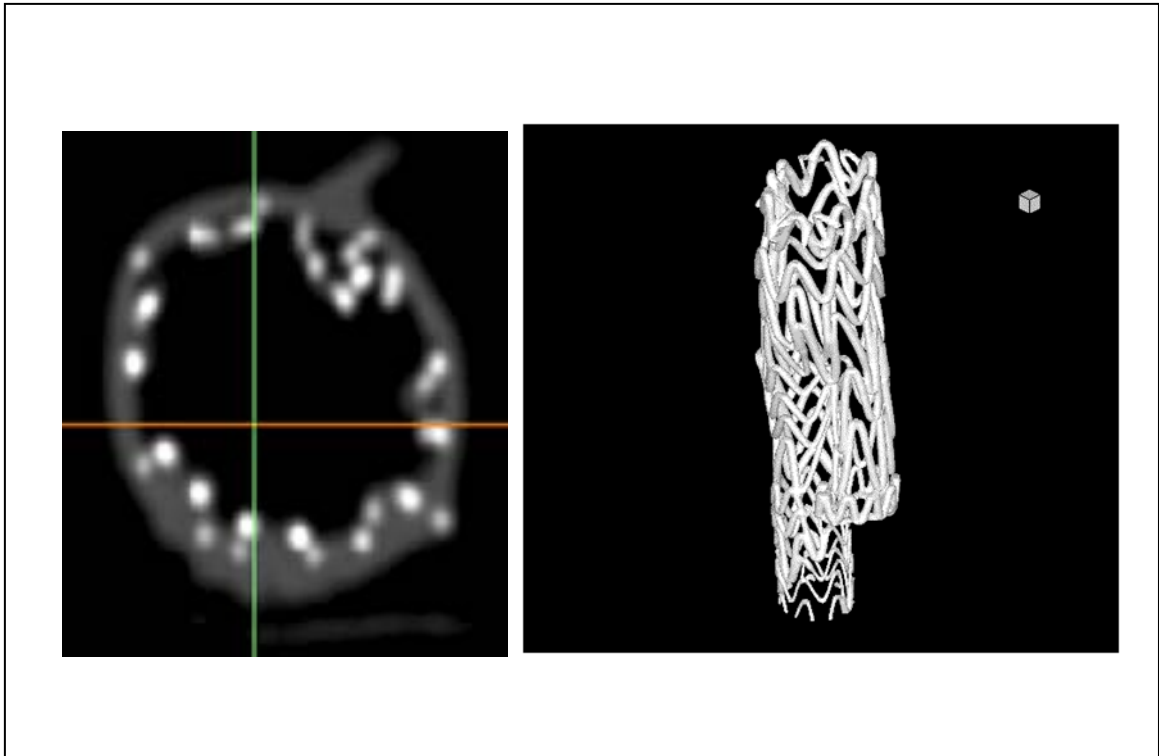
Figure 6: Example of folding observed in Kratzberg et al study. Left picture shows cross sectional of the stent. Note the fold of the stent into the lumen. Right picture is a 3D volume rendering of folded EVG. (Oversizing: 43%, Barb length: 2mm, Barb Angle: 20^0)

CHAPTER 2: MOTIVATION AND PRELIMINARY WORK

A causative relationship between high oversizing and folding is plausible but remains unclear. Other factors such as barbs may play an important role as well due poor barb penetration that aggravates folding risk. As such, the role of graft oversizing, barb length, and barb angle on stent graft folding was investigated to test this hypothesis using imaging and mechanical testing data collected from Kratzberg et al's in vitro bench top studies on the effect of oversizing on barbed endograft attachment strength.

<u>Experimental study on the role of oversizing on barbed</u>

<u>endograft attachment strength</u>

Disclosure: This work was performed by Jarin Kratzberg, then PhD candidate in the Biomechanics of Soft Tissues Lab (M.L. Raghavan, advisor), University of Iowa. My contribution to this work was the later analysis of the data obtained from the experiments. This work was published in a conference proceedings: Jarin A Kratzberg, Kathleen Lin, William Barnhart, Jafar Golzarian, Madhavan L Raghavan, "Experimental and computational optimization of aortic endovascular graft variables", Annual Meeting, Biomedical Engineering Society, St. Louis, MO, 2008 Sep.

Kratzberg et al [36] investigated the effect of three stent graft variables on proximal fixation strength: oversizing (rang, 4%-45%, n=20), proximal barb length (rang, 0-7 mm; n=13), and barb angle (range, $10°$-$90°$ to graft axis; n=7). Oversizing was defined as the percent difference between the stent graft diameter and the systolic diameter of the aorta it was deployed in. Barb length was defined as the length of the barb protruding downward from the stent. The chosen range of study for barb length of 0 to 7 mm captured the range of barb lengths in commercial devices. Barb angle was defined as the angle that the barb makes with the axis of the graft when freely deployed. The range studied covered the entire range possible from 0° (vertical, hugging the stent) to 90°

(horizontal). When one of these three variables was perturbed, the other two variables were maintained constant. Gore Excluder grafts with custom nitinol barbs varying in length and angle were fabricated in-house. The barbs were sutured on the second stent layer of the device. The stent grafts were then deployed into a mock flow loop with a time-averaged physiologic flow rate of ~2.5 L/min, pressure of ~80/140 mmHg at 80 beats/min, and an idealized biosynthetic aneurysm phantom.

Descending thoracic bovine aorta obtained from an abattoir was attached to the synthetic aneurysm phantom. The device was compressed into a 24 Fr catheter and introduced to the flow loop via the iliac bifurcation. The proximal end of the device was deployed into the fresh bovine aortic tissue to ensure realistic deployment and barb penetration conditions (Figure 7). Deployments were conducted under continuous flow, and devices remained under flow for roughly 30 seconds to 2 minutes post deployment to ensure stabilization of flow and pressures.

The flow loop was stopped and the graft–aorta complex was removed and stored in saline at body temperature. Within 1 hour after removal from the flow loop, the graft–aorta complex underwent high-resolution CT scanning on a 64-slice Siemens Cardiac Sensation scanner (Siemens Medical Siemens Medical, Malvern, Pa) with scan parameters of 100 effective mAs, 140 kV, pitch of 1, and a rotation speed of 0.5 seconds. A collimation of 64 x 0.6 mm was selected with a reconstructed slice of 0.6-mm width and recon increment of 0.4 mm to obtain the best resolution and achieve isotropic voxel images. Subsequently, mechanical pullout tests of the graft-aorta complex were conducted to evaluate the fixation strength of the stent-graft [34, 36].

<u>Preliminary studies: Investigation of oversizing and barb</u>

<u>characteristics on endograft folding</u>

Methods

Discloser: This work was performed by Kathleen Lin, PhD candidate in the Biomechanics of Soft Tissues Lab (M.L. Raghavan, advisor), University of Iowa. This work was published in a journal: Kathleen Lin, Jarin Kratzberg PhD, Madhavan L Raghavan PhD, "Role of aortic stent graft oversizing and barb characteristics on folding", Journal of Vascular Surgery, ePub before print, 2/07/2012.

CT scans from Kratzberg et al's [36] study on the effect of oversizing and barb characteristics on fixation strength were obtained and used for this study. The proximal stent graft deployed in the bovine aorta/AAA phantom was evaluated with rigor for the level of folding. Two forms of visual assessments of the stent graft apposition and deployment characteristics were performed: First, the image volume was obliquely sliced based on local graft axis at the fixation site using Syngo CT (Siemens Medical), an image-processing platform. This allowed for visualization of the stent and barbs at the proximal end of the graft along its true cross section (Figure 8a). A coronal section was also used where needed. Second, 3-dimensional (3D) reconstructions of the stent and barbs were generated using Mimics (Materialise Inc, Plymouth, MI), a 3D solid-modeling software (Figure 8b). Data visualization software (Tecplot Inc, Bellevue, Wash) was used for further visualization of the 3D objects.

All data analysis was performed on the proximal region of the device (first few stent layers, especially where the barbs generally attach). Folding in the proximal region of the stent graft is of particular concern because it directly affects its proximal apposition with the aortic wall. Where necessary, 3D models were also sliced along the transverse, sagittal, and coronal planes to better visualize and confirm folding along the perimeter of

the stent. For control, a 26-mm stent graft with a 7-mm barb length and a 20° barb angle was deployed freely in air and imaged in a similar manner. The control deployment represents the best-case scenario with no deformation or folding (Figure 9). The images obtained and processed from the control deployment served as the gold standard while studying the stent grafts deployed within the bovine aortic neck of the biosynthetic AAA phantom. An initial evaluation of the CT data revealed two types of folding: longitudinal and circumferential (Figure 10). Longitudinal folding occurs when the stent graft folds along the length of itself (Figure 10b). Circumferential folding occurs when the stent graft folds into the lumen of the device (Figure 10c) or when there is overlapping of neighboring stent struts. Folds observed by image processing and visualization were ranked on a scale of 0 to 3 for severity (Table 2) by comparing with the control. Because some stent grafts may have multiple folds, rank values for all folds within a graft (regardless of fold type) were summed to obtain a cumulative folding rank. Ranks for all cases in this study were assigned by the same investigator according to the criteria in Table 2. The investigator was blinded to all oversizing and barb characteristic information during the ranking process.

Results

Forty stent grafts were deployed with various oversizings, barb lengths, and barb angles, followed by imaging and pullout testing. We failed to obtain CT scans in 3 stent grafts, resulting in 37 devices used in this analysis. A summary of CT imaging data of deployments used to assess folding is provided in Table 3. In these cases, the CT scan volumes were processed to characterize graft folding on an ordinal scale, as laid out in Table 1. In the study population, incidences of almost all combinations of folding ranks and types (circumferential and longitudinal) were noted. Representative examples for various ranks and types of folding may be found in Figure 11.

The relationship between cumulative fold level and oversizing, barb length, and barb angle are shown in Figure 12. Of the 37 cases, 12 deployments showed one or more folds (5 mild, 5 moderate, 3 severe), and 11 of these 12 were from the study where oversizing was perturbed. Three of the 12 fold cases (38%, 13%, 38% oversizing) experienced two folds and one (30% oversizing) experienced three folds. A total of 17 folds were identified in 12 stent graft deployments, of which 4 (23%) were longitudinal and 13 (77%) circumferential. Among the 37 deployments, at least one instance of folding was noted in the five stent grafts with oversizing >30%. One severe folding (cumulative fold level of 6) occurred in a 13% oversized stent graft, a suspected outlier in the data.

The cumulative fold rankings were (mean ± standard deviation) 3.4 ± 1.7 for oversizing >30% (n = 5) vs. 0.5 ± 1.2 for oversizing < 30% (n = 7), which was statistically significant (Mann-Whitney U test $P < .005$). The results were similar with statistical significance when experiments where only oversizing was perturbed were compared between oversizing >30% and <30% (3.4 ± 1.7 vs. 1.1 ± 2; $P < .05$). When barb length was held at 10%-20%), folding was noted in 1 of 11 cases (mild folding in a stent graft with a 7-mm barb, (Figure 13). When barb angle was varied from 0° (vertical) to 90° (horizontal, oversizing held constant at 10-20%), folding was not noted in any of the seven cases (Figure 14).

Pullout force data were available for assessment of the relationship between graft–aorta attachment strength and folding (Figure 15). Pullout force was not significantly different between stent grafts with and without folding (5.4 ± 1.95 vs. 5.12 ± 1.89 N, respectively; $P > .5$).

Discussion

Graft folding may result in poor apposition between the stent graft and aortic wall, a phenomenon whose impact on short-term fixation strength and long-term endoleak and/or migration risk remains poorly understood. Recall the study reported by Wolf et al. on folding and poor wall apposition, as well as the studies on factors favoring device folding reported by Jonker et. al [43], and Canaud et. al [44]. Empiric data from patient outcome studies are indispensable for gaining a true understanding of graft folding and its effects on migration. But measurements made in such studies are unlikely to be detailed enough to reveal the mechanisms involved in folding or be sufficiently controlled for a deterministic understanding of this process and its association with fixation strength. In vitro bench-top studies, however, may allow for controlled investigations, although they admittedly suffer from limited realism to the physiologic situation. Further, bench-top studies at best only provide insights into short-term aspects of deployment rather than long-term outcomes.

Thus, bench-top studies compliment empiric patient outcome studies by driving hypotheses that may be tested prospectively or clarifying findings in retrospective data, or both. This bench-top investigation was motivated by patient outcome reports noting empiric associations between stent graft oversizing, folding, and migration rates [37, 43, 44]. We have assessed some of the factors that may conceivably be associated with and causative of folding and its effects on attachment strength in a retrospective analysis of data obtained from our bench-top investigation. Quantifying folding levels is beneficial because it captures the level of apposition to the host vessel and may have implications on device migration or endoleak. Folds may form a "ledge" in the perimeter of the device, resulting in an elevated axial force on the device from blood flow that can aggravate migration risk.

A link between oversizing and folding in stent grafts is to be expected. For an oversized stent graft to fit inside an aorta, it needs to expand the aorta or compress itself, or both. If the level of compression breaches some threshold, it will likely fold at one or more spots. Thus, the precise relationship between oversizing and folding is likely nonlinear. Anecdotal observations in an earlier study by our group suggested that folding particularly occurs with oversizing >30%. This study was undertaken to more definitively verify those observations with some level of quantification. Our analysis of detailed image volumes of the deployed stent graft show that oversizing >30% does result in folding; indeed, folding was observed in all grafts oversized >23.5%. But for one suspected outlier, where a 13% oversized graft showed severe folding (cumulative fold level of 6; also see Figure 11, *D* and *G,* and Figure 12), folding was minimal or nonexistent in stent grafts oversized < 23.5%. This suggests that the aorta is not expanding to accommodate the stent graft, but rather forces it to fold when oversized greatly. This is only understandable when one considers the nonlinear stiffening of the aorta at higher pressures and that the additional radial pressure from the stent graft onto the aortic wall is about 30 mm Hg, even when oversized greatly.

We performed a quick finite element simulation of the dilation of a circular 2D cross-section of a human aorta (1.9-cm inner diameter; 1.5-mm thick; finite elastic tissue constitutive model) under mean aortic pressure (100 mm Hg), followed by the additional radial pressure by 15% and 40% oversized grafts. The aorta inflates by an additional 0.8% from mean aortic pressure for deployment of a 15% oversized graft and by an additional 1.1% for a 40% oversized graft. Clearly, oversizing greatly will invariably result in folding of the stent graft, as noted in our experiments. An in vitro study by Schurink et al [53] also reported some positive correlation between oversizing of Gianturco (William Cook Europe, Bjaeverskov, Denmark) and Palmaz (Cordis, Miami Lakes, Fl) stent grafts and the size of the largest fold in these grafts.

It is conceivable that barbs interfere with and perhaps aggravate folding risk, especially when they do not penetrate the wall but rather protrude from the wall and push against it. However, results here suggest that barbs in stent grafts oversized in the 10% to 20% range, regardless of their length (2-7 mm) or angle (10°-90° with respect to graft axis), do not aggravate folding risk. This is irrespective of whether and by how much the barbs penetrate into the aortic wall. The study did not investigate whether barbs are similarly of no consequence in folding at other oversizing ranges. Interestingly, stent grafts that had folding did not necessarily have lower pullout strength when compared with those with no folds. Caution is warranted in interpreting this to mean that folding is unlikely to affect short-term attachment strength, mainly because pullout strength was also affected by other factors such as oversizing and active fixation effects from barbs that were perturbed independently in this study.

Some limitations in this study are worth noting. Fold was quantified on an ordinal scale by visual observation by one investigator. However, all observations were performed by leveraging advanced 3D reconstruction methods by a single investigator, and fold severity determination was based on comparative level to the condition of all stent grafts within the 37 devices, especially the control deployment. Further, the investigator was blinded from information on oversizing and barb length and angle for a given stent graft whose images were being assessed. Therefore, we are confident that the findings are valid, especially for comparative purposes. The results observed are also only representative of short-term cases, because the devices remained in the flow loop for a very short period. If the devices remained under flow conditions for a longer period, infolding may become more severe but barb embedment may also be more efficient. Although we did not find a statistically significant difference in pullout forces between devices with and without folds, there may be long-term implications of this occurrence. As previously mentioned, devices with folding do not have proper apposition to the host

vessel and may lead to a lower threshold attachment strength immediately after deployment. Over time, this could put the patient at higher risk for complications associated with migration. Migration is also a very complex occurrence because of all the factors that influence it (oversizing, barb characteristics, etc.). No conclusive statement can be made regarding the role of folding in migration from this study.

Furthermore, because this study was also a retrospective analysis of data gathered from experiments designed to assess how pullout strength was affected by oversizing, folding was not varied in a highly control manner. Studies focused on perturbing other potential causative factors in a controlled manner may provide further insights.

Conclusion

In this in vitro investigation, stent graft folding occurred at all oversizing ranges but was especially prevalent at oversizings >30%. This confirms suspicions that oversizing is a large factor in folding risk. Logic dictates that an increase in oversizing would obviously cause an increase in folding. However, we are unfamiliar with the behavior of folding as well as the whether or not the relationship is linear or non-linear.

Within the recommended range of 10% to 20%, large variations in barb length and angle did not aggravate folding risk. Despite this finding, the relationship of barbs, oversizing, and folding is still not clear. Interactions between the barbs at various oversizing ranges were not evaluated in this study and may provide a stronger correlation with folding.
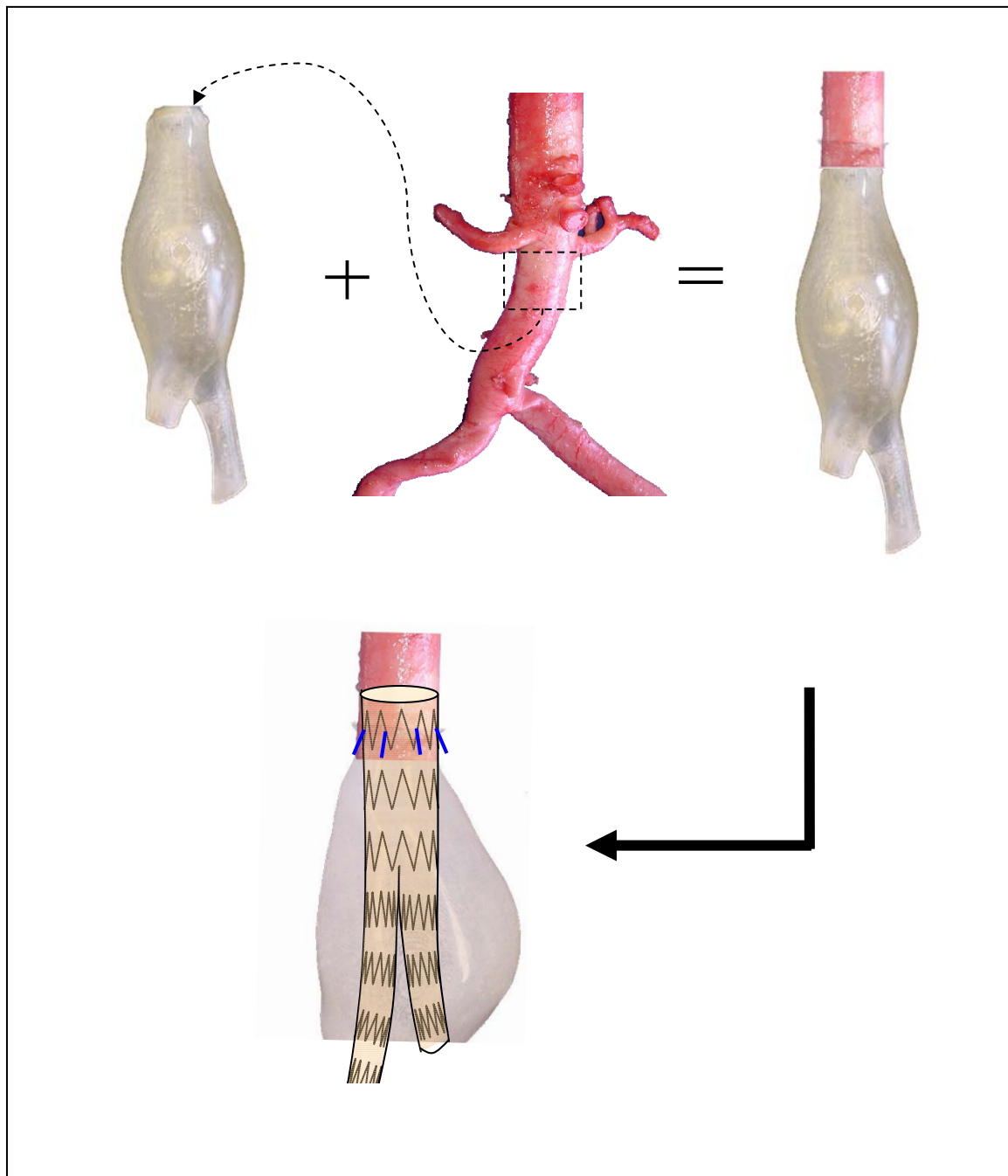
Figure 7: Aorta-AAA complex used by Kratzberg et al for his project. The stent graft was target deployment landing site was in the bovine aortic region a few centimeters higher than the bioprosthetic AAA model
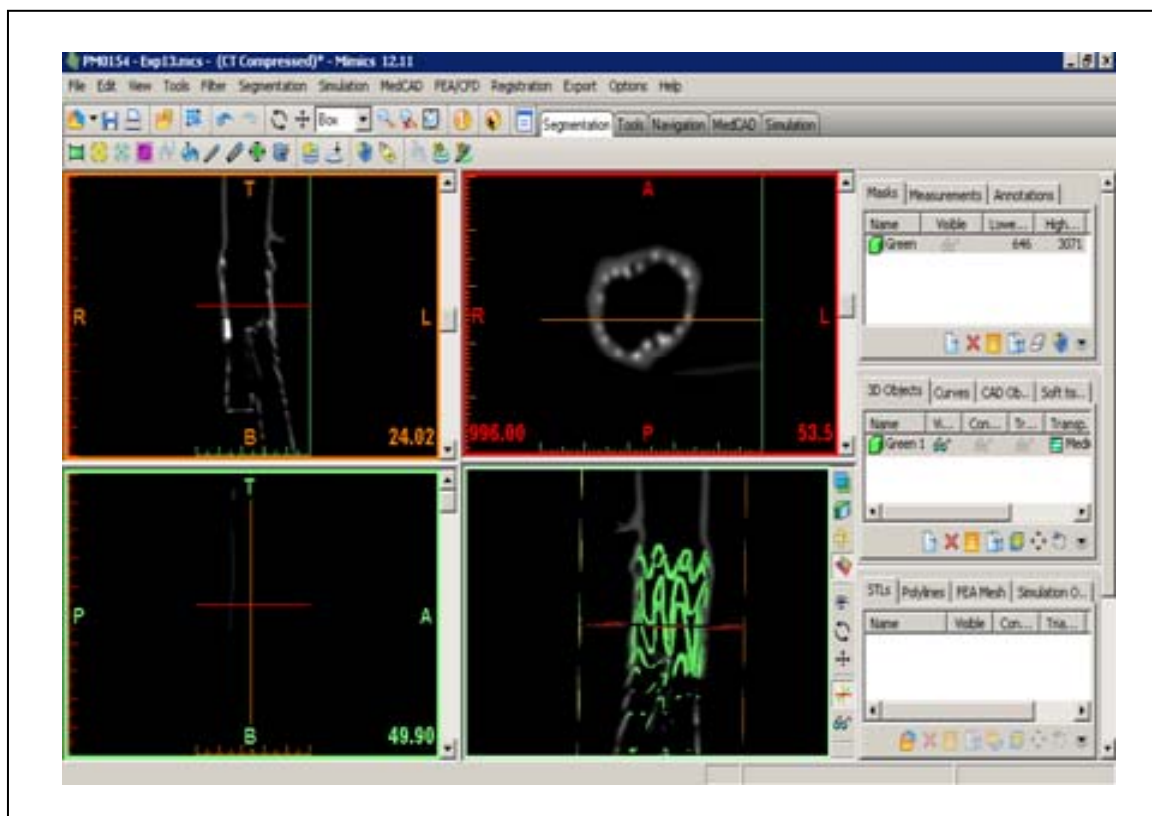
Figure 8: Syngo CT scanner software visualization of stent graft. Syngo allows for rotation and oblique slicing of EVG for better evaluation (left). Mimics software allowing for volume rendering and visualization of image slices (right).

(A)

(B)
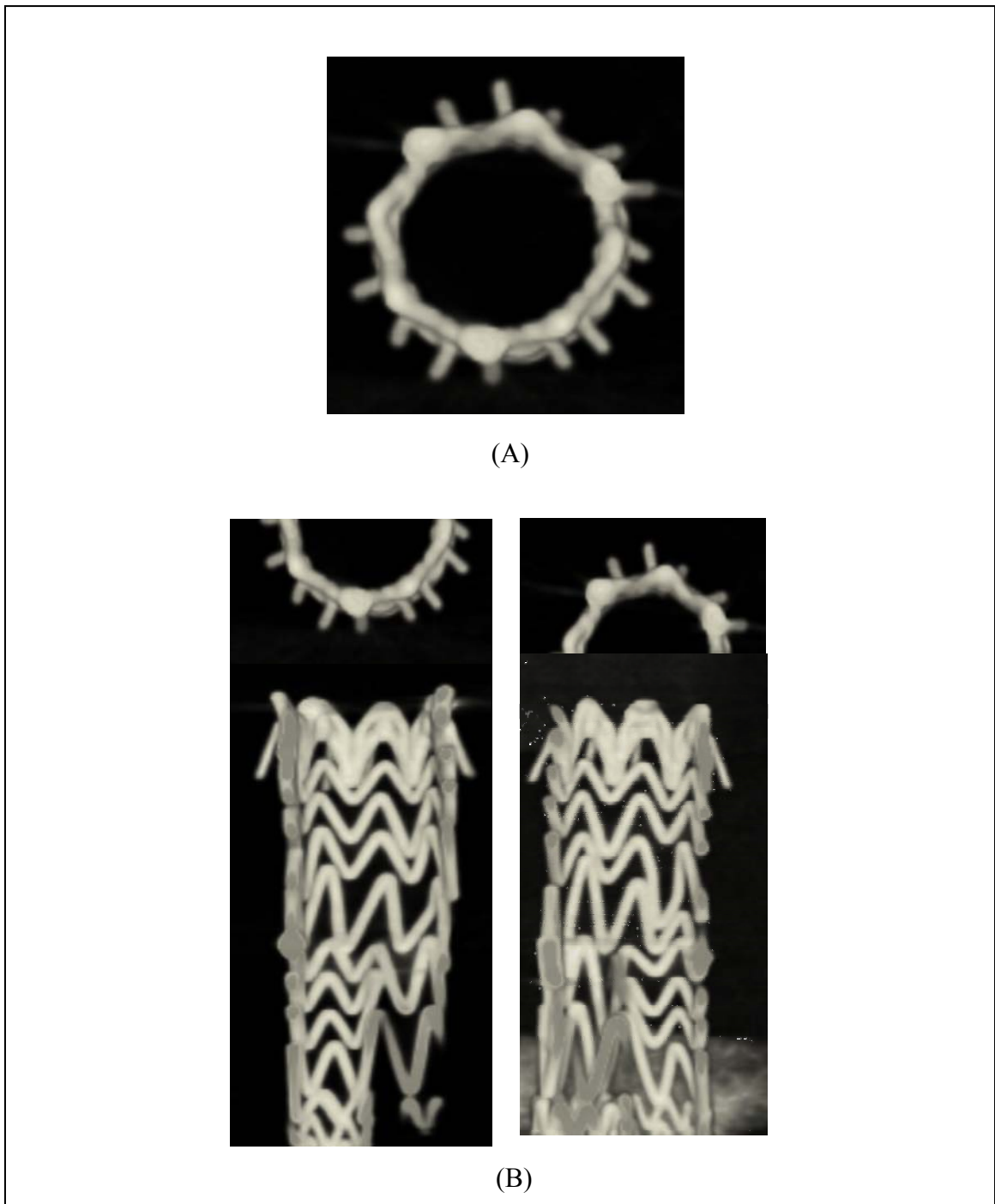
Figure 9: CT scans of endografts deployed in air to use as control. (A) Cross sectional view of 26mm diameter EVG (B) Front half of EVG after coronal slice. (C) Back half of EVG after coronal slice.
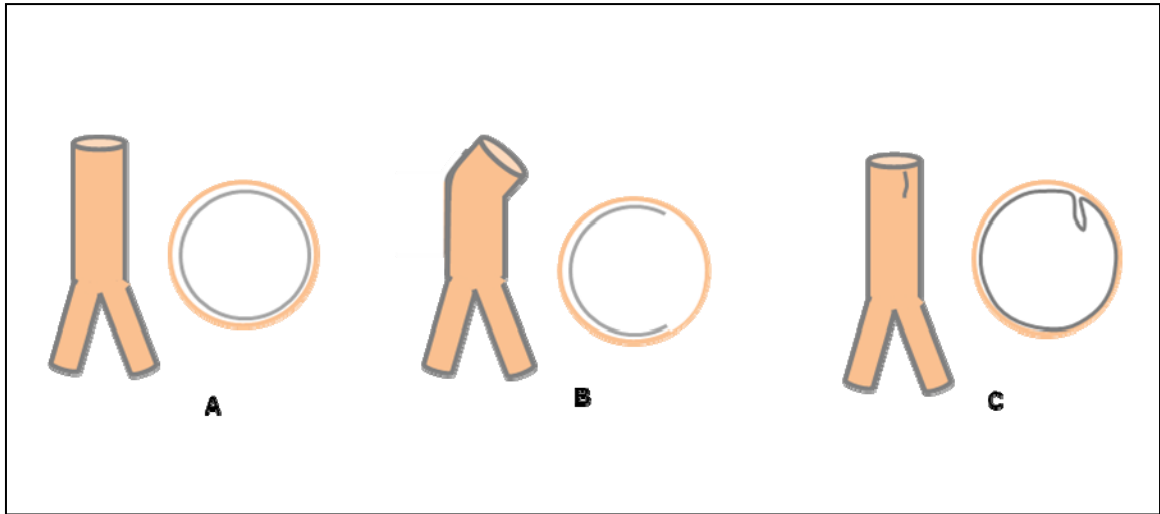
Figure 10: Schematic of folding phenomenon.(A) No folding, (B) Longitudinal folding, (C) Circumferential folding.

Table 2: Fold ranking criteria.

Fold Rank	Criteria
0	No evidence of folding in stent.
1	Minimal folding. Slight overlap of neighboring stents. General circular shape of stent still retained. Slight bend in length of device.
2	Moderate folding. More noticeable overlap of neighboring stents. Circular stent configuration has been compromised in certain areas and is now irregular in shape. More noticeable bend in length of device.
3	Severe folding. Stent configuration is completely deformed. Severe stent overlap of neighboring stents. Extreme protrusion into lumen or against aortic wall of stent. Severe bend in length of device.

Table 3: Experimental parameters investigated by Kratzberg et al on the effect of oversizing and barb characteristics on device fixations strength.

Parameter Perturbed	Range	Sample Size	Other Characteristics
Oversizing (OS)	5-45%	20	BL=5mm, BA=20°
Barb Length (BL)	0-7mm	11	OS=10-20%, BA=20°
Barb Angle (BA)	10-90°	9	OS=10-20%, BL=2mm
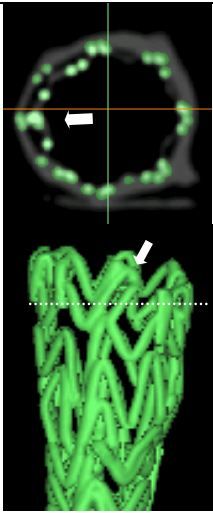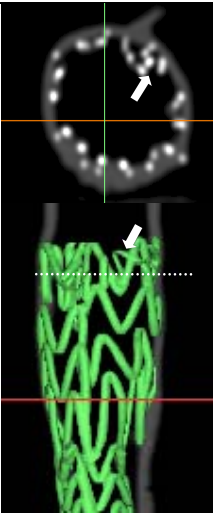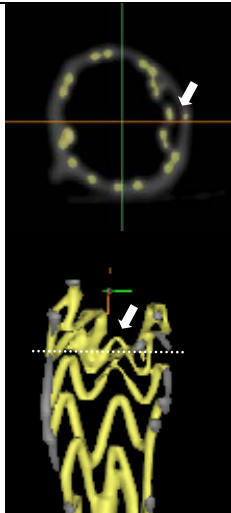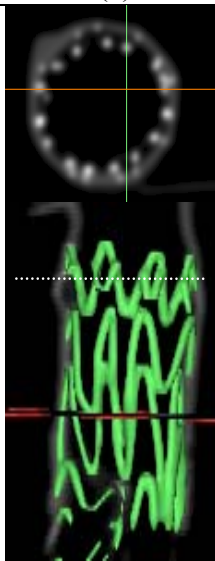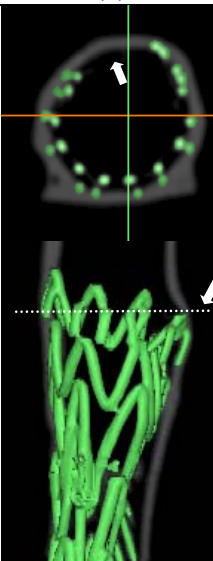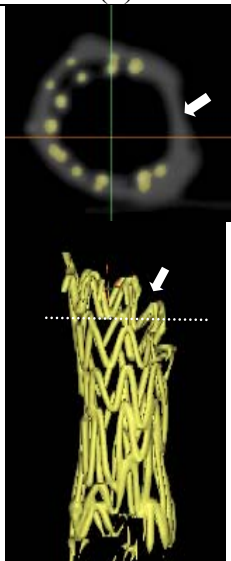
Folding	None [0]	Mild [1]	Moderate [2]	Severe [3]
Circumferential	12% oversizing (a)	11%oversizing (b)	43% oversizing (c)	13% oversizing (d)
Longitudinal	12% oversizing (e)	N/A	34% oversizing (f)	13% oversizing (g)

Figure 11: Representative examples of fold rankings given to each EVG with observed folding. There were no cases of mild longitudinal folding. Dotted lines indicate location of cross sectional slice. Arrows indicate regions of folding.
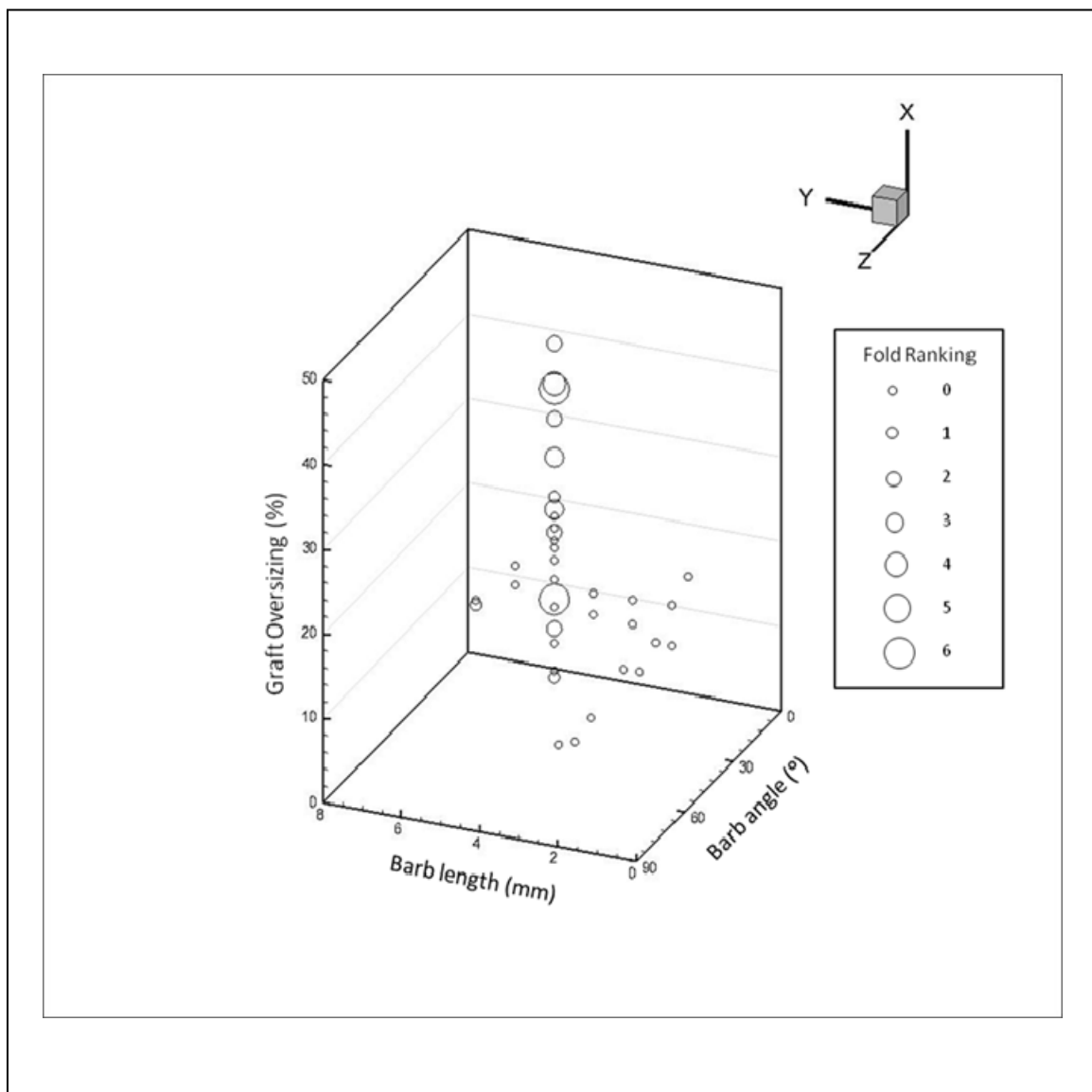
Figure 12: Effect of graft oversizing, barb length, and barb angle on folding ranking.
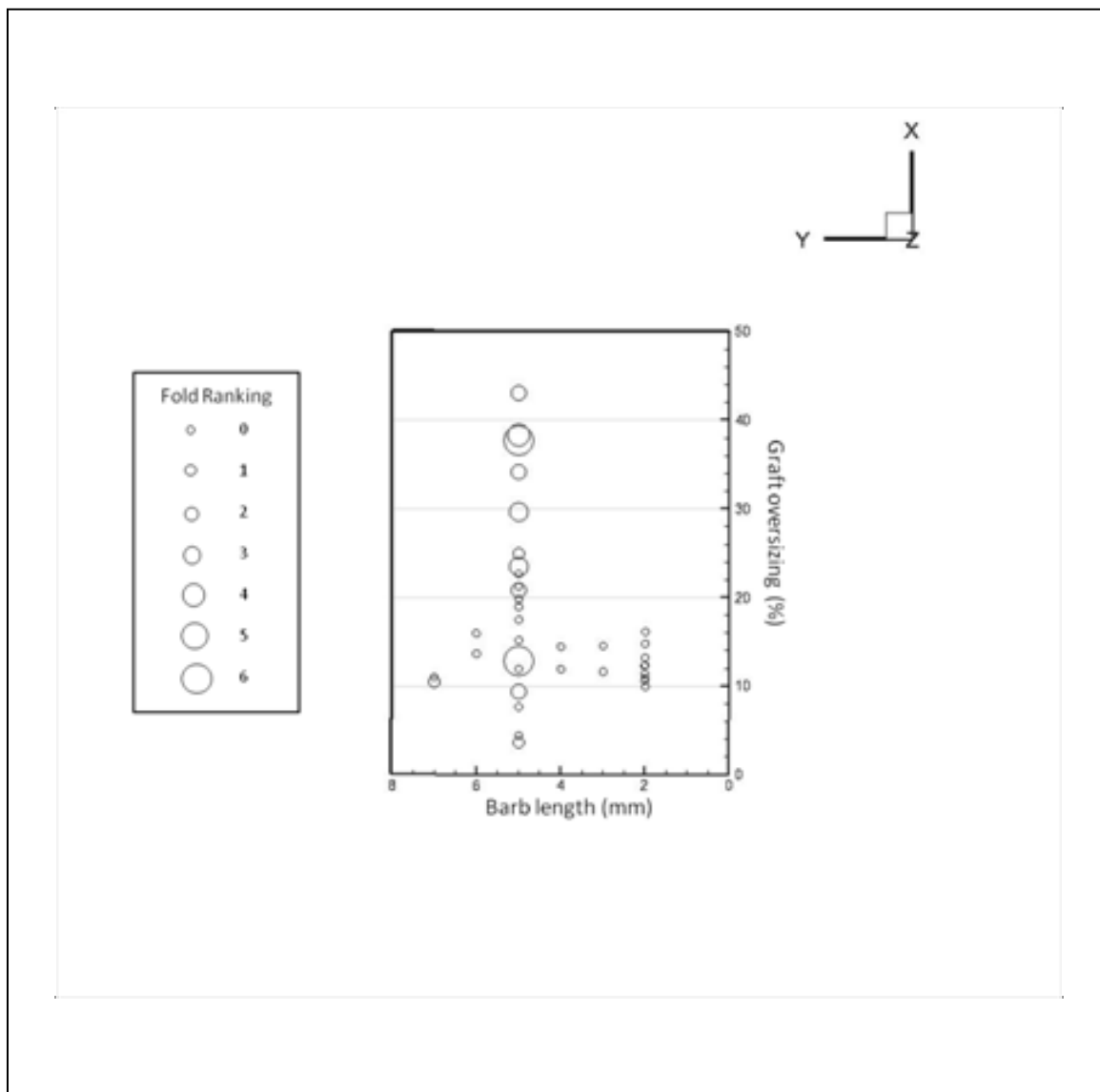
Figure 13: Effect of barb length and graft oversizing on fold ranking. Perturbations for the barb length parameter were conducted in the 11-20% oversize range with a barb angle of 20°.
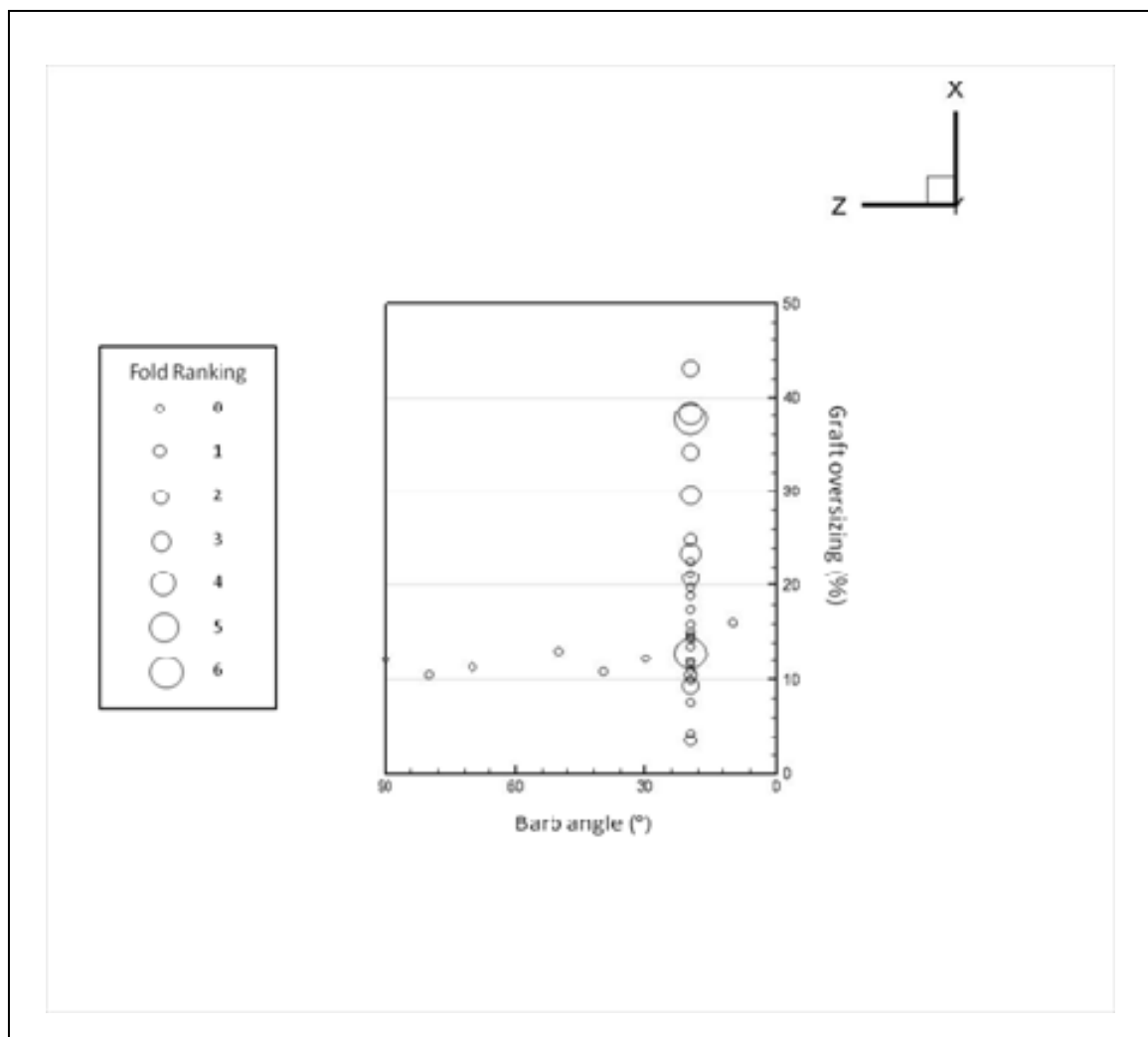
Figure 14: Effect of barb angle and graft oversizing on fold ranking. Perturbations for the barb angle parameter were conducted in the 11-20% oversize range with a barb length of 2mm.
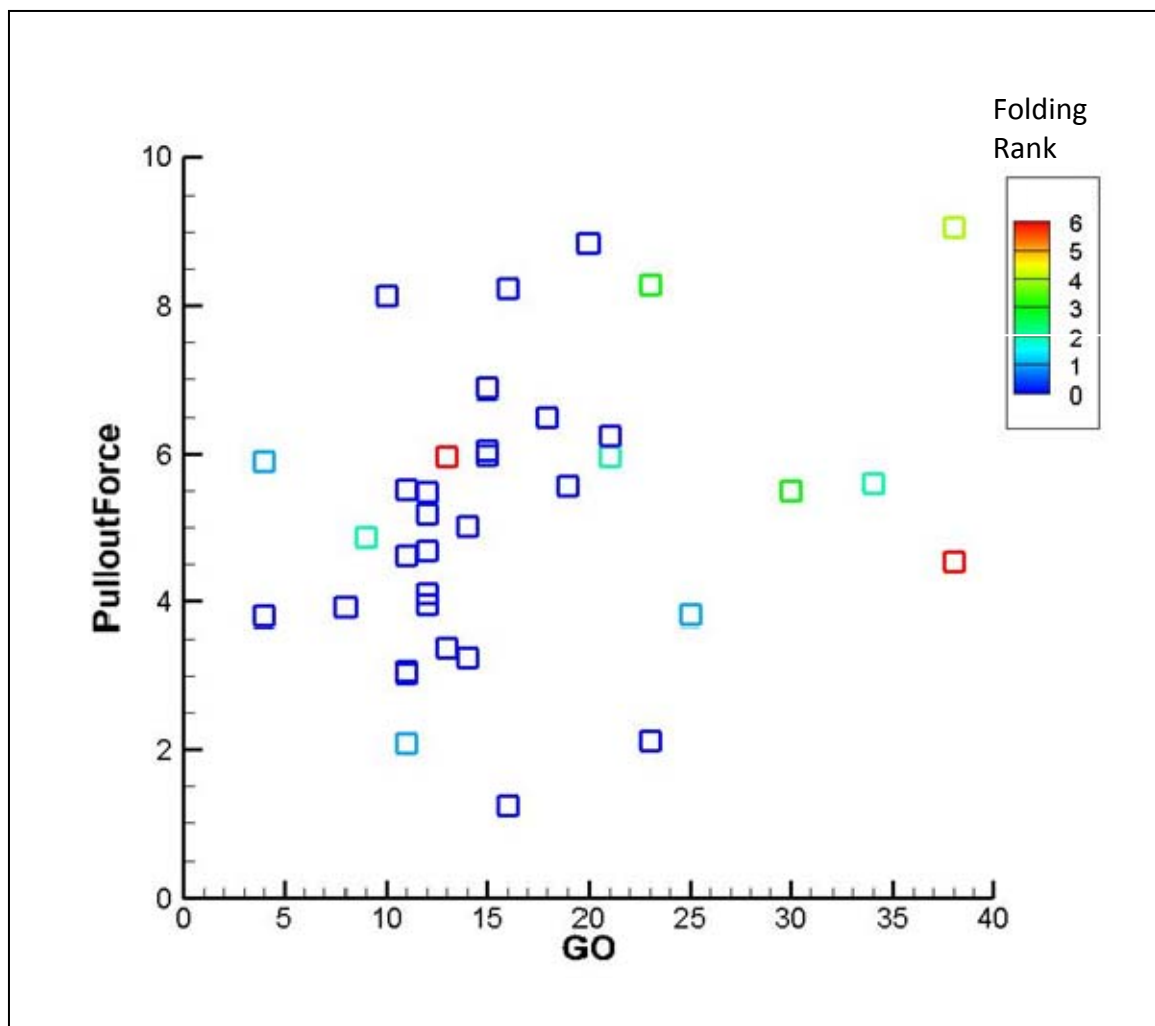
Figure 15: Impact of folding on pull out force as oversizing is increased.

CHAPTER 3: SPECIFIC AIMS

Results from the preliminary studies described in the previous chapter provided a foundation for understanding the implications of endograft folding. Although folding has been observed clinically and in experimental models, factors that cause this phenomenon are poorly understood. Reports from literature suggest a relationship between oversizing, folding, and migration but this relationship has not been carefully investigated. This dissertation project aims to assess some factors that increase endograft folding risk and its impact on device fixation strength.

Plausible risk factors for folding are barbs, stent geometry, oversizing, and patient anatomy (neck angulation). Poor penetration of the barb may push against the aortic tissue and cause the attached stent section to protrude into the lumen and fold. The barb can also become trapped between the device and aortic wall if the barb is too long or has a low barb angle. This may cause the stent strut attached to the barb to protrude and fold into the lumen (Figure 16a). Stent geometry can impact folding my affecting radial rigidity. Radial rigidity can be varied by changing the angle between stent struts as well as the height of the stent struts. Uniformity of the stent design throughout the perimeter of the device also prevents localized areas of weakness that may be targeted for folding (Figure 16b). Excessive oversizing can cause folding as the host vessel is unable to strength to accommodate the significantly larger diameter of the device. Although experimental data indicates increased radial and frictional forces with higher oversizing, the device is no longer capable of evenly distributing the negative radial force exerted by the aorta. Neck angulation has also been reported to induce folding because of difficulties associated with ideal deployment. Stent struts that land in the bend of the neck region will invariable experience a lot of overlapping and folding in of adjacent apices. Highly

angled aortas also cause deformation of the stent graft throughout the length that may prevent a proper seal.

Although all four factors are plausible in effecting folding risk, only two of the factors will be investigated in this project: device oversizing and neck angulation. These factors were chosen because they have been cited as factors increasing folding risk. They are also variables that are encountered during every procedure. Patients will always have a certain level of neck angulation and will be required to choose an appropriate device and oversizing for the patient. Barbs and stent geometry however, is device specific and depends on physician preference.

<u>Hypotheses & Questions Driving this Project</u>

In a series of bench top experiments, folding risk was assessed by varying neck angulation and oversizing. Stent graft attachment strength was then investigated. *Bench top testing will be used to investigate the hypothesis that endograft folding negatively impacts attachment strengths of devices with higher oversizings. Neck angle and excessive oversizing are hypothesized to increase folding risk.* The following sub-hypothesis below provides a clear outline to facilitate in understanding the relationship between folding and fixation strength.

1. Folding will increase as neck angle and oversizing increases.
   This hypothesis seems obvious but whether this relationship is linear or non-linear remains unknown. Also, it is also unclear if there is an optimum oversizing and neck angle range that avoids folding.

2. An increase in oversizing will result in decreased fixation strength across all neck angles.

As oversizing and neck angle increases, folding is expected to increase. Is the drop in pull out force is more severe at specific neck angulations or oversizings?

3. Higher neck angles will result in higher average pull out forces across all oversizings.

   As neck angle increases, frictional forces will increase due to the bend that the endograft must passes through. Is level of folding or neck angle the dominating factor?

The following specific aims will test the hypothesis and questions outlined above:

Specific aim #1: Develop physiologically representative bench top flow model with a synthetic aorta-aneurysm model to serve as a deployment substrate.

The flow loop will have pulsatile flow and compliance chambers to accomplish physiological flow waveforms and pressures. A synthetic aorta-AAA model with biomechanical properties comparable to live aortic tissue must be developed to serve as the deployment site. The model must allow for clear visualization of stent-graft behavior post deployment.

Specific aim #2: Determine the impact of oversizing and neck angulation on folding.

The impact of 3 neck angles and 5 oversizes on folding risk will be experimentally tested by deployment into the synthetic aorta-AAA model. A "folding metric" will also be developed to objectively quantify folding Relationship between oversizing and neck angulation with respect to folding will be identified.

Specific aim #3: Determine the impact of folding caused by neck angulation and oversizing on post-deployment attachment strength.

After deployment in the flow loop, the devices will be removed placed on the uniaxial a tester for assessment of fixation strength. The maximum pull out force will be used as a

measure of device fixation strength. Relationships between folding due to folding or neck angulations will be identified.

      A flow chart of the dissertation project is shown in Figure 17.
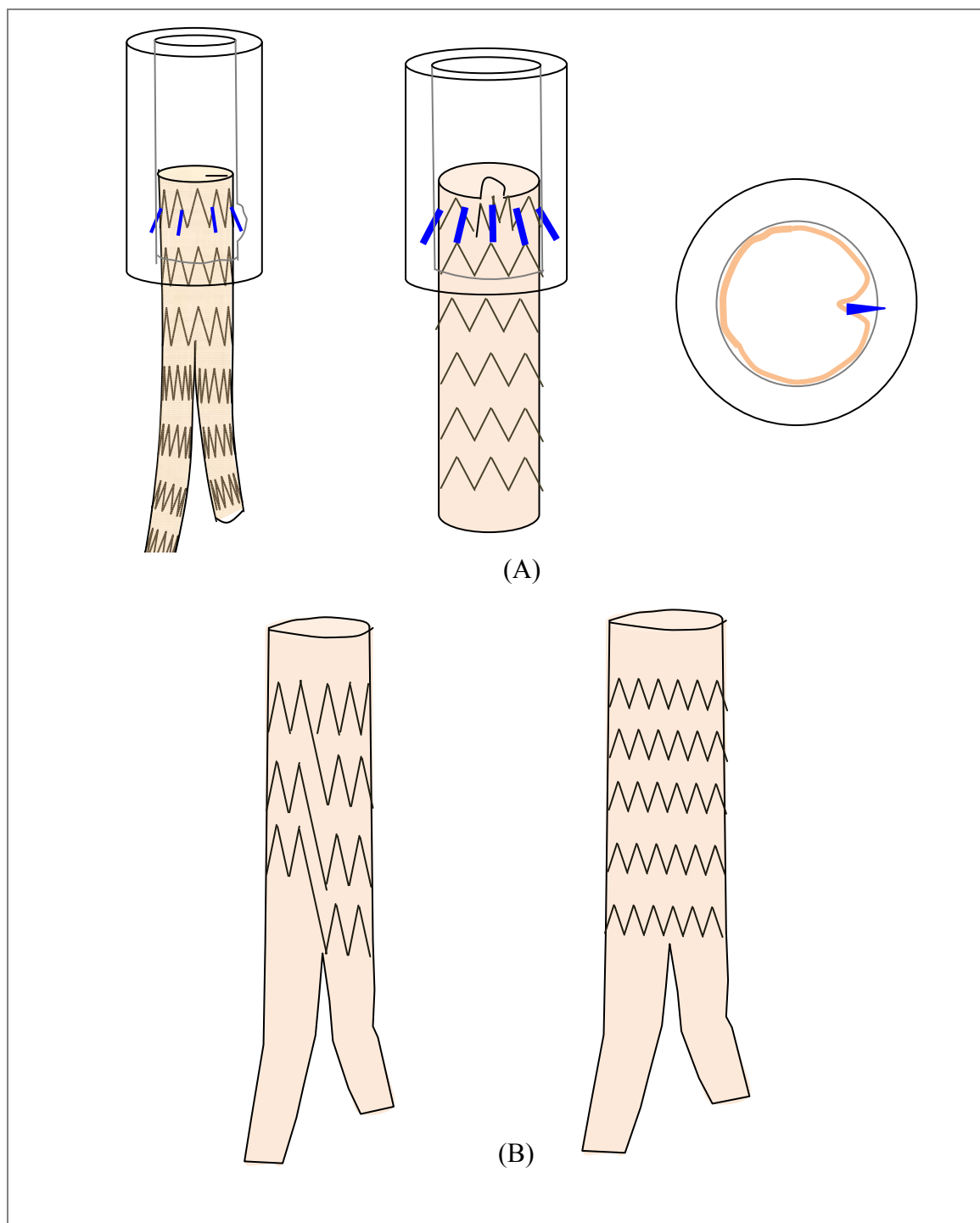
Figure 16: Schematic of potential folding risk factors. (A) Schematic of side, front and cross sectional view of folding caused by improper penetration of barb causing the stent graft to protrude into the lumen. (B) Schematic of non-uniform (left) and uniform (right) stent design that may impact folding risk.

Findings from Kratzberg et al. study on "Role of graft oversizing in the fixation strength of barbed endovascular grafts" J Vasc Surg 2009 reported that devices oversizing >30% had lower pull out forces. I hypothesized that folding causes a compromised seal resulting in the drop in pull out forces.

Preliminary work
Investigation of folding in barbed endografts using Kratzberg et al data

Study Plan: Specific Aims

Specific Aim 1:
Develop physiologically representative flow loop

Specific Aim 2:
Assess impact of neck angulation and device oversizing on endograft folding

Specific Aim 3:
Assess impact of endograft folding on device attachment strength

Investigate folding due to oversizing, barb length and barb angle using CT scans of devices deployed in bovine aortic tissue. CT scans investigated for folding instances were obtained from Kratzberg et al

- Oversizing: 4-43%, BL: 5mm, BA: 20°
- Barb length: 0-7 mm, Oversizing: 11-20%, BA: 20°
- Barb angle: 0-90°, Oversizing: 11-20%, BL: 2mm

Figure 17: Dissertation project flowchart. The genesis for this project stemmed from results reported by Kratzberg et al. Preliminary studies were performed to test hypotheses and the dissertation study plan was decided.

CHAPTER 4: BENCH TOP FLOW LOOP AND SYNTHETIC MODEL
DEVELOPMENT

<u>Flow Loop Design</u>

A mock circulatory flow loop was designed to provide a realistic environment for the endograft deployment. The flow loop consisted of a programmable pump, compliance chambers, pressure and flow sensors, resistance valves, and AAA flow phantom (Figure 18).

A representative flow waveform for the descending abdominal aorta [54] was programmed into the CardioFlow 5000 programmable pump (Shelley Medical, Toronto, Ontario, Canada). The cardiac output programmed into the pump ranged from -0.1 L/min to 18 L/min, the minimum and maximum flow rates throughout a cardiac cycle. The pump software allowed for extreme control of flow parameters such as cycle period, stroke volume, stroke rate, etc. The heart rate was set to 75 bpm with a time averaged flow rate of 3.5 L/min that is typically observed in the aorta. A silicone tube was placed in the system upstream from the deployment site to serve as a compliance chamber that creates enough back pressure for diastolic pressure of 80 mmHg. The compliance in the system was controlled by shortening the length or changing the thickness of the silicone tube. Resistance valves in the flow loop also allowed for additional control of the pressure and flow rates in the system. Finding the optimal setting of each control mechanism in the flow loop was a very difficult process. When one parameter was optimized, the others would be negatively affected. For example, the flow output from the pump matched the flow rates measured upstream of the deployment site when there was no compliance in the test system. Although the flow waveform was optimized, pressure ranged from 20 mm to 120 mm. When pressure was optimized by including the compliance in the test system, the flow waveform was dampened. The compliant

synthetic aorta-AAA model served as another "compliance chamber" because of the stretchy qualities of the silicone. Attempts were made to modify the output waveform so that the measured waveform would be physiologically representative. Unfortunately, this was unsuccessful as the pump has a maximum output of 18 L/min and compensation required for the dampened waveform once in the proper pressure range was outside of the pump's capabilities. After significant tweaking of several aspects in the system, it became apparent that reasonable compromise on flow waveform accuracy must be made to continue progress on the project. The flow loop and pump was not sophisticated or powerful enough to ensure accuracy of flow waveform and pressure simultaneously. The flow waveform was compromised because the correct pressure range would have greater influence on the endograft post deployment since it is directly involved in the slight expansion and collapse of the device under pulsatile motion. Despite the compromise, the flow loop had pulsatile flow with a dampened flow abdominal aortic flow waveform and a time averaged flow rate of 3.0-3.5 L/min (Figure 19). The general shape of the waveform was maintained but the magnitude of the physiologic flow waveform was not reflected in the measured waveform experienced by the flow loop. However, the systolic and diastolic periods of the flow waveform correspond. Similarly, the pressure waveform shape and systolic/diastolic periods match the physiologic target.

Temperature of the flow loop was maintained at 37.5 ℃ by a water bath that also served as the water reservoir. The water bath had a capacity of 2.5 L and an air tight lid that was manufactured in-house allowed for a closed-system flow loop if needed. Once sealed, the bath provided another method of compliance management for the flow loop by allowing air to be pumped into the system through the attached syringe.

<u>Synthetic AAA and Aorta Model Development</u>

An idealized synthetic aorta-AAA model was included in the mock flow loop to ensure that the deployments were performed in a representative surgical environment. Any difficulties in deployment should be as well mimicked as possible to reduce any bias in the results. The model had to be compliant and mimic compliance in the aorta and AAA as well as be optically clear so that the stent behavior could be easily visualized. Silicone was decided upon as the model material because it is inexpensive and easily manipulated to have the desired compliance properties. The lost wax technique was used to make the silicone molds. To begin this process, creation of an idealized AAA was required so that aluminum female molds could be made.

The idealized AAA was created using a Gaussian distribution curve adopted from Raghavan et al and Vorp et al [55, 56]. A population representative maximum diameter of 4.5 cm was used [57]. The equations used to develop the model were:

$$r(z) = (R-1)e^{-0.5\{\{z-h/2\}/\rho]^2} + 1 \qquad \text{Equation 2}$$

$$a(z) = \alpha e^{-0.5[\{z-h/2\}/\rho]^2} + 1 \qquad \text{Equation 3}$$

Where α is defined by

$$\alpha = \beta/1.4 * R \qquad \text{Equation 4}$$

Equation 2 describes the radius of each circular cross section at a given height along the length of the aneurysm. Equation 3 describes the radius offset of each cross section. The length of the aneurysm is designated by the variable h and the standard deviation of the Gaussian curve is ρ. The variable β represents the level of asymmetry of the anterior and posterior walls of the aneurysm while R represents the maximum radius.

The parameters used to design this AAA model were an R of 2.25, β of 0.4, and standard deviation of ρ of 2.5. Data points from this curve generation were imported into the NURBS based modeling software Rhino3D (Version 4.0, Seattle, WA). Circles were fit to the data points and connected together to form a surface. The centerline of the circle cross sections followed the Gaussian distribution curve defined previously. The iliac bifurcation was generated by creating two circles 30⁰ apart with a 1.2 cm diameter and then applying the loft command that joined the aneurysm body to the two iliac arteries.

A solid block was then place around the AAA surface and a Boolean subtraction operation was performed so that the solid block now has a void in the shape of the aneurysm. This block was then split using a plane that followed the centerline of the AAA. This block would serve as the mold for the wax core. A similar drawing was created by offsetting the aneurysm surfaces by x mm so that the finished silicone model would have a wall thickness of x mm to have a compliance of 2% [58]. The drawings were then exported to Mastercam CAD/CAM (CNC Software, Inc. Gig Harbor, WA) and milled onto aluminum blocks with a CNC machine (Figure 20).

The AAA silicone model was made using the lost wax technique. This technique uses a mold and core that is sacrificed at the end of the process so that the remaining project is a shell in the desired geometry with desired thickness. The smaller of the aluminum molds was filled with wax and then spun until the wax cooled. Spinning the mold created a thin wax shell to use as the core. This facilitated in the core removal process. Once the wax core has cooled, it was placed in the larger aluminum mold and the gap between the wax and the aluminum mold is filled with silicone (Figure 21). A clear, two-part platinum catalyzed addition cure silicone with high tensile strength and low shore A hardness (XP 565, Silicones Inc., High Point, North Carolina) was used to make the AAA model. The stretchy nature of the silicone was very forgiving towards rough handling during removal of the core. It was also more resilient when fitting the

aneurysm with the hemodynamic ports for the flow loop. Thickness of the silicone determined the compliance of the model; the thicker the silicone, the less compliant the model. Once the silicone cured, it was removed from the aluminum mold and the wax core was crushed into small pieces and dumped out of the silicone AAA model (Figure 22).

After the silicone AAA was made, it was placed back into the larger aluminum mold so that the silicone aorta could be joined to the AAA body. Appropriate adapters that allowed for aortic diameter and neck angle variation was attached to the top of the larger aluminum mold (Figure 23). Two acrylic pipes served as the mold for the silicone aorta. The pipe sizes were dependent on the thickness of silicone required to give a compliance of 5-6%. The outer diameter of the inner pipe served as the inner diameter of the finished silicone aorta. The inner diameter of the outer pipe served as the outer diameter of the finished silicone aorta. Once the proper acrylic pipes were placed into the adapters, silicone was poured into the gap between the pipes so that bonded and cured with the previously made AAA model (Figure 24). After the silicone cured, the acrylic pipes were removed, leaving a completed silicone aorta-AAA model (Figure 25).

<u>Development of Aorta-AAA Silicone Model with</u>
<u>Biomechanically Matching Properties</u>

Disclosure: A portion of this work was performed in collaboration with Ben Berkowitz, a MS candidate in the Biomechanics of Soft Tissues Lab (M.L. Raghavan, advisor), University of Iowa. This work was published in a conference proceeding: Kathleen Lin, Benjamin M. Berkowitz, Madhavan L Raghavan, "Penetration Mechanics of Endovascular Stent Graft Barbs in Aortic Tissue", Annual Meeting, Summer Bioengineering Conference, Farmington, Pennsylvania, 2011.

Compliance and barb penetration mechanics were two biomechanical properties that would further substantiate the use of silicone as an abdominal aortic substitute during experimentation. Compliance of the aorta (5-6%) and AAA (2-3%) was controlled by the wall thickness [56, 58]. Trial and error was used to determination the appropriate wall thicknesses to achieve appropriate compliance for the aorta and AAA model. Silicone tubes and AAA of various thicknesses were placed into the flow loop to measure compliance using a laser micrometer. The AAA and silicone tube started out at roughly 2 mm in thickness. If compliance was too high, a coat of silicone was added to increase the thickness. The new thickness was measured and placed in the flow loop for compliance testing. Fresh bovine aorta was also obtained from an abattoir and placed into the flow loop to measure compliance and use as a comparison. Figure 26 shows diameter change for bovine aortic tissue and two silicone aortas with difference wall thicknesses under pulsatile flow. A wall thickness of ~ 3.3 mm for the aorta and 4mm for the AAA was finally determined to be appropriate wall thickness for a compliance of 5-6% and 2-3%, respectively.

In additional to compliance matching, barb penetration properties were also evaluated and compared to that of bovine aorta. Fresh bovine aorta was procured from an abattoir, dissected, and cut open longitudinally. Three square pieces 4-5cm in length was removed to use as testing specimens. Three square silicone samples of similar size (XP 565, Silicones Inc., High Point, NC) were also cut and prepared for testing. The thickness of both types of testing specimen ranged between 1.5 to 1.9 mm. The specimens were then placed on a drum fixture that applied a radial strain of 30% to the test samples. This simulates the circumferential strain from in vivo pressure and longitudinal strain from tethering. Care was taken to ensure that the inner surface (intimae) of the aorta was facing the needle to simulate barb penetration during endovascular graft deployment. The fixture was placed in a vice clamp that allowed for angle adjustment between 90° (perpendicular

to plane of specimen) to 30° (almost parallel to plane of specimen) in 10° intervals. A protractor was used to ensure proper angling of the drum fixture during testing. The vice clamp with the drum fixture was then placed on the platform of the uniaxial extension tester (Lloyd Instruments, UK) for penetration force testing. A flat-tip pin 0.305 mm in diameter was attached to the moving crosshead of tester. A machine extension rate of 0.2 mm/sec was used to penetrate the specimen until the pin had exited its other side. All pin insertions were conducted within 60% of the total drum radius to avoid artifacts due to edge effects. Each entry angle was tested 3 times for each specimen. Pin displacement and force were recorded. The forces at the instant the pin first pierced through the specimen and at the instant it exited the specimen on the other end of its thickness were documented and compared. A distinct popping sound coupled with recoil of the tissue upon penetration provided clear visual and audio cues to correlate with force measurements recorded by the uniaxial extension tester (Figure 27).

Comparison of entry forces between the two types of samples show that the silicone material falls well within the penetration forces observed for bovine aortic tissue and is a suitable substitute for aortic tissue from a barb penetration standpoint as well (Figure 28).
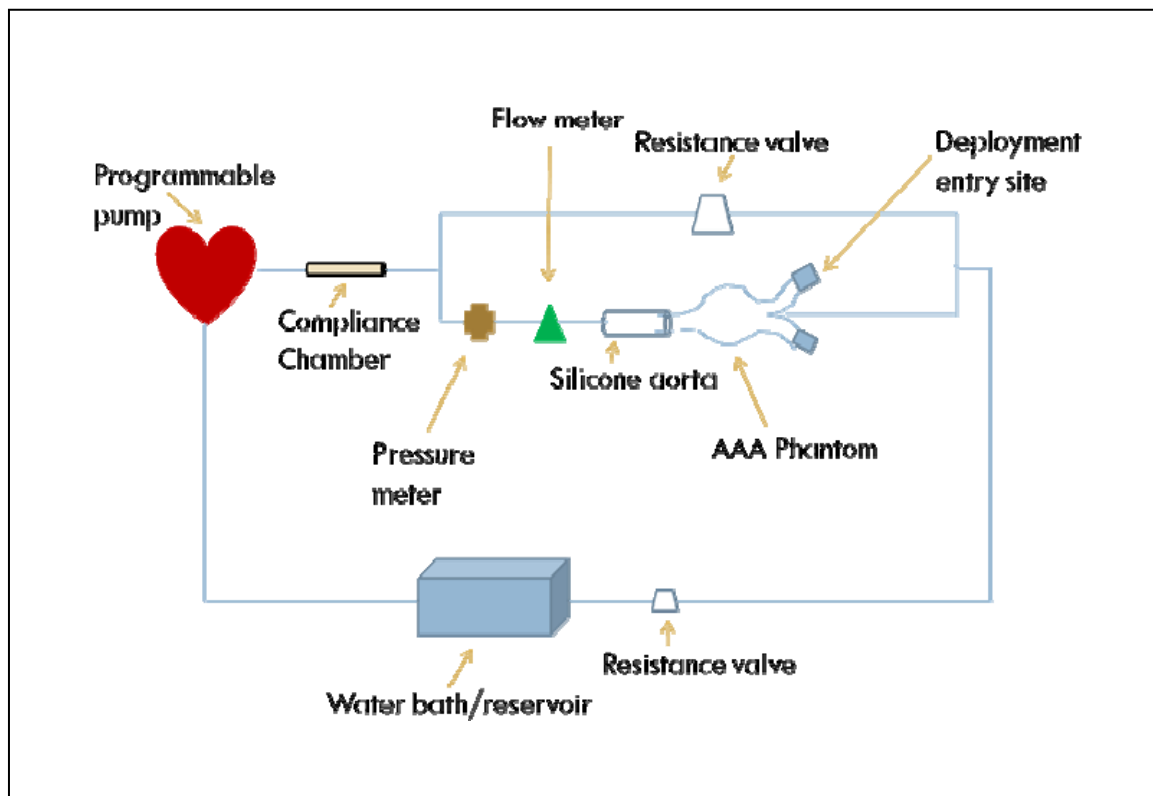
Figure 18: Schematic of bench-top flow loop system used during deployments. EVGs are deployed via the haemostatic valves at each iliac bifurcation that serves as an access sight. Haemostatic valves prevent leakage when delivery catheter is introduced and removed to the system.
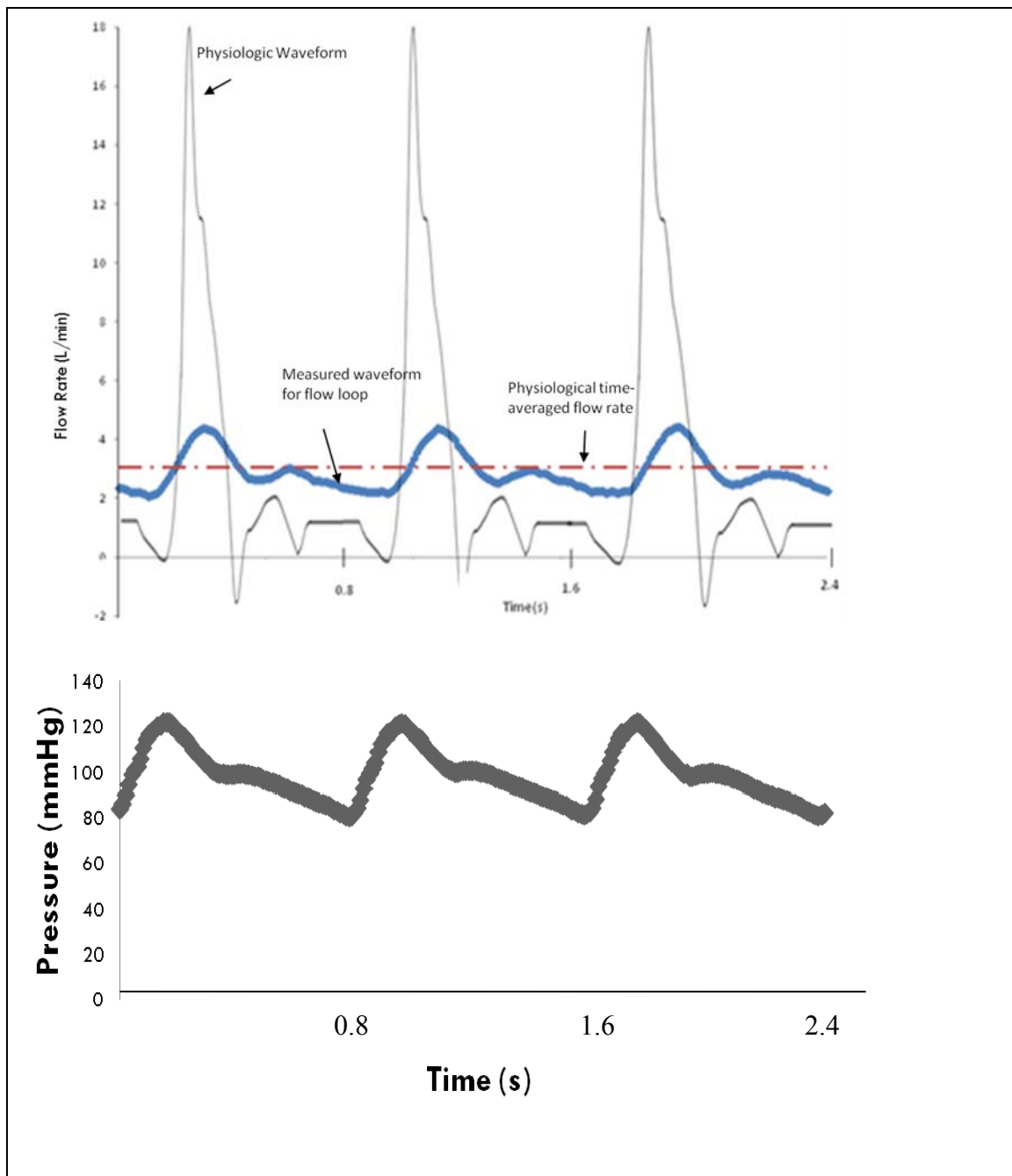
Figure 19: Representative flow and pressure waveforms measured in the bench top flow loop. (Top) Plot of physiologic flow waveform in the abdominal aorta [54] and flow waveform measured in the system. The general shape is more representative of the physiologic waveform. Time periods in the systole/diastole phases are also closer to target. (Bottom) Pressure waveform measured in the system that is physiologically representative.

Figure 20: AAA mold aluminum blocks milled using a CNC machine. Dowel pins are used to ensure the two halves of the aluminum block are perfectly aligned.

Figure 21: Placement of wax core into silicone mold milled from aluminum blocks. The gap between the wax core and aluminum mold will be filled with silicone. Thickness of the finished silicone model is the same as the gap between the wax and aluminum surface (4mm).

Figure 22: Finished transparent silicone AAA model with wall thickness of 4 mm.

Figure 23: Blue adapters are connected to aluminum mold to allow for creation of different neck angles while using the same AAA body.

Figure 24: Clear acrylic pipes used as the silicone aorta mold. Two different aorta sizes with 19 mm (wall thickness 3.3 mm) and 25.4 mm ID (wall thickness 3.9 mm).

Figure 25: Finished silicone aorta-AAA complex connected into the flow loop. The top picture shows a model with 0⁰ neck angle and bottoms shows 30⁰.
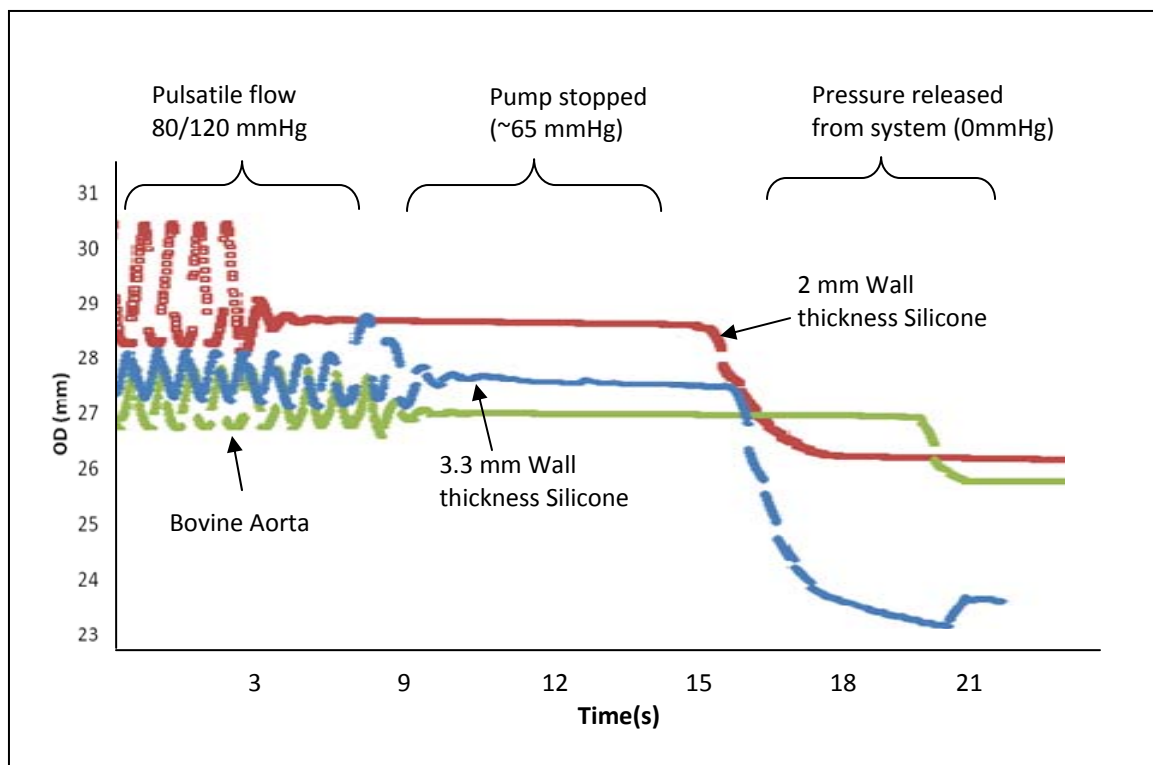
Figure 26: Compliance matching of silicone aorta to bovine aorta (desired compliance ~5-6%) in pulsatile flow loop. Comparison of outside diameter changes for silicone tubes and bovine aorta. Heart rate: 75 bpm, pressure 80/120 mmHg, time-averaged flow: 3.2 L/min.
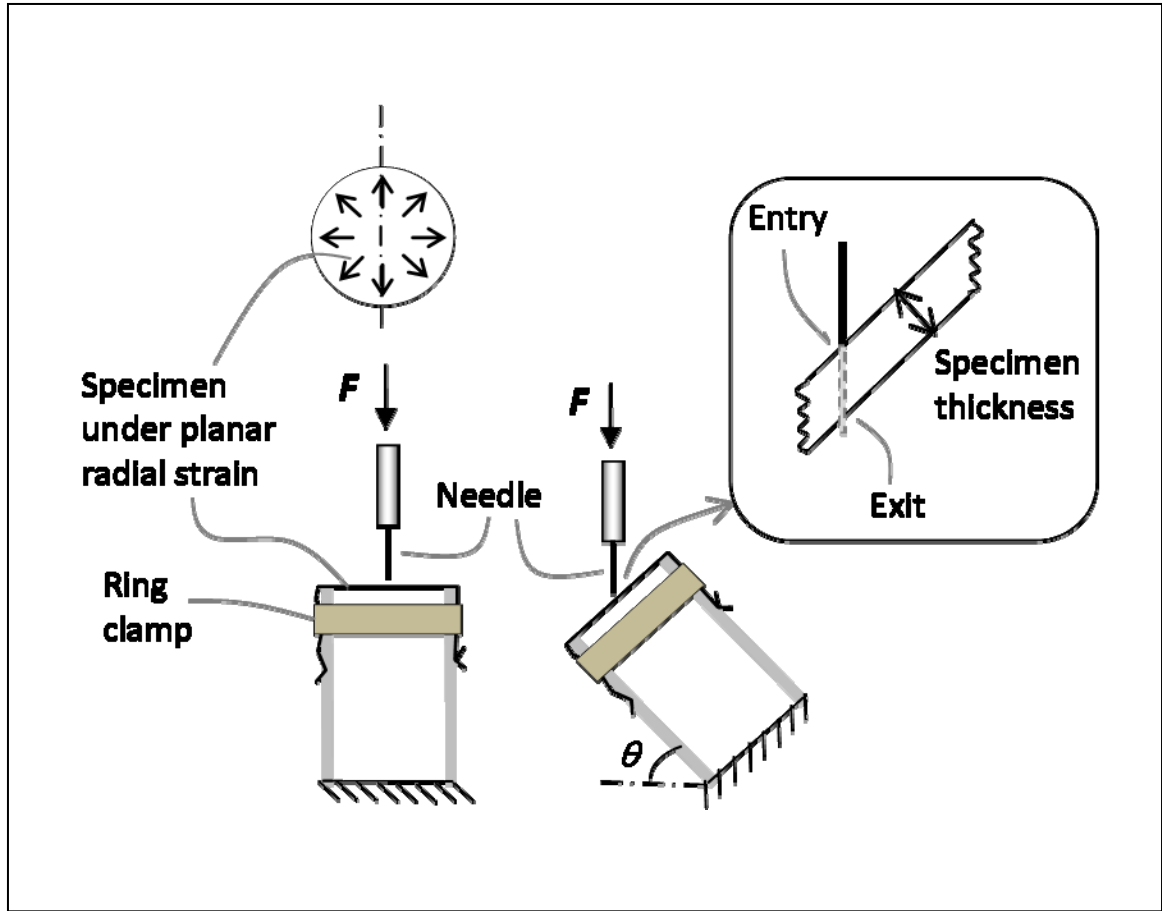
Figure 27: Schematic of entry force test setup on uniaxial extension machine. The specimen was angled between 0º-90º at 10º intervals.
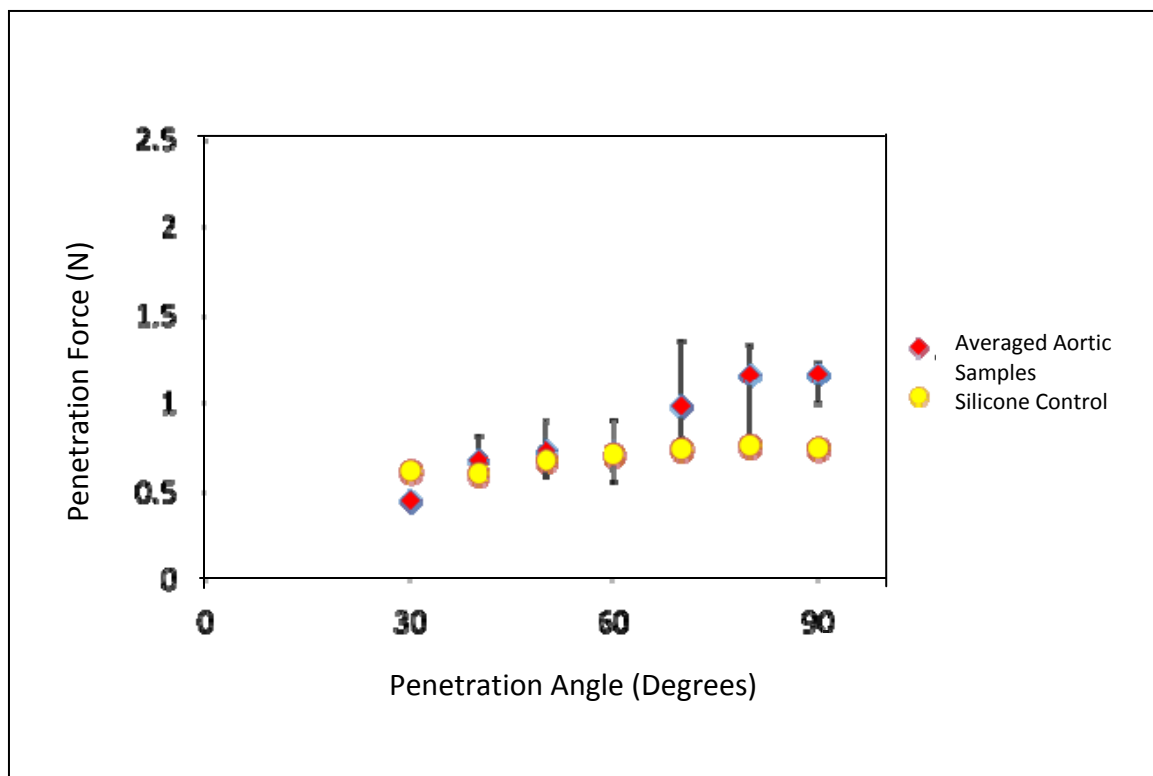
Figure 28: Entry forces measured for each penetration angle for averaged samples of bovine aortic tissue (N=3) and silicone analog.

CHAPTER 5: INVESTIGATION ON THE ROLE OF OVERSIZING

AND NECK ANGULATION ON FOLDING RISK

Test Matrix

To investigate the role of oversizing and neck angulation on folding, five oversizes and three neck angles were evaluated in this study. Three endovascular graft sizes of 23 mm, 26 mm, and 28.5 mm were deployed into two aortic sizes 20.7 mm and 29 mm pressurized diameter (19 mm and 25.4 mm at 0 mmHg) to give oversizings of -7%, 2%, 12%, 24%, and 38%. Neck angles of 0°, 30°, and 60° were evaluated at each oversizing for a total of 45 deployments (N=3 for each oversizing, Table 4) in this study. The testing parameters chosen were intended to be a comprehensive representation of aortic diameter, oversizing and neck angles encountered in the patient population. A large range within the test parameter also provides a more comprehensive understanding of the relationships between the test parameters.

The average abdominal aortic diameter is roughly 2 cm (range, 1.6-3.0 cm when pressurized). The two aortic diameters chosen in this study chosen largely due to the convenience in manufacturing the models and because they fall within the range of population aortic diameters, even though one of them is on the higher end of the spectrum (2.9 cm when pressurized) [59]. Furthermore, the limited endovascular graft sizes available to use required a larger aortic diameter to for testing at the lower oversize ranges. The silicone aorta sizes were also chosen to ensure that there would be an oversizing sample from the -10-0%, 1-10%, 11-20%, 21-30%, and >30% oversizing ranges. The proposed oversizing range of -10% to 40% was chosen to include a control range (-10-0% oversizing) with the representative range of oversizings used clinically [33]. Oversizing of in the -10-0% range allows for a clear comparison with a device that will have no folding. Neck angles of 0°, 30° and 60° were chosen for a comprehensive

investigation that included the best, average, and worst case scenarios in patient anatomy that were still within the permitted anatomical limits stipulated in the Gore Excluder instructions for use [60].

Experimental Method

Silicone Model Creation

A total of 45 silicone models were created in three sets in order of smallest to largest neck angle. For each neck angle subset, a total of nine 19 mm and six 25.4 mm aortic diameter silicone models were made. All experiments for a neck angle subset were completed before beginning testing on a different angle. Oversizing during deployments were randomized to minimize any bias to the data (deployment order, -7%, 38%, 2%, 2%, etc.).

Flow Loop Setup and Priming

A silicone aorta-AAA model was placed into the flow loop and clamped to ensure no water leakage. 0.9% saline solution was circulated through the system until all air bubbles were eradicated. Once the system was properly primed, it was adjusted to give pressures of ~ 80/120 mmHg with a time averaged flow rate of 3.0-3.5 L/min. The flow loop circulated while the rest of the experimental set up process was completed. This practice also ensured that the circulating fluid was at 37.5 °C. This temperature was critical to ensure the Gore Excluder nitinol stents expand to its intended diameter.

Loading of the EVG into the Delivery Catheter

While the flow loop was warming up, an endovascular graft was collapsed into a funnel. The funnel facilitates in loading the 24 Fr delivery catheter by collapsing the device into a diameter smaller than the ID of the catheter. Four apices are each threaded (alternative apices) with string 1 m in length. The strings from each connection point

were knotted together, enabling a more even distribution of the load induced when pulling the device through the funnel. Once the EVG was collapsed through the funnel and flush with the narrow tip of the funnel, the excess string was pushed through the delivery catheter. The funnel tip should be in contact with one end of the catheter. Holding the funnel and catheter in line, the string was pulled so that the funnel collapsed the entire EVG is as it passed through and into the delivery catheter (Figure 29).

Surgical Deployment

The delivery catheter was introduced to the flow loop via the surgical access sites connected to the silicone model through one of the bifurcated legs. The haemostatic valves allowed for easy entry and exit into the flow system while maintaining blood flow and pressures during insertion and removal of the catheter from the system. Deployment was performed under pulsatile flow with a consistent landing site is roughly 2-2.25 cm above the neck of the aneurysm. Care was taken to ensure that the length of contact between the silicone aorta and EVG were consistent through all 45 deployments. This was important to insure that there wasn't an artificial increase in pull out forces due to a longer proximal seal. In cases where there was negative oversizing, deployment of the iliac leg secured the device at the initial deployment site rather than floating downstream. A video of the deployment process was also recorded.

After successful deployment, the system was allowed to reach equilibrium (~2-5 min) with the deployed EVG in place. During this time, a Canon EOS 40D high speed camera was used to take aerial photos of two adjacent stent peaks. Once a pair of stent apices was photographed, the entire silicone aorta-AAA model was rotated as a unit to capture the stent apex behavior of the next two stents. This process was repeated eight times per device so that a photo of every apex and its adjacent apices was obtained. A scale was also included in the photograph to use during data analysis. An aerial view of

the stent behavior is important so that curvature of the device during measurement is negligible. After confirmation that all eight apices have been photographed, the pump is stopped and the silicone model is removed for pull out testing.

<u>Oversizing and Neck Angulation Data Analysis</u>

Visual identification of folding is a simple task but it is not a reliable method to differentiate between severity of folding between devices. Assigning a quantitative description for folding provides a better idea of folding level. As such, an objective folding metric was also developed to quantify the level of folding for an endograft.

Folding Metric Development

As previously mentioned, a certain level of folding is inherent and unavoidable when the device is oversized. It was important that the folding metric distinguished between uniform folding and localized regions of folding. Numerous methods to quantitatively characterize folding levels were explored before the method of using variance of the peak to peak distances was proposed as the folding metric (Figure 30).

Variance in the peak to peak distances throughout the circumference of the device would accurately capture any outliers, or localized regions where the apices are exceptionally close or overlapping. In an ideally deployed endograft, the distance between each stent strut would be relatively uniform and the variance of all peak to peak distances throughout the device would be very low. This would be visually confirmed by a relatively straight line when plotting variances of peak to peak distances. A large variance value would clearly indicate non-uniformity in the distribution of the stent apices and would result in a variance plot with an obvious outlier.

The peak to peak measurements were made using ImageJ, an open source, public domain image processing software. The ruler in the photographs served as a scale for measurement. The distance between the centers of two adjacent stent apices was

measured for the top three stent layers to ensure that we fully capture folding in the device in case folding occurred further along the length of the stent body. After all measurements were made, the distances were normalized with the EVG diameter; variances in the apex to apex distances were calculated for each stent layer and summed to represent the folding metric (Equation 5 & 6).

$$P = \frac{d_p}{d_{evg}}$$

Equation 5

$$F = \sum_{j=1}^{s} \sum_{i=1}^{n} \frac{(P_{i,j} - \bar{P})^2}{n}$$

Equation 6

Where n=8 for the number of peak to peak measurements and s=3 for the total number of stent layers. The variable d_p is the measured peak to peak distance and d_{evg} is the diameter of the endograft.

A visual confirmation of folding was also used to validate the folding metric. Another graduate student in the lab was asked to identify folding for all of the devices deployed at 0° neck angle by stating if folding was: present, possibly present, and not present. Results from this study supported the calculated folding metric trends.

User Sensitivity Study

Since all measurements used to calculate the folding metric was based on measurements obtained from images, concerns of user bias prompted a side study to test user sensitivity of the measurement method. Twelve experiments in the 0° neck angle subset were given to another graduate student in the lab to for folding metric calculations. The values were normalized to the EVG diameter and folding metric was calculated for the twelve studies. A comparison of folding metrics calculated by User 1 and User 2 can be seen in Figure 31. As seen from the cluster of data points near the diagonal line, User

1 and 2 agree very well, indicating the measurement method was not user sensitive. On average, User 2 only had a 1.4% higher estimation of the folding metric. Pearson's correlation coefficient and Spearman's rank was also calculated to be 0.98 and 0.925, respectively. The plot along with the Pearson's coefficient and Spearman's rank suggest that the methodology for obtaining the folding metric is valid.

<u>Neck angulation and Oversizing Results</u>

Representative pictures of folding observed at three different oversizings (12%, 24%, and 38%) for each neck angle are shown in Figure 32. The images focus on the same location of each EVG deployed for easy comparison. At 12% oversizing for 0° and 30° neck angulation, the stent apices are close together but not overlapped. At 24% oversizing, adjacent stents are beginning to overlap and at 38% oversizing, this becomes more severe as you can clearly see stent graft material folded under itself. At 0° and 30°, folding also tends to occur in a specific area of the device where stent geometry is non-uniform. In this region, a stent strut drops down from one stent layer to the next allowing for the helical wrapping of the stent around the graft material . At a neck angle of 60°, folding is not observed at the same location regardless of oversizing.

Folding becomes more severe as oversizing and neck angulation increases, specifically at the outer radius of the bend (Figure 33). Figure 34 shows peak to peak stent behavior throughout the perimeter of the stent graft for a conservative oversizing of 12% at 0° neck angle. Notice that the stent apices are relatively uniformly distributed throughout the perimeter. In the 24% oversized case, notice that folding is concentrated in one region while the rest of the stent perimeter displays no folding or overlapping of stent struts (Figure 35).

Figure 36a shows the average folding metric for 0°, 30° and 60° neck angle at oversizings from -10% to 40%. shows the averaged folding metric for 0°, 30°

and 60⁰ neck angle at oversizings ranging from -10% to 40%. Folding metric increased as oversizing and neck angle increased. Variation in folding metric also increases as neck angle increased. Comparison of folding metric between 0⁰ versus 30⁰ and 0⁰ versus 60⁰ neck angle showed statistical significance (Mann-Whitney U test, $p < 0.05$). The relationship between folding, oversizing, and neck angle is non-linear. Folding metric increased at 0⁰ and 30⁰ neck angle for oversizing >12%. There is a distinct increase in folding metric from 0.0014 to 0.0039 (178%) at 0⁰ neck angle and from 0.0023 to 0.0099 (330%) at 30⁰ neck angle. At 60⁰, oversizing > 2% caused a significant increase in folding metric (Figure 36b).

Neck Angulation and Oversizing Discussion

Folding in endovascular repair for abdominal aortic aneurysms is a topic that is poorly understood but has been clinically observed. Wolf et al [37] reported incidences of folding, or eccentric compression, in patients treated with the AneuRx device. The patients that experienced folding also had migration and late type 1 endoleak. In the thoracic endovascular field, folding risk has been linked with neck angle and oversizing. This study aimed to elucidate the relationship between neck angulation and oversizing on folding risk through a set of controlled experiments.

It is expected that oversizing and neck angulation would induces folding of the endograft. However, whether this increase was of a linear nature was not clear. In this study, a significant increase in folding occurred at oversizing > 12% for 0⁰ and 30⁰ neck angles and at oversizing >2% for 60⁰ neck angle. The noticeable increase in folding metric at such a low oversizing for the 60⁰ scenario is likely due to the awkward deployment of the device. The stiffness of the delivery catheter prevents a conforming travel pathway around the neck angle bend. As such, the endograft is now deployed at an angle where the top end of the EVG contacts exactly at the aortic neck bend rather than

parallel with and along the centerline axis of the aorta. Recall from Figure 32 that the similar folding behavior observed at 0° and 30° neck angles for oversizing ≥ 24% was not observed at the same location in the 60° case. This occurrence can be attributed to the larger cross sectional area for the device to fully expand. However, the stent struts that are situated near the outer radius of the bend are forced together and overlap. At 30°, navigation through the angled anatomy was not as difficult so deployment was not as angled. Although there is a linear increase in neck angulation, the difficulties associated with accessing the targeted deployment site for optimal deployment increases exponentially.

When folding was observed, the folding nature of devices in this study differed from those observed in Kratzberg et al's study [34]. A cross sectional view of the deployed endograft in this study showed that although the stent graft would fold under itself, it did not protrude severely into lumen as observed in Kratzberg et al's results. This can be attributed to the absence of barbs on the endografts used for this study. Without the presence of barbs, the stent graft is more likely to lie flatter against host vessel rather than pushing against the aortic wall (Figure 38). The pushing force also affects the stent section attached to the barb, causing it to protrude into the lumen.

Another observation was that folding always occurred at the region of stent non-uniformity. In this region, one stent strut spans two stent layers Figure 37 to allow for the helical winding structure of the stent along the length of the graft. Folding always occurred and was most severe at this region in the 0° and 30° cases. This suggests that stent design may also be an important risk factor for folding. As previously mentioned, the aorta behaves like a rigid tube with very little expansion when pressurized in the physiological range. With increased oversizing, the aorta is less and less capable of accommodating the larger stent graft diameters. As such, the device must collapse down in some manner to fit within the host vessel. Basic mechanics dictates that failure in

radial rigidity will occur at the weakest point of the stent perimeter. Findings from this study suggest that these weaknesses are the localized points of stent non-uniformity. When a section of the stent is dissimilar in design, it becomes the weak point and is targeted to buckle when oversized aggressively. A stent design with uniform structure throughout the perimeter can maintain its radial rigidity as the forces applied by the aorta to collapse the endograft is evenly distributed among all stent struts since they are identical. Even with excessive oversize, uniform stent design would be more successful at collapsing in a uniform manner so that a localized fold is less likely to occur.

A crude experiment was performed on a stent graft with uniform stent design throughout the entire device. As the EVG was collapsed radially, the stent collapsed uniformly with no evidence of folding unlike the Excluder where folding occurred in the region where a stent strut spanned two stent layers. As previously mentioned, the portion of the stent that is different becomes targeted as a weak point in the perimeter is the first buckling point. To clarify, this is not to say that stent design must be identical for the entire device. For example, Medtronic's "M" stent alternates between large and small stent apices. Although the stent apex varies within each stent cell, folding risk isn't as high due to the uniform stent pattern. Experimentation on those devices would be required to truly determine the impact of stent design on folding risk and whether uniformity is a dominating factor.

As previously mentioned, the aorta behaves like a rigid tube with very little percent expansion when pressurized in the physiological range. With increased oversizing, the aorta will not accommodate the larger diameter of the stent graft so the device must collapse down in size to fit within the host vessel. Basic mechanics dictate that failure in radial rigidity will occur at the weakest point of the stent perimeter. Findings from this study suggest that localized points of apex non-uniformity are at higher risk for folding.

Neck Angulation and Oversizing Conclusion

High oversizing and neck angulation increases the folding risk. There is a non-linear relationship between neck angulation/oversizing with folding indicated by the significant increase in folding metric. For neck angles of 0º and 30º, this occurs at oversizings over 12% and at oversizings over 2% at a neck angle of 60º. Non-uniformity in stent design impacts folding risk.

Table 4: Parameters tested in the assessment of factors inducing folding and its impact on fixation strength.

Neck Angles	EVG Sizes (mm)	Aorta Diameter (mm) (Pressurized)	Oversizing Achieved
0˚, 30˚, 60˚	23, 26, 28.5	19 (~20.7)	-7%, 2%, 12%, 24%, 38%
		25.4 (~29)	
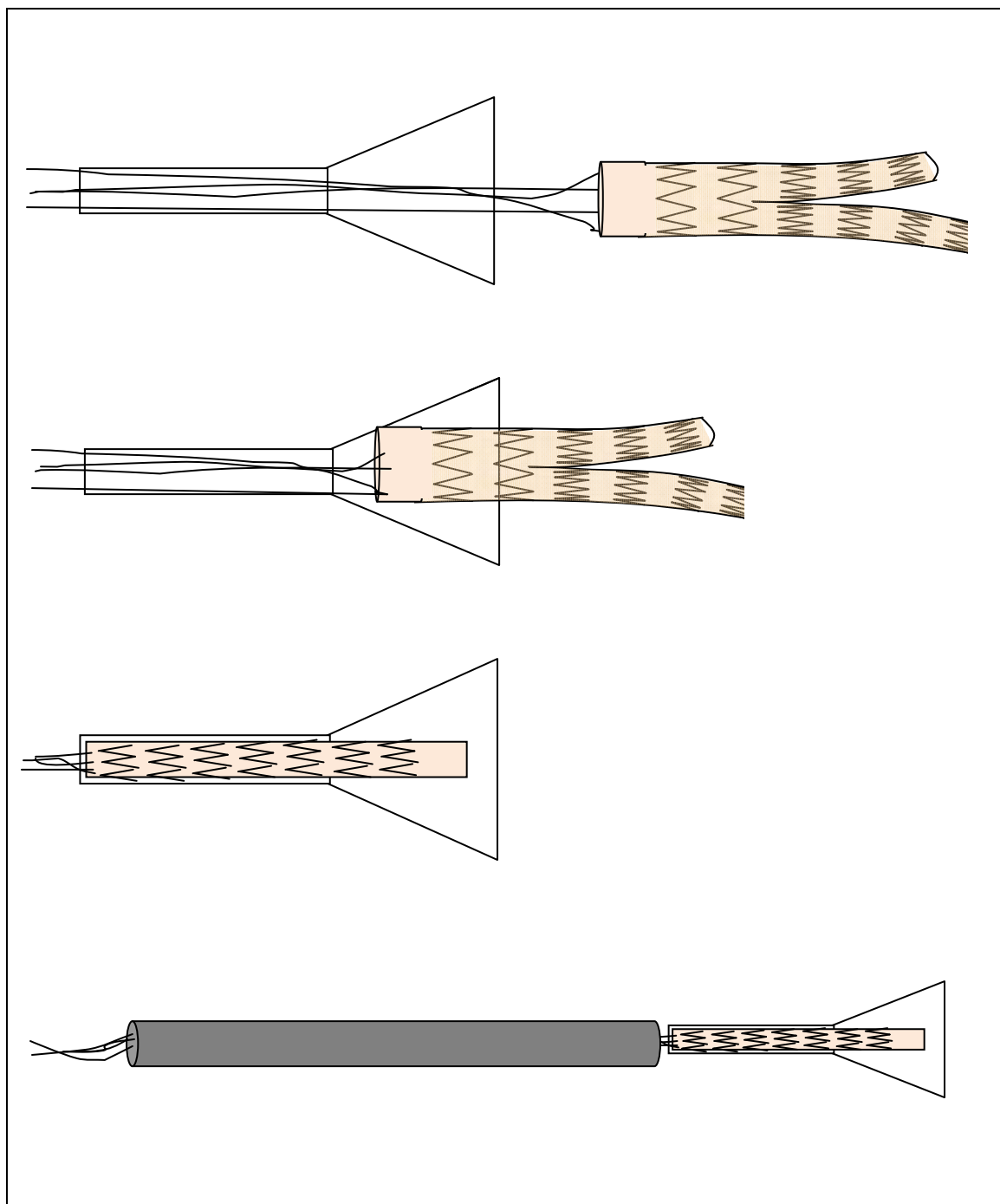
Figure 29: EVG collapse into the funnel for reloading into deployment catheter.
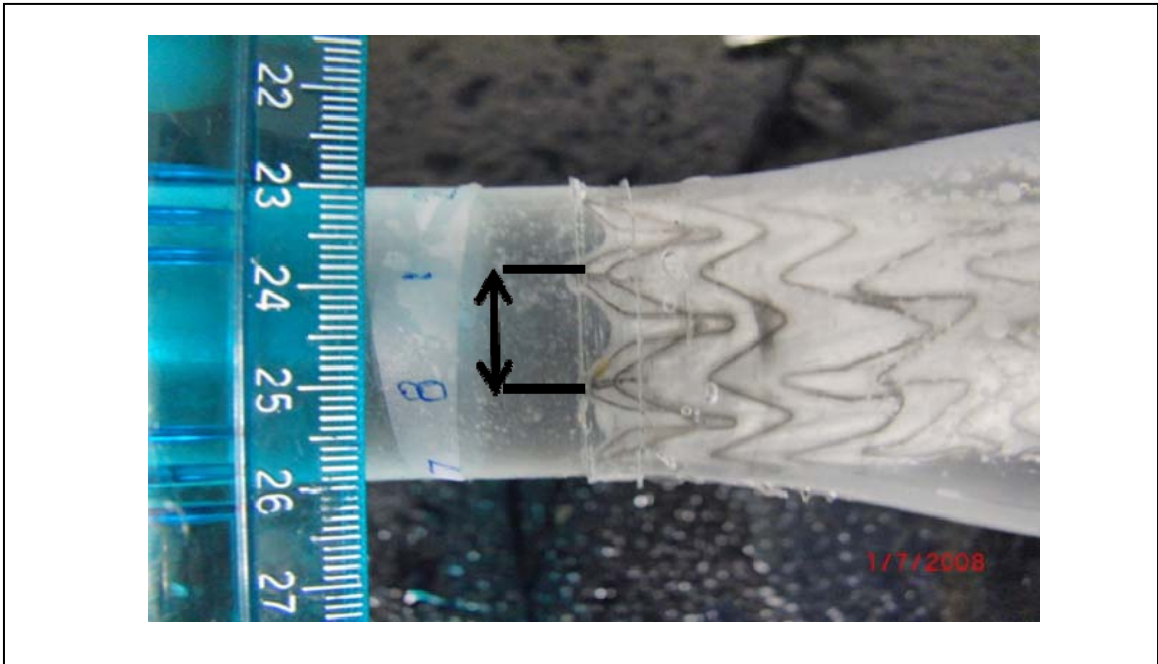
Figure 30: Apex to apex distance measurements for top three stent layers that was used for folding metric calculations.
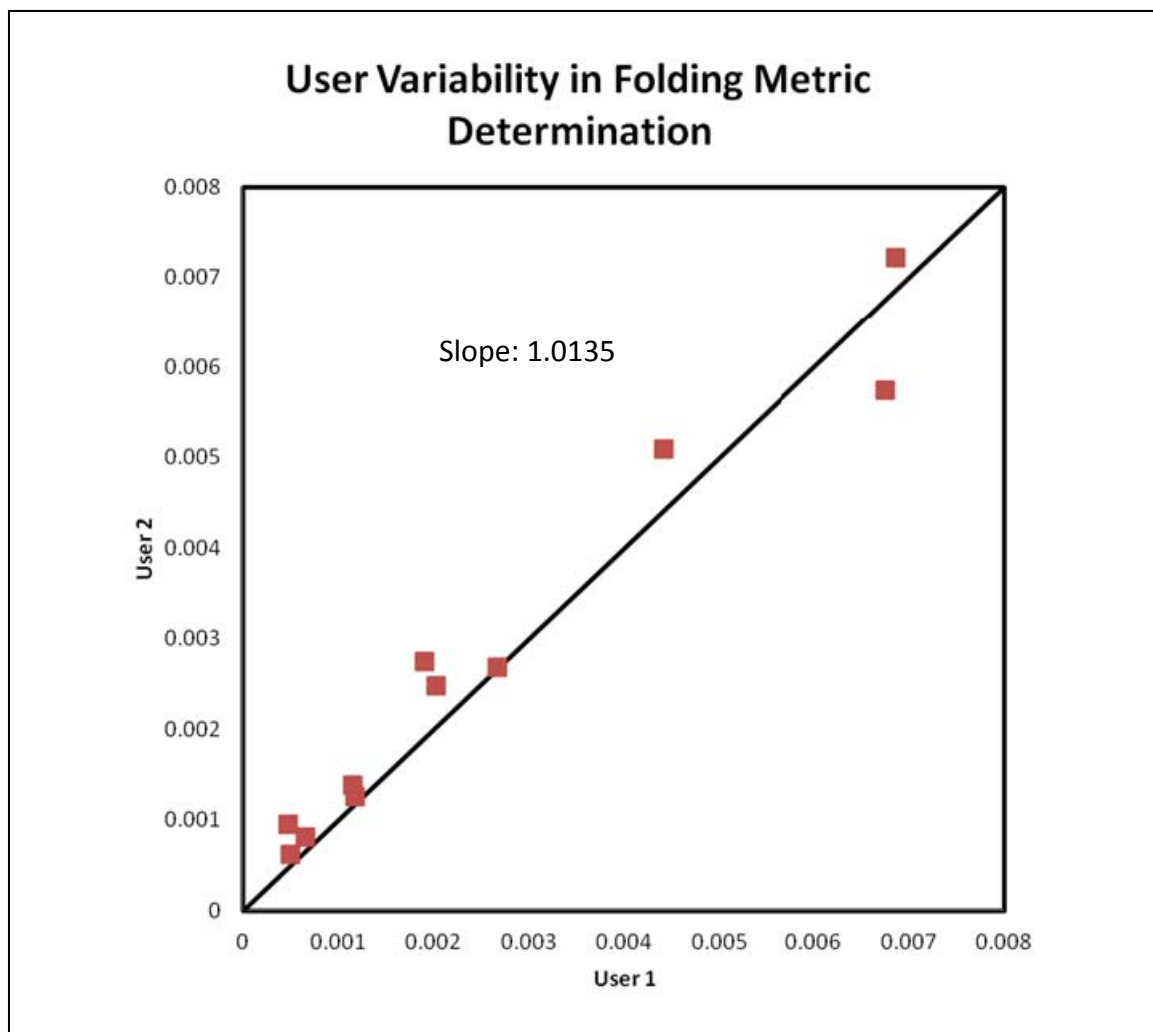
Figure 31: Comparison of folding metric values obtained between two users for user sensitivity study and validation of measurement method.
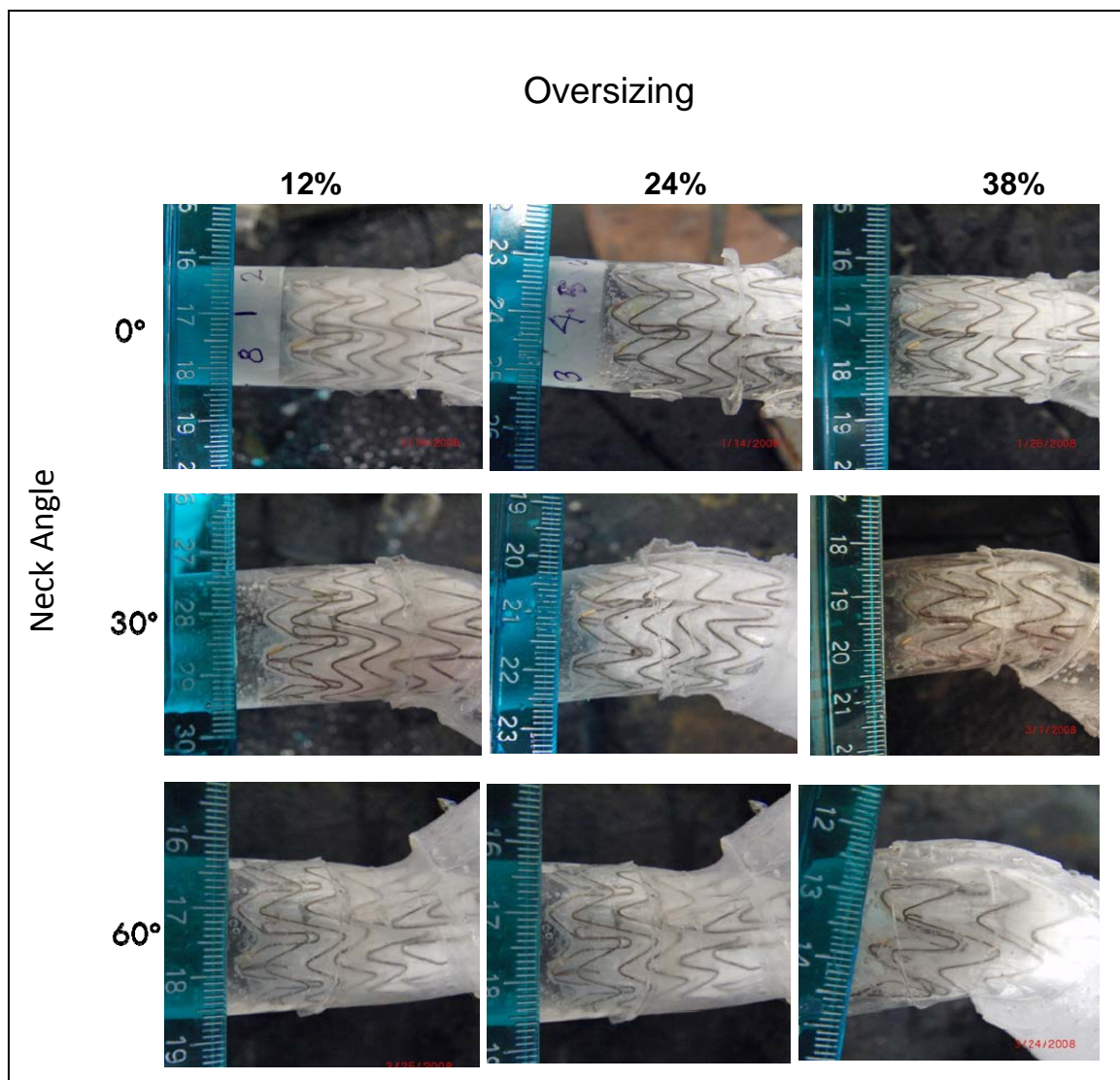
Figure 32: Representative images of deployed EVG at various oversizing and neck angles combinations. The images have the same location on each EVG stent in view for easy comparison.
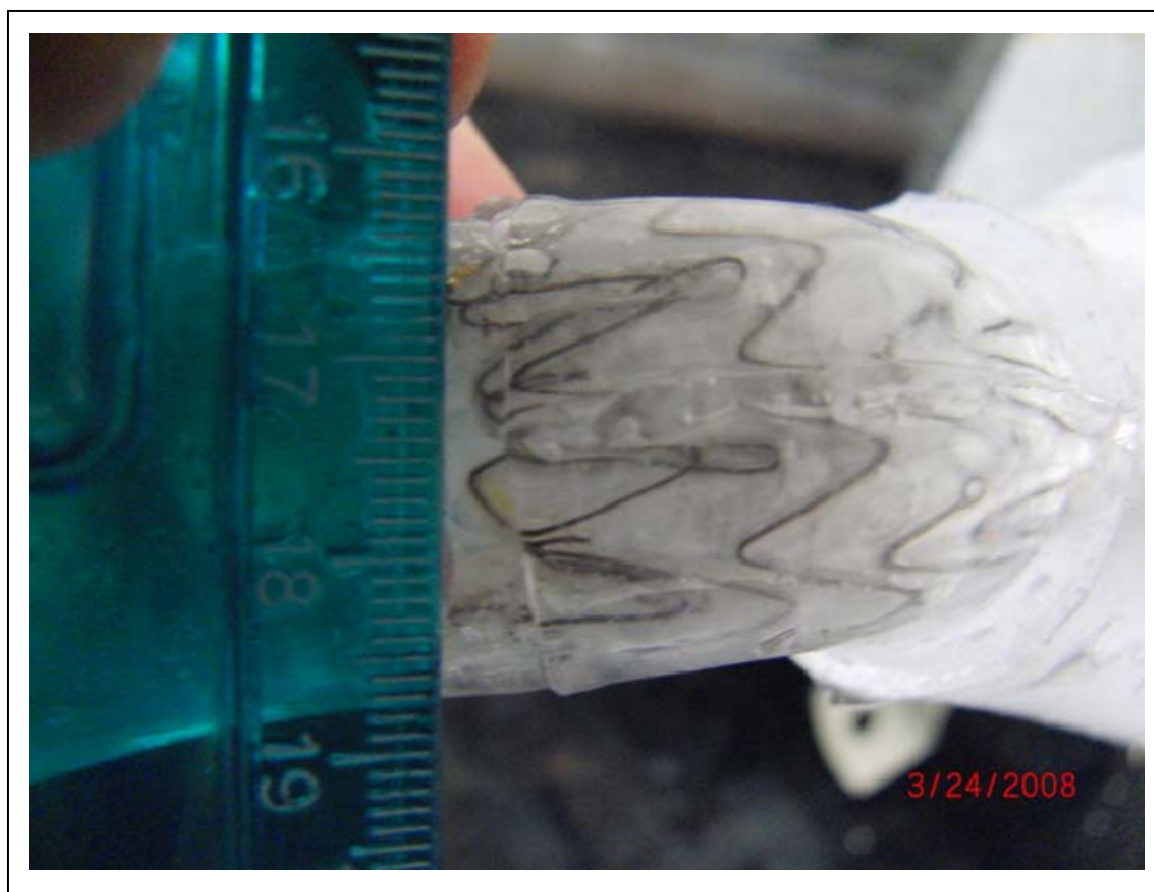
Figure 33: Folding and overlap of endograft stent struts at outer radius of the 60º neck angle bend.
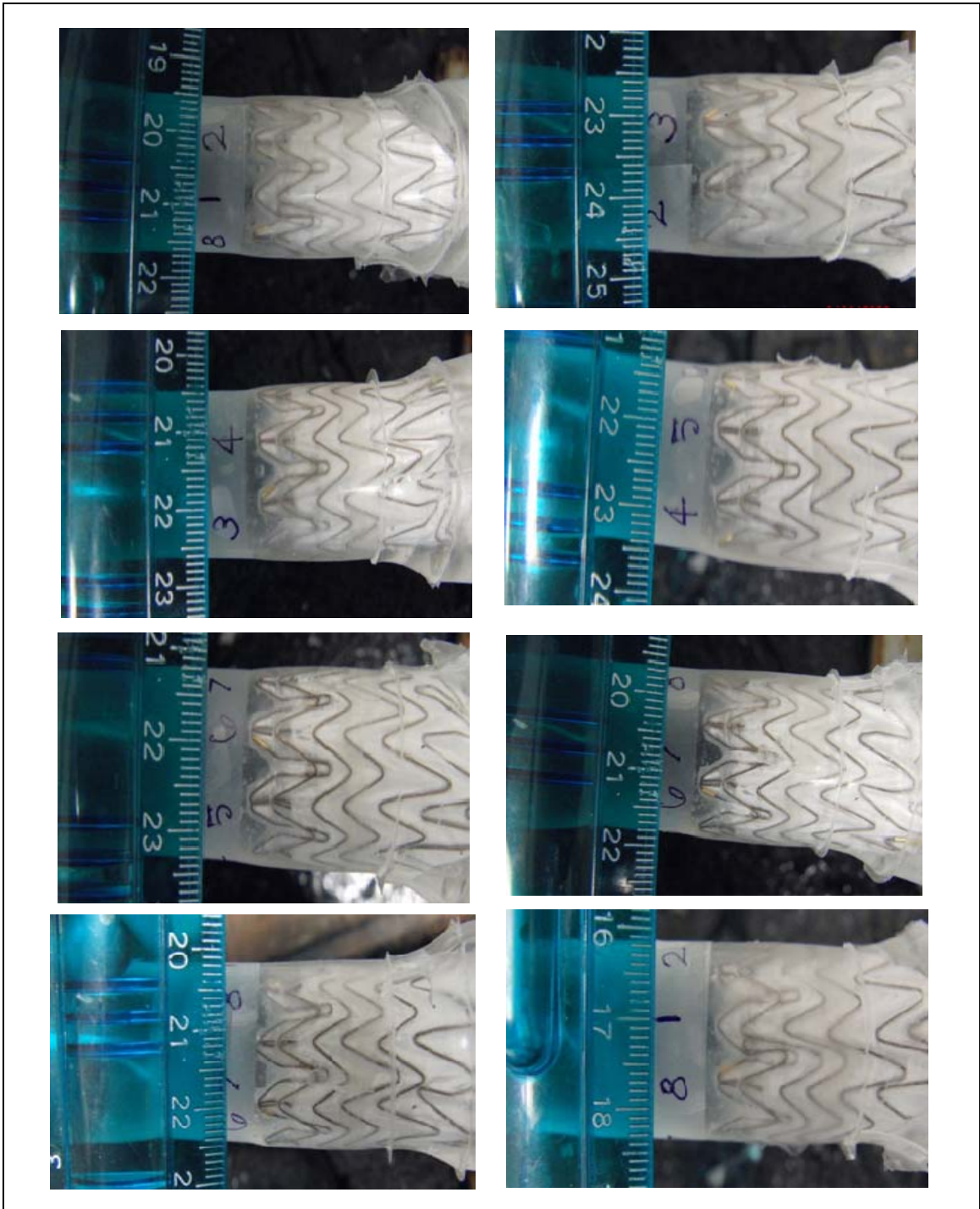
Figure 34: Representative images of apex to apex stent behavior throughout entire EVG perimeter for 0⁰ neck angle, 12% oversizing.
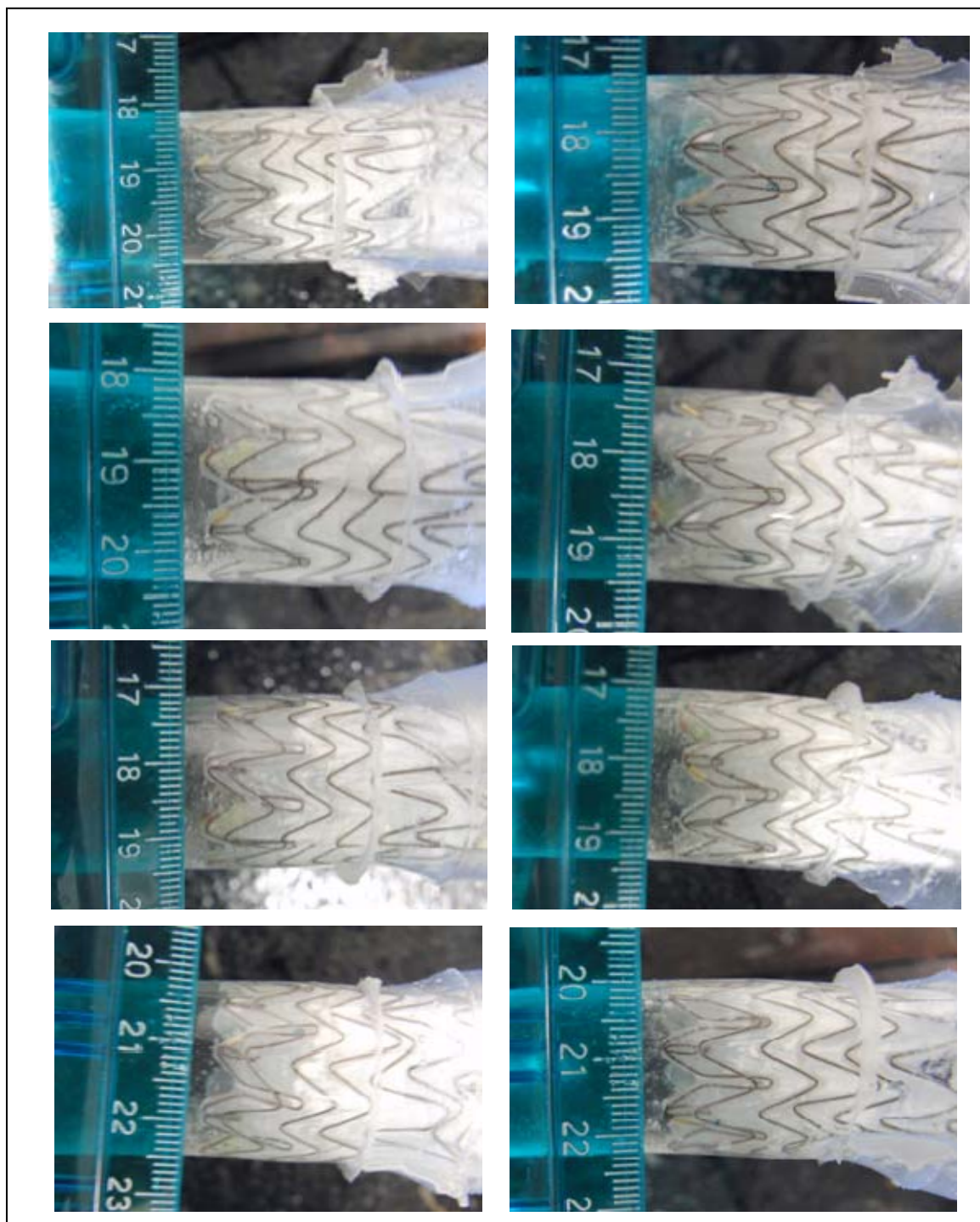
Figure 35: Representative images of apex to apex stent behavior throughout entire EVG perimeter for 0⁰ neck angle and 24% oversizing.
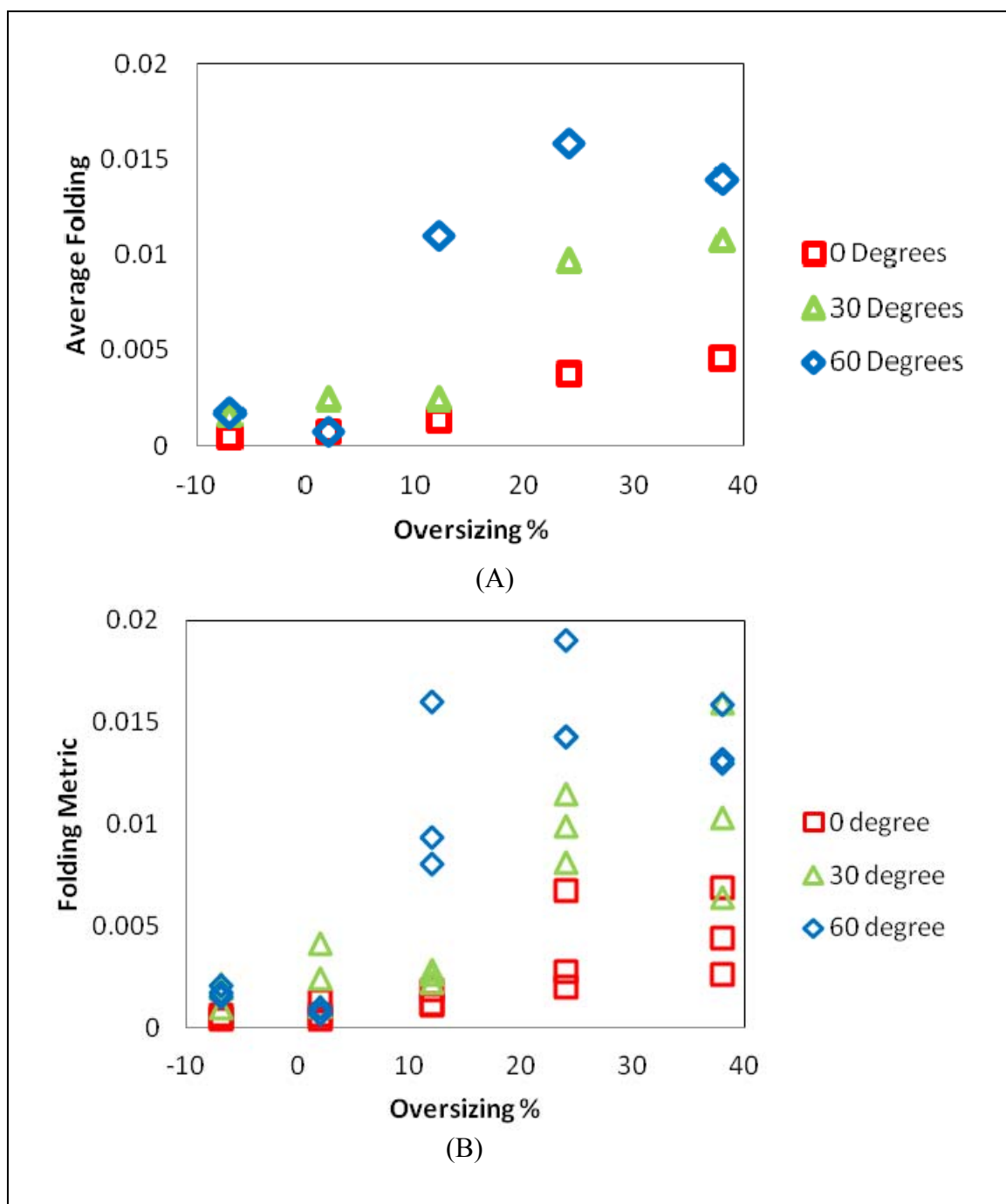
Figure 36: Effect of neck angle and oversizing on folding risk. (A) Averaged folding metric in oversizing range of -10-40% across neck angle of 0°, 30°, and 60°.
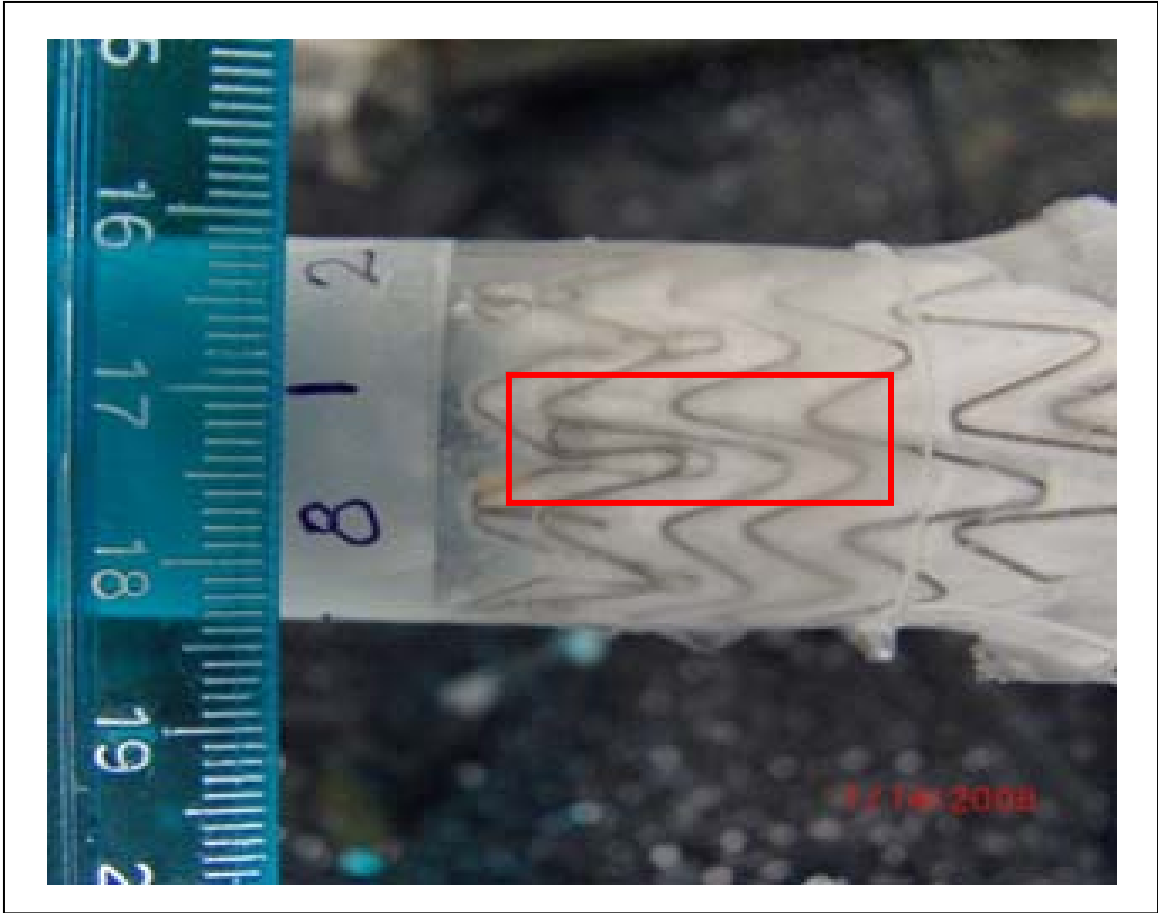
Figure 37: Non-uniform section of the stent perimeter. Notice part of stent apex that spans two stent layers.
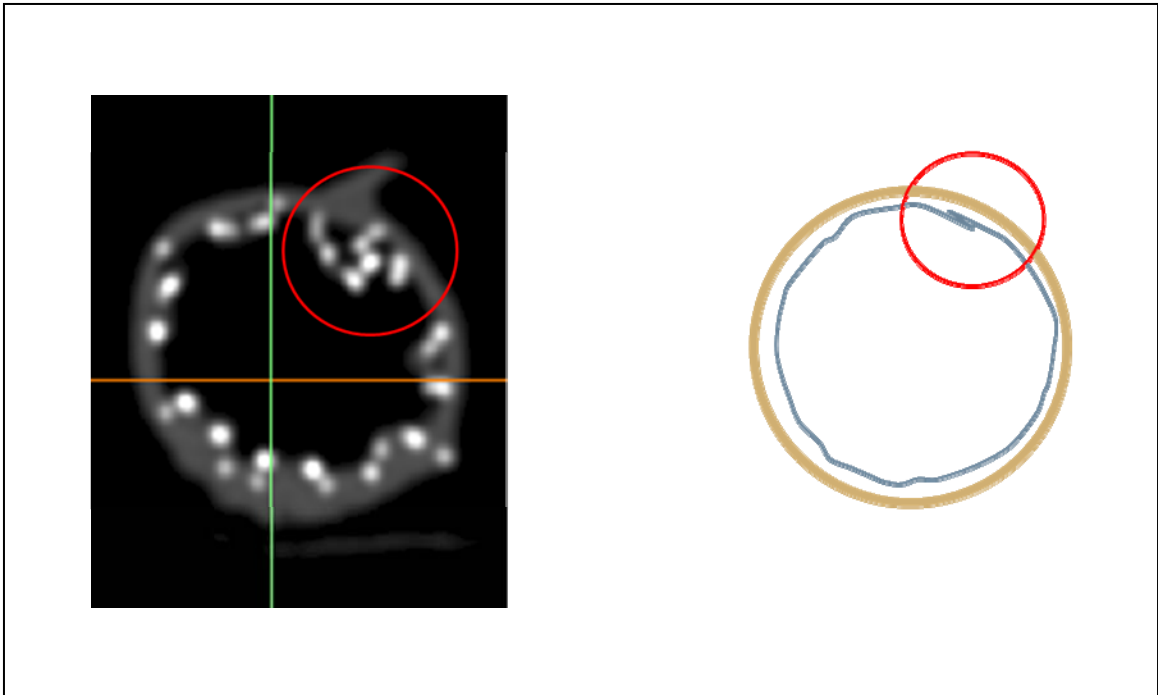
Figure 38: Depiction of different endograft folding phenomenon. (Left) Folding behavior of stent grafts from Kratzberg et al's study. (Right) Folding behavior of stent grafts from this study. The folding was flatter against the silicone aortic wall, similar to the behavior of creased paper.

CHAPTER 6: ASSESMENT OF FOLDING ON ENDOGRAFT

ATTACHMENT STRENGTH

Folding is of clinical importance because of the potential impact it may have on device attachment strength. In the preliminary studies, the relationship between folding and attachment strength was poorly understood. This project investigated the impact of folding induced by oversizing and neck angulation on endograft attachment strength using bench top experiments. The maximum force required to cause distal movement was used as a measure of fixation strength.

Pull Out Testing Setup

After the silicone aorta-AAA models were removed from the flow loop, the AAA portion of the model was cut from the aorta and discarded. Excess length in the silicone aorta material was also trimmed approximately 1" from the top stent layer. An adapter with two prongs that fit into the iliac legs of the EVG was used to connect the device to the cross head of the uniaxial tester. (LF*Plus*, 25 lbf load cell, Lloyd Instruments Ltd., West Sussex, UK). The load cell was zeroed with the weight of the aorta-EVG complex before attaching the proximal end of the complex onto the platform of the uniaxial tester. The silicone aorta was fitted over a cylinder adapter secured on to the base of the tensile tester and zip tied roughly 1.5-2 cm from the top stent layer (Figure 39a). Adaptors were designed for pull out testing of 30° and 60° neck angles to accommodate for the bend. The distance between the EVG and the secured point on the silicone aorta was minimized to reduce potential noise caused by silicone stretching or necking (Figure 39b). The crosshead position was adjusted to a load reading of "0". This ensured that the aorta-EVG complex did not experience artificial loads caused by the zip-tying process. Once the device was secured onto the tensile tester, a tensile extension rate of 0.2 mm/second was

selected. Testing was completed once the endograft was completely separated from the silicone aorta. (Figure 39c).

For test samples with angled necks, two testing methods were proposed to most accurately evaluate pull out forces. Since the tester only has a load cell in the axial direction, lateral forces wouldn't be measured. This first method would be to measure the pull out force along the centerline axis of the aorta, regardless of the neck bed. This would be a true assessment of the effects of folding due to oversizing and neck angulation during and after deployment. The second method would be to measure the pull out force it would be experienced physiologically by the stent graft during migration. The aorta-EVG complex should be set up so that the EVG would be dislodged from the silicone aorta in the same manner that an EVG would migrate in the body.

After much deliberation and discussion, it was decided that the second moth would be more appropriate for the study. Although the first method results in the true measurement of fixation strength due to oversizing and neck angle from deployment, it assumes that the interaction between oversizing, neck angle, and folding is only dependent on deployment. This may not be an accurate representation of migration. The second method closely resembled the mechanics of migration observed physiologically and would give more clinically oriented findings.

To accomplish this, two adapters were drawn in ProEngineer (PTC, Needham, MA) and rapid prototyped. The adapters were designed as cylinders with diameters slightly smaller than the ID of the aortas, consisting of a 90° bend and then a 30° or 60° bend (Figure 39a/b). The adapters allowed for the proximal region of the device to be secured at an angle off from the longitudinal axis of the device and tester. The same setup methods mentioned above for pull out tests performed on the 0° samples were employed. Pull out force data for each sample was exported into excel where the maximum pull out forces for each device was identified.

Pull Out Force Results

Folding metric and pull out force data was averaged to identify general trends in the relationship between pull out force and folding metric for all neck angles as oversizing increased (Figure 40). As folding metric increased, average pull out forces increased for 0° and 30° neck angles across all oversizings. Folding has no impact on pull out forces for a neck angle of 60°. When discrete data points were plotted for all trials in the study, a slight decrease in pull out force was observed as folding metric increased for 0° and 30° neck angles. Figure 41 shows a negative trend line between folding metric and pull out forces at the 0° and 30° neck angles correlating with an oversizing >24%.

Figure 42a shows the relationship between neck angulation, folding, and pull out forces. The color scale represents the folding metric for each data point. Marker colors with more severe/higher incidence of folding tend towards red while less severe/lower incidences of folding tend towards blue. Folding prevalence is decreased as neck angle decreased. Variation in pull out force for each neck angle also decreased as neck angle increased. Test samples in the 0° neck angle subset had the largest spread of pull out forces, claiming the lowest and highest maximum pull out force out of all the tests conducted in this project. Pull out forces for all three neck angles were in the same range with no statistical difference when oversizing was perturbed. Comparisons of pull out forces between 0° and 30°, 0° and 60°, as well as 30° and 60° neck angles were not statistically significant (Mann-Whitney U, $p > 0.05$).

In Figure 42b, the relationship between oversizing, folding, and pull out force for all neck angles is plotted. An increasing trend across all neck angles in pull out forces and folding is observed as oversizing was increased, especially for oversizings greater than 12%. Figure 43 shows averaged pull out forces for each neck angle as oversizing was varied. As neck angle was increased, pull out force remained around the same value,

regardless of oversizing. For 0⁰ and 30⁰ neck angle, as oversizing increased, pull out forces increased as well.

<u>Pull Out Force Discussion</u>

Folding of the stent graft compromises the radial rigidity of the device and decreases contact surface area between the aorta and the device. Theoretically this translates to a decrease in radial and frictional forces that facilitate in device fixation, potentially causing migration. This occurrence was investigated as the reason for the drop in fixation strengths for devices oversized >30%.

In this study, migration was experimentally captured by the maximum pull out force measured. The maximum force recorded represents the moment the stent begins to move in the host aorta. The higher the pulls out force, the higher the resistance to movement of the stent graft inside the aorta. Identifying factors that reduce migration risk is of clinical interest as it is the leading cause of complication for endovascular repair.

Results from the preliminary studies mentioned above reported no clear correlation between folding and attachment strength in a retroactive study investigating the impact of oversizing on barbed attachment strength. Devices with high fold rankings did not necessarily have corresponding low pull out strengths. Oversizing and neck angle was varied to intentionally induce folding in the device. The effect of these two parameters on device fixation strength was evaluated through pull out testing. Results from this study suggest that folding does not have an overall affect device attachment strength. However, there might be a slight correlation between higher folding level and lower pull out forces for 0⁰ and 30⁰ neck angles with oversizing ≥24% within the trial set. As the neck angle becomes more extreme in the 60⁰ case, folding and device oversizing become less relevant in impacting attachment strength. This may be due to the effect of the neck angle bend in the aorta. The angled neck becomes the dominant factor affecting

device attachment strength at higher neck angles. This is supported by the relatively flat slope of the best fit line through the data points. Figure 42a also supports this as seen by the tighter cluster pull out forces at 60°, even though folding metrics were the highest observed. This pattern is less obvious at a 30° neck angle, and even less so at 0° indicated by the spread of pull out strength data. At lower neck angles, the bend does not provide a tortuous enough anatomy for the stent graft "locked in" at the neck angle bend. At higher neck angles, the proximal end of the device deployed in the aorta upstream to the bend forms a "lever" or switch that resists migration until the pulling force from the extension tester is able to overcome the axial and transverse resistance from the device attempting to move in the angled anatomy. At higher neck angles, severe stent and graft overlap as oversizing increases drops surface area contact but the resistance provided by the lever arm is such a dominating factor that pull out strength is not affected. Interestingly enough, even at low oversizing where folding is less severe but still present, pull out force is still not affected. In cases where very low oversizing was used, the stent graft would not be able to form a seal in its expanded state because the diameter of the device was much smaller than the now angled cross sectional area (Figure 44). In agreement with the collected data, at a neck angle of 0°, a low oversize would still allow for a uniform proximal seal that would maximize the device to aortic wall contact area so that frictional forces can be employed in increasing pull out strengths.

Findings from this study are in direct contradiction with the results from Kratzberg et al [34]and Sternbergh et al [28]. Recall that there was no decrease in the averaged pull out forces as oversizing was increased across all neck angles. An important difference to note is that the devices in Kratzberg et al's and Sternbergh et al's studies had barbs on the proximal stent layer while the devices in all other studies were barbless. Barbless grafts were also used in this study and our results are in agreement with the groups reporting no correlation between oversizing and migration risk. Interestingly, the

devices the devices used for this study were the same exact devices used by Kratzberg et al with the barbs removed. This strongly suggests that barbs are actually the main contributing factor to migration risk at higher oversizings. There is already difficulty in accommodating a barbless device in the aorta when severely oversized. When barbs are added to a highly oversized device, this task becomes even more difficult. There is even more material that must compress and fit into the aorta and the protruded nature of the barbs increases the difficulty in proper seal formation with the aortic wall. The interaction between the barbs and the surrounding stent struts may cause more severe folding. Poor penetration of the barb further aggravates folding as it can cause the stent attached to the barb to protrude further into the lumen of the device. Partial penetration of the barbs may also cause protrusion into the lumen or prevention of stent strut repositioning for even distribution throughout the circumference of the device. Conducting similar studies with the addition of barbs will elucidate the relationship between oversizing, decreased fixation strength, and pull out forces.

<div align="center">Pull Out Force Conclusion</div>

Maximum pull out force was used as a measurement of device fixation strength as variables were perturbed. Overall, folding did not cause a drop in attachment strength of the devices. At 0° and 30° neck angles, once folding metrics exceeded 0.0027 and 0.006, respectively, a drop in pull out forces was observed. At higher neck angles, folding does not impact pull out forces. As the neck angle increases, interaction of the stent graft with the bend in the aorta becomes the dominating factor effecting pull out force. Similarly, a positive trend between pull out forces and oversizing was observed. There was also no statistical difference in pull out forces measured across all oversizings for all neck angles.

Figure 39: Pull out force test setup. (A) Pull out force test setup for angled aortic neck samples (30⁰ neck angle in the photo). (B) Stretching of silicone aorta during pull out testing. Angle of pull out not fully maintained throughout pull out process. (C) Test stopped when EVG is fully separated from silicone aorta.
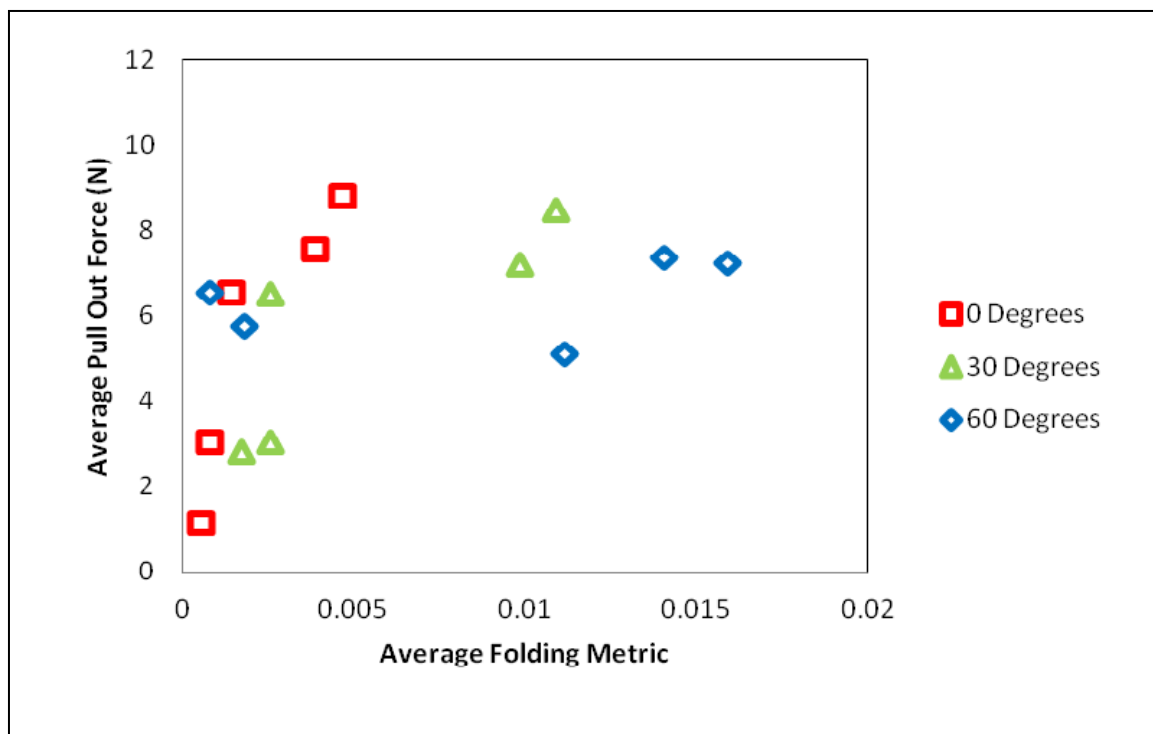
Figure 40: Averaged effect of folding on attachment strength across all tested oversizing and neck angles.
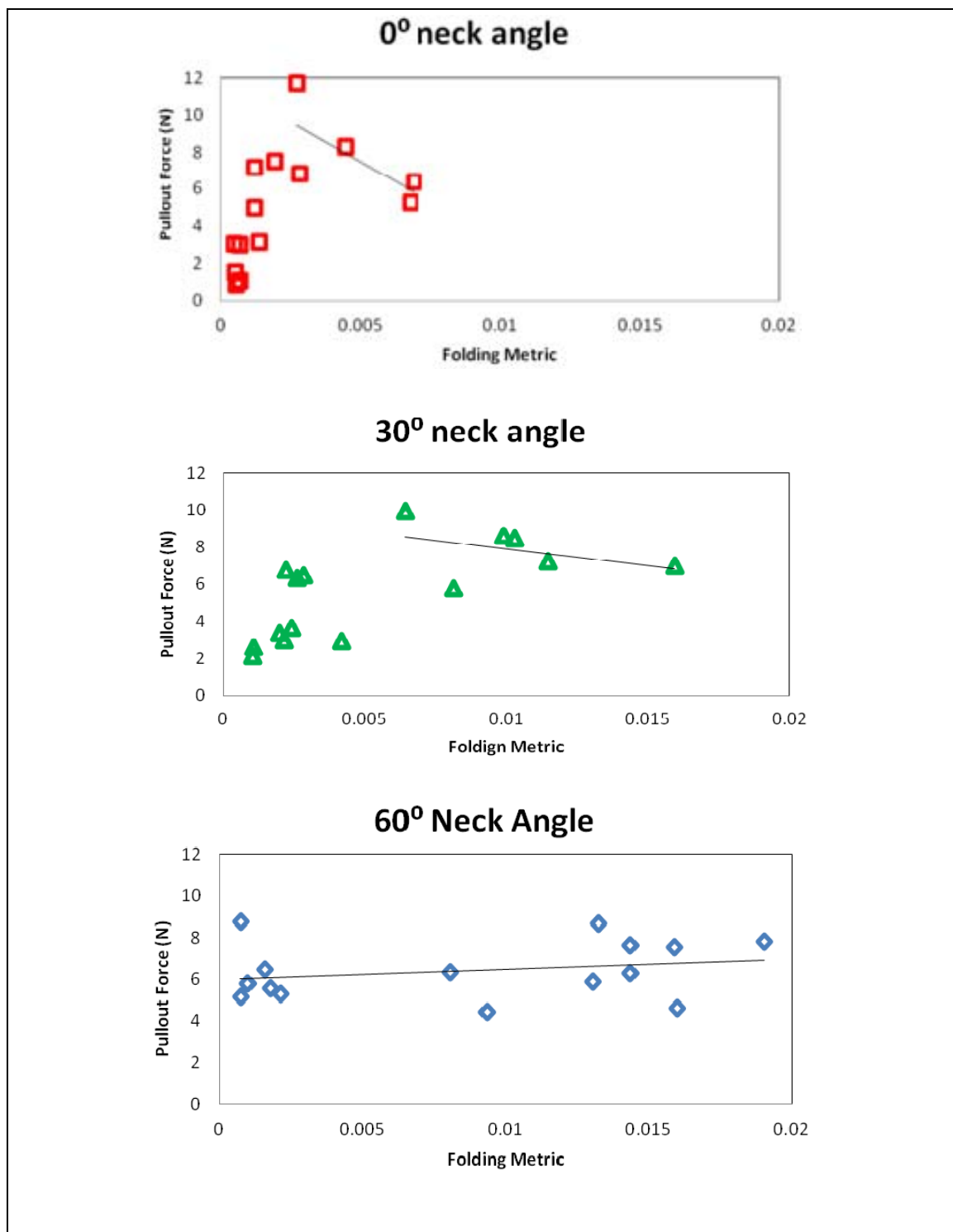
Figure 41: Effect of folding on fixation strength. Line shows decreasing trend in pullout force as folding increased for each neck angle subset.

(A)

(B)
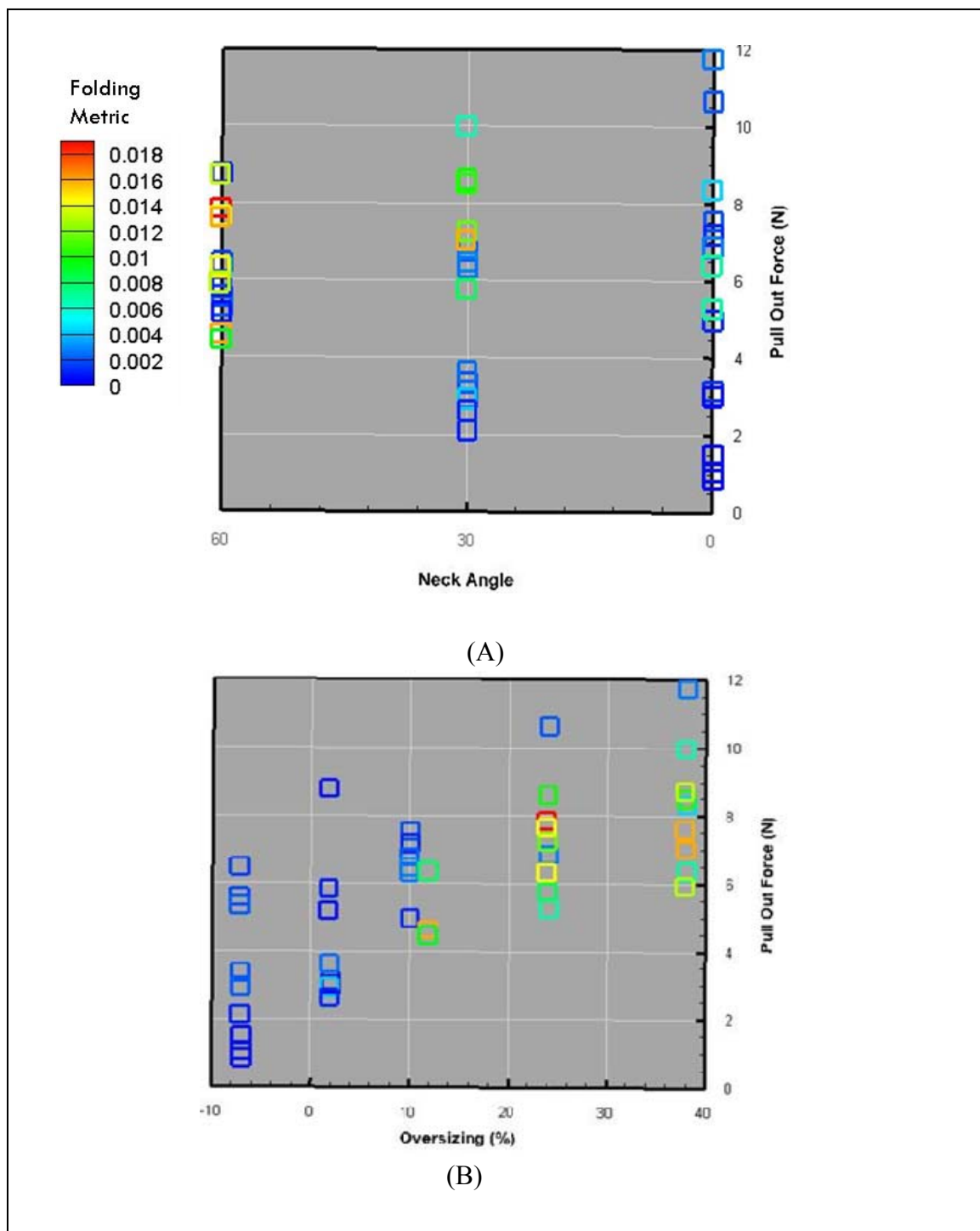
Figure 42: Effect of folding variables on pull out force (A) Effect of neck angle on fixation strength across all EVG oversizings. (B) Effect of EVG oversizing on fixation strength across all neck angles.
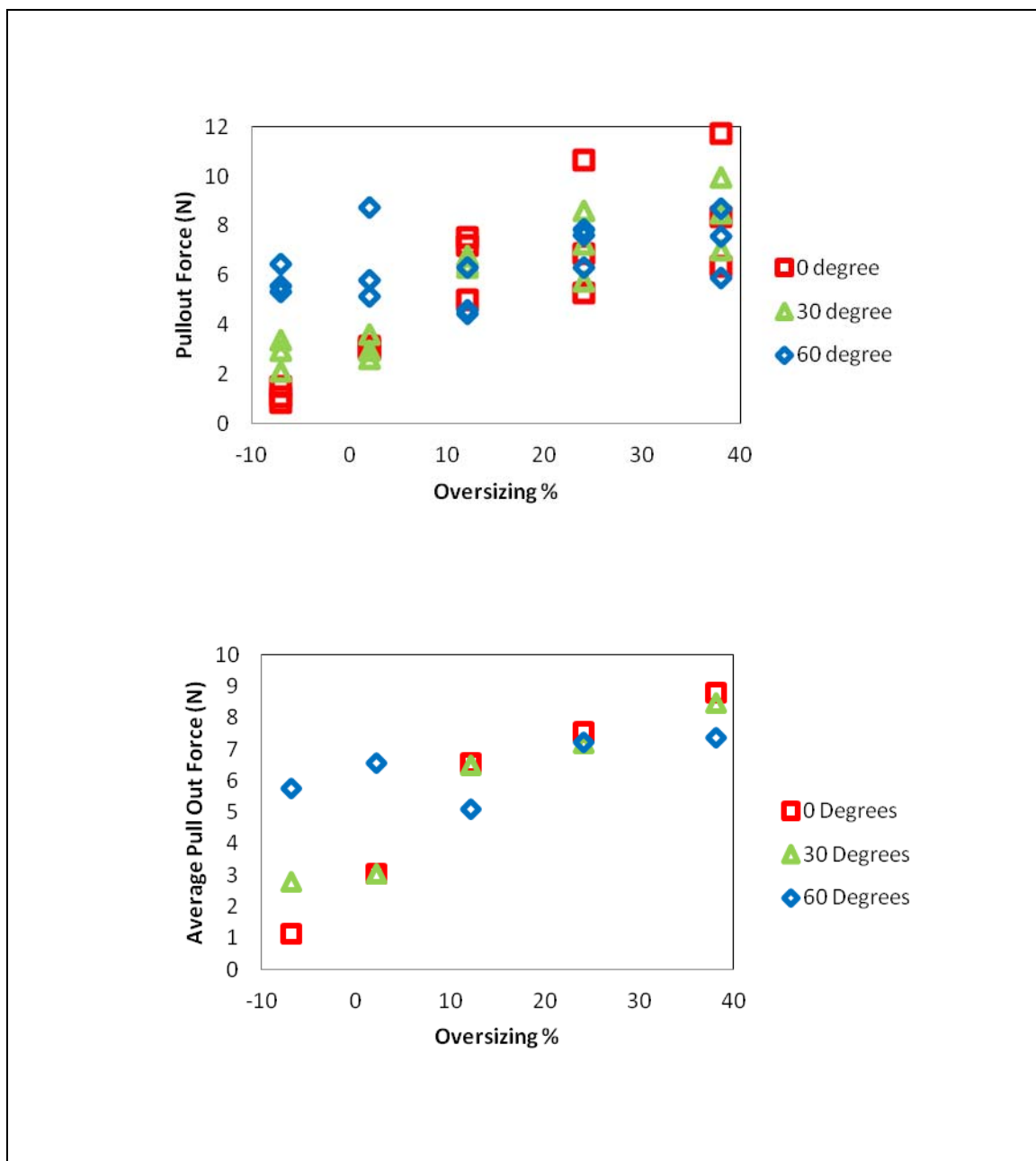
Figure 43: Effect of EVG oversizing on averaged fixation strength across all neck angles. Bottom graft shows the averaged pull out force for each oversizing.
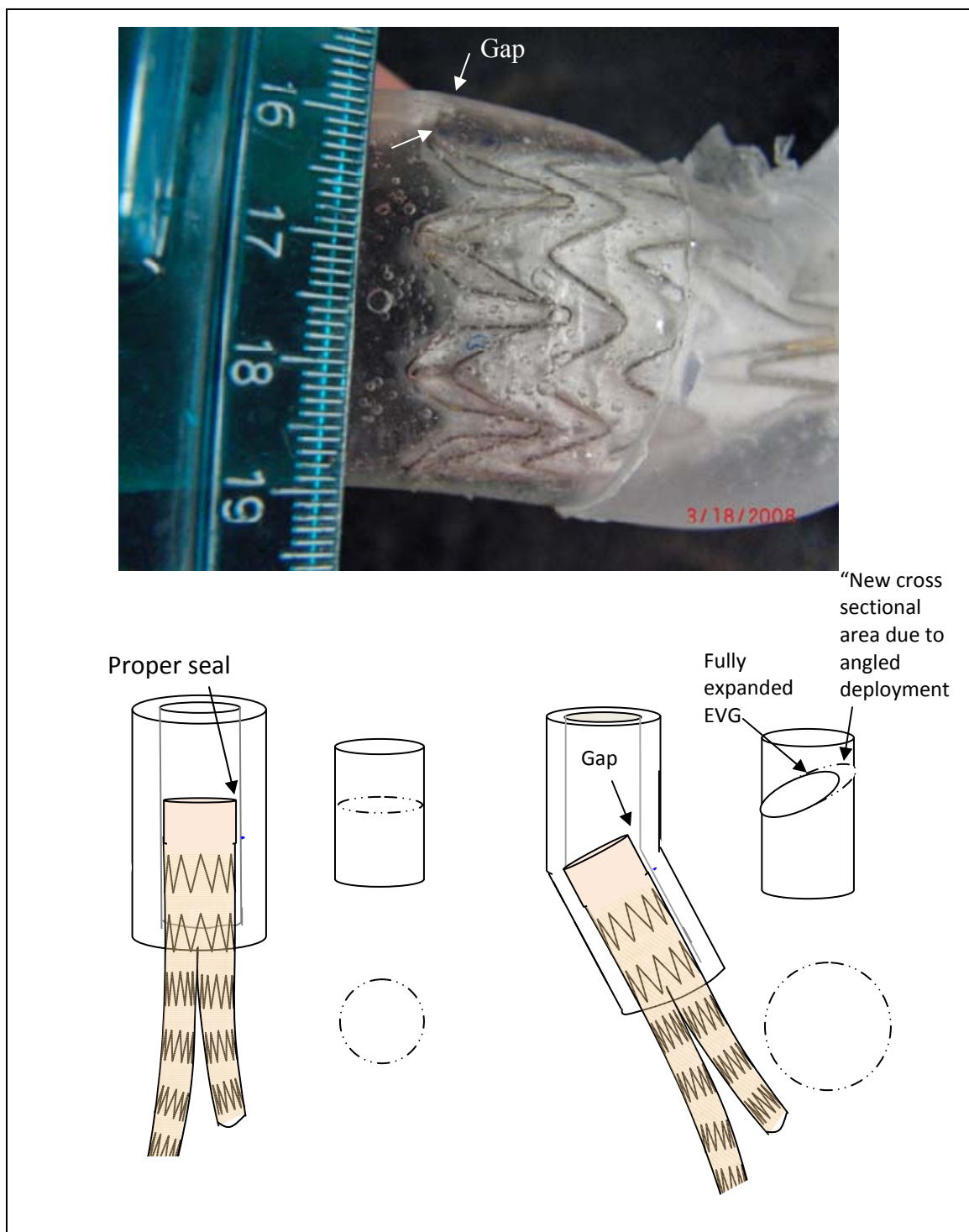
Figure 44: Improper seal with aortic wall at 60 neck angle with very 2% oversizing. Angle of deployment creates a larger expansion area inside the aorta as shown in the schematic.

CHAPTER 7: STUDY CONCLUSION

Study Motivation

Project Genesis

Kratzberg et al [34] performed a bench top study on the effect of oversizing on attachment strength of barbed endografts and reported that endografts oversized greater than 30% had lower pull out forces. Sternbergh et al [28] also reported excessive oversizing as a migration risk in a clinical study. A 14% migration rate was observed for endografts oversized >30% vs. only 0.9% migration rate for endografts oversized less than 30%. These results are counter intuitive to mechanical theory as higher oversizing should induce higher radial and frictional forces. This would then increase fixation strengths of the device post deployment. Experimental data also supports the theory that higher oversizing increases radial and frictional forces [30-32]. Other researchers have reported that excessive oversizing has no impact on migration risk [23, 24, 35]. The contradicting data suggests lack of a consensus regarding the role of oversizing on migration rates. Our group further explored the impact of oversizing on device migration and proposed the phenomenon of endograft folding as the for decreased fixation strength at high oversizings. Anecdotal observation of CT volume rendered data from Kratzberg et al's study [34, 36] showed instances of stent graft collapse or folding. Folding is described as a localized deformation of the stent adjacent struts begins to overlap or protrude into the lumen. We hypothesized that endograft folding may explain the decreased fixation strength observed at higher oversizings.

Clinical Support for Hypothesis

Wolf et al [37] reported clinical findings to support this hypothesis for 100 patients treated with the AneuRx device. Five of the 100 (5%) treated patients displayed

evidence of folding and of these 5 patients, 4 (80%) experienced device migration. Factors that contribute to endograft folding are poorly understood and there is little literature on this topic. However, thoracic endovascular repair have numerous cases of stent graft folding or stent graft collapse. These reports often suggest that device oversizing and aortic neck angle are large determinants in folding risk [43, 44].

<u>Study Findings</u>

We hypothesized that folding contributes to migration risk. Folding of the stent graft reduces surface contact between the device and aortic wall, decreasing frictional and radial forces. Attachment strength is potentially compromised when there are incidences of folding and factors believed to induce folding are neck angulation and endograft oversizing.

Effect of neck angulation and oversizing on folding

Three neck angles $0°$, $30°$, and $60°$ were tested at five oversizings of -7, 2, 12, 24, and 38%. **Neck angulation and oversizing increase folding in endografts. This relationship is non linear as there is a significant increase in folding metric for oversizing >12%.** Folding risk is also higher when stent geometry is non-uniform or irregular at a singular point, suggesting that stent design is also an important factor in folding risk.

Effect of folding on pullout forces (migration resistance)

Folding does not increase migration risk across all neck angles and oversizings tested. There was an overall increasing trend in pull out forces measured when oversizing and neck angulation was increased. However, pull out forces did decrease as folding metric increased within the trial sets for oversizing of 24 & 38% at $0°$ and $30°$ neck angles. Folding would occur at oversizing $\geq$ 12% but didn't negatively

impact pull out forces until oversizing ≥24%. In the 60° case, folding and oversizing did not impact attachment strength.

No drop in pull out forces was observed as oversizing was increased. This study did not find similar results reported by Kratzberg et al [34]and Sternbergh et al [28] but did support claims by other researchers [23-25, 35]that found no correlation between oversizing and migration risk. One important difference to note is that Kratzberg et al and Sternbergh et al reported on barbed devices while the other groups reported on barbless devices. **This highlights the importance of barbs in the relationship between oversizing, folding, and compromised fixation strength**.

<u>Study Limitations</u>

Flow waveform

There are a few limitations that must be noted in this study. Although great care was taken to ensure a physiologically representative experimental environment, the flow loop did not accurately simulate all aspects of the circulatory system. Although the time averaged flow and percentage of time in the systolic/diastolic phases matched, the magnitude of the flow rates did not match. The programmable pump was unable to output flow rates high enough to compensate for the dampening effects of the compliant components of the flow loop. Despite this limitation, the flow loop was still very effective in simulating the deployment process as the general shape and cycle periods in the systole/diastole phases are representative. The pressure waveform was also more physiologically representative and was decided to be the more important parameter to maintain.

Flow loop test fluid

The 0.9% saline solution used in the flow loop did not have comparable fluid dynamic properties as blood. Ideally, a viscosity matching fluid such as 40/60 glycerin/DI water mixture would be used during experimentation to accurately simulate the hemodynamics in the aorta. The blood analog fluid would provide more lubrication during deployment and may induce drag forces on the stent graft that may affect its deployment characteristics. The extra lubrication may facilitate in uniform strut distribution in the host aorta. Fluid dynamic effects may also impact folding of the stent grafts, specifically on the graft material. Glycerin was not used in this study because it is logistically difficult to handle. The fluid is extremely messy and slippery, making it difficult to handle the stent grafts and keep them clean for multiple uses.

Effects from drag forces and fluid dynamic effects were assumed to be negligible due to the short time period of the experiments. In addition, all stent grafts were deployed in similar conditions so that the trends observed still provide valuable insight. The blood analog fluid would also be more lubricating than saline water which may also facilitate in uniform placement of stent struts though the circumference of the device. Silicone has a much higher friction coefficient than aortic tissue so it is possible that stent graft folding is exaggerated because it is sticking to the silicone wall rather than distributing itself uniformly.

Potential stent fatigue due to reloading of devices

The endografts used in the study had been collapsed and redeployed numerous times. They have also been used by Kratzberg et al for his studies. The structural integrity of the stent, specifically radially, may be compromised from continually collapsing and expanding the device. The stent material is nitinol and will retain its heat treated shape once in the appropriate temperature range but may become fatigued after so much use.

The true diameter of the fully expanded device may be less than the manufacturer intended diameter. This may also impact radial rigidity negatively. At the beginning of the dissertation research project, measurements of the outer diameter of the devices were made using a laser micrometer. Between experiments, crude measurements of the device diameter were measured using calipers before reloading into the deployment catheter. Despite the crude measurements made with a caliper throughout the dissertation process, the effect of continual reloading on the stent grafts is definitely a concern that needs to further investigated. Radial rigidity of the device must also be assessed as that may impact folding risk.

Pull Out Testing

Pull out testing was used to evaluate migration resistance of the stent graft in the host aorta. This test setup used in this project physiologically mimics device migration in the body but was not performed in a pressurized state. Accurate simulation of device migration mechanics provides the most clinically relevant findings. Consideration was given to performing pull out tests while the device was in the flow loop but this would require the use of a hand held force gauge and proved to be a difficult task in pulling the device at a constant rate and in a perfectly straight line. Logistically, this test method allowed for maximum control in pulling the device out of the aorta and was easiest to accomplish. Although this test method was more feasible and allowed for more control, the oversizing during pull out testing was higher, resulting in elevated pull out force measurements. Folding of the stent graft may be exaggerated as the silicone collapses to its smaller, unpressurized diameter. Despite this, trends observed in the results by comparison within the data sets still provide plausible lines of connection between the test parameters.

The isotropic nature of the silicone also caused difficulty in maintaining a consistent neck angle throughout the pull out test. The longitudinal mechanical properties of the material were not physiologically representative. During testing, the silicone began to stretch as the device is being pulled out of the host aorta due to higher coefficient of friction for silicone. Average pull out force for barbless Gore Excluder devices deployed in bovine aorta at 0 neck angle in the 10-15% range was 1.75 N [36] compared to 6.6 N (2.8 times higher) when deployed in silicone. Maintaining a consistent neck angle for the entire duration of the pull out tests was difficult due to stretching of the material. The silicone material was isotropic so longitudinal mechanical properties were not representative. As the device is pulled from the silicone aorta, the material begins to stretch at the attachment site and attempts to straighten as the EVG migrates through the bend. The neck angle during pull out testing was slightly smaller than the intended 30° or 60° (Figure 39b). Despite this, the results still provide valuable insight as the stretching of the silicone results in a longer time frame before the radial and frictional forces exerted by the device is overcome. In addition, although the angles were not perfectly at 0°, 30°, and 60°, they testing angle for the 30° cases were still smaller than the testing angle for the 60° cases. Although the exact pull out force values are not physiologically representative, the trends observed do provide insight regarding the effect of folding on migration resistance.

Future Work

This project successfully addressed the hypothesis and questions posed at the beginning of the study. An objective method for characterizing a folding metric was also developed to quantify folding in an endograft. The results from this study also stresses that we still have a relatively poor understanding of oversizing, folding, and fixation strength. We have investigated two variables that were reported in literature to be large

contributors in folding risk. However, the interaction of barbs and stent geometry in relation to folding and migration risk are not well understood and were not addressed by this study. Findings from this study indicate that those variables are extremely important in folding risk as well. Future work incorporating the role of barbs and/or stent design would provide a clearer picture of variable interactions that impact folding and pull out force.

REFERENCES

1. Lederle, F.A., et al., *Relationship of age, gender, race, and body size to infrarenal aortic diameter. The Aneurysm Detection and Management (ADAM) Veterans Affairs Cooperative Study Investigators.* J Vasc Surg, 1997. **26**(4): p. 595-601.

2. Lederle, F.A. and D.L. Simel, *The rational clinical examination. Does this patient have abdominal aortic aneurysm?* JAMA, 1999. **281**(1): p. 77-82.

3. Campos-Outcalt, D., Sr., *US Preventive Services Task Force: the gold standard of evidence-based prevention.* J Fam Pract, 2005. **54**(6): p. 517-9.

4. *Summaries for patients. Screening for abdominal aortic aneurysm: recommendations from the U.S. Preventive Services Task Force.* Ann Intern Med, 2005. **142**(3): p. I52.

5. Darling, R.C., et al., *Autopsy study of unoperated abdominal aortic aneurysms. The case for early resection.* Circulation, 1977. **56**(3 Suppl): p. II161-4.

6. Hall, A.J., et al., *Aortic wall tension as a predictive factor for abdominal aortic aneurysm rupture: improving the selection of patients for abdominal aortic aneurysm repair.* Ann Vasc Surg, 2000. **14**(2): p. 152-7.

7. Raghavan, M.L., et al., *Biomechanical failure properties and microstructural content of ruptured and unruptured abdominal aortic aneurysms.* J Biomech, 2011. **44**(13): p. 2501-7.

8. Venkatasubramaniam, A.K., et al., *A comparative study of aortic wall stress using finite element analysis for ruptured and non-ruptured abdominal aortic aneurysms.* Eur J Vasc Endovasc Surg, 2004. **28**(2): p. 168-76.

9. Hertzer, N.R., et al., *Open infrarenal abdominal aortic aneurysm repair: the Cleveland Clinic experience from 1989 to 1998.* J Vasc Surg, 2002. **35**(6): p. 1145-54.

10. Becquemin, J., et al., *Mid-term results of endovascular versus open repair for abdominal aortic aneurysm in patients anatomically suitable for endovascular repair.* Eur J Vasc Endovasc Surg, 2000. **19**(6): p. 656-61.

11. Goueffic, Y., et al., *Midterm survival after endovascular versus open repair of infrarenal aortic aneurysms.* J Endovasc Ther, 2005. **12**(1): p. 47-57.

12. Rutherford, R.B. and W.C. Krupski, *Current status of open versus endovascular stent-graft repair of abdominal aortic aneurysm.* J Vasc Surg, 2004. **39**(5): p. 1129-39.

13. Krupski, W.C. and R.B. Rutherford, *Update on open repair of abdominal aortic aneurysms: the challenges for endovascular repair.* J Am Coll Surg, 2004. **199**(6): p. 946-60.

14.   Lee, W.A., et al., *Perioperative outcomes after open and endovascular repair of intact abdominal aortic aneurysms in the United States during 2001.* J Vasc Surg, 2004. **39**(3): p. 491-6.

15.   Moore, W.S., et al., *Five-year interim comparison of the Guidant bifurcated endograft with open repair of abdominal aortic aneurysm.* J Vasc Surg, 2003. **38**(1): p. 46-55.

16.   Elkouri, S., et al., *Perioperative complications and early outcome after endovascular and open surgical repair of abdominal aortic aneurysms.* J Vasc Surg, 2004. **39**(3): p. 497-505.

17.   Upchurch, G.R., Jr. and T.A. Schaub, *Abdominal aortic aneurysm.* Am Fam Physician, 2006. **73**(7): p. 1198-204.

18.   Parodi, J.C., J.C. Palmaz, and H.D. Barone, *Transfemoral intraluminal graft implantation for abdominal aortic aneurysms.* Ann Vasc Surg, 1991. **5**(6): p. 491-9.

19.   Hausegger, K.A., et al., *Complications in endoluminal repair of abdominal aortic aneurysms.* Eur J Radiol, 2001. **39**(1): p. 22-33.

20.   Harris, P.L., et al., *Incidence and risk factors of late rupture, conversion, and death after endovascular repair of infrarenal aortic aneurysms: the EUROSTAR experience. European Collaborators on Stent/graft techniques for aortic aneurysm repair.* J Vasc Surg, 2000. **32**(4): p. 739-49.

21.   England, A., et al., *Device migration after endovascular abdominal aortic aneurysm repair: experience with a talent stent-graft.* J Vasc Interv Radiol, 2004. **15**(12): p. 1399-405.

22.   Flora, H.S., et al., *Secondary intervention following endovascular repair of abdominal aortic aneurysm: a single centre experience.* Eur J Vasc Endovasc Surg, 2003. **26**(3): p. 287-92.

23.   Conners, M.S., 3rd, et al., *Endograft migration one to four years after endovascular abdominal aortic aneurysm repair with the AneuRx device: a cautionary note.* J Vasc Surg, 2002. **36**(3): p. 476-84.

24.   Cao, P., et al., *Device migration after endoluminal abdominal aortic aneurysm repair: analysis of 113 cases with a minimum follow-up period of 2 years.* J Vasc Surg, 2002. **35**(2): p. 229-35.

25.   Zarins, C.K., et al., *Stent graft migration after endovascular aneurysm repair: importance of proximal fixation.* J Vasc Surg, 2003. **38**(6): p. 1264-72; discussion 1272.

26.   Li, Z. and C. Kleinstreuer, *Analysis of biomechanical factors affecting stent-graft migration in an abdominal aortic aneurysm model.* J Biomech, 2006. **39**(12): p. 2264-73.

27. Resch, T., et al., *The impact of stent design on proximal stent-graft fixation in the abdominal aorta: an experimental study.* Eur J Vasc Endovasc Surg, 2000. **20**(2): p. 190-5.

28. Sternbergh, W.C., 3rd, et al., *Influence of endograft oversizing on device migration, endoleak, aneurysm shrinkage, and aortic neck dilation: results from the Zenith Multicenter Trial.* J Vasc Surg, 2004. **39**(1): p. 20-6.

29. van Prehn, J., et al., *Oversizing of aortic stent grafts for abdominal aneurysm repair: a systematic review of the benefits and risks.* J Vasc Surg, 2009. **39**(1): p. 20-6.

30. Malina, M., et al., *Endovascular AAA exclusion: will stents with hooks and barbs prevent stent-graft migration?* J Endovasc Surg, 1998. **5**(4): p. 310-7.

31. Lambert, A.W., et al., *Experimental assessment of proximal stent-graft (InterVascular) fixation in human cadaveric infrarenal aortas.* Eur J Vasc Endovasc Surg, 1999. **17**(1): p. 60-5.

32. Zhou, S.S., et al., *Comparison of the fixation strength of standard and fenestrated stent-grafts for endovascular abdominal aortic aneurysm repair.* J Endovasc Ther, 2007. **14**(2): p. 168-75.

33. van Prehn, J., et al., *Oversizing of aortic stent grafts for abdominal aneurysm repair: a systematic review of the benefits and risks.* Eur J Vasc Endovasc Surg, 2009. **38**(1): p. 42-53.

34. Kratzberg, J.A., J. Golzarian, and M.L. Raghavan, *Role of graft oversizing in the fixation strength of barbed endovascular grafts.* J Vasc Surg, 2009. **49**(6): p. 1543-53.

35. Sampaio, S.M., et al., *AneuRx device migration: incidence, risk factors, and consequences.* Ann Vasc Surg, 2005. **19**(2): p. 178-85.

36. Kratzberg, J.A., *Modification of endovascular graft parameters in order to decrease graft migration*, in *Biomedical Engineering*. 2008, University of Iowa: Iowa City. p. 147.

37. Wolf, Y.G., et al., *Eccentric stent graft compression: an indicator of insecure proximal fixation of aortic stent graft.* J Vasc Surg, 2001. **33**(3): p. 481-7.

38. Melissano, G., et al., *Disappointing results with a new commercially available thoracic endograft.* J Vasc Surg, 2004. **39**(1): p. 124-30.

39. Idu, M.M., et al., *Collapse of a stent-graft following treatment of a traumatic thoracic aortic rupture.* J Endovasc Ther, 2005. **12**(4): p. 503-7.

40. Mestres, G., et al., *Symptomatic collapse of a thoracic aorta endoprosthesis.* J Vasc Surg, 2006. **43**(6): p. 1270-3.

41. Hinchliffe, R.J., et al., *Observations on the failure of stent-grafts in the aortic arch.* Eur J Vasc Endovasc Surg, 2007. **34**(4): p. 451-6.

42.   Muhs, B.E., et al., *Anatomic factors associated with acute endograft collapse after Gore TAG treatment of thoracic aortic dissection or traumatic rupture.* J Vasc Surg, 2007. **45**(4): p. 655-61.

43.   Jonker, F.H., et al., *Endograft collapse after thoracic endovascular aortic repair.* J Endovasc Ther, 2010. **17**(6): p. 725-34.

44.   Canaud, L., et al., *Factors favoring stent-graft collapse after thoracic endovascular aortic repair.* J Thorac Cardiovasc Surg, 2010. **139**(5): p. 1153-7.

45.   Jonker, F.H.W., et al., *Endograft Collapse After Thoracic Endovascular Aortic Repair.* Journal of Endovascular Therapy, 2010. **17**(6): p. 725-734.

46.   Chong, C.K., et al., *Computer aided design and fabrication of models for in vitro studies of vascular fluid dynamics.* Proc Inst Mech Eng H, 1999. **213**(1): p. 1-4.

47.   Berry, E., et al., *Flexible tubular replicas of abdominal aortic aneurysms.* Proc Inst Mech Eng H, 2002. **216**(3): p. 211-4.

48.   Doyle, B.J., et al., *3D reconstruction and manufacture of real abdominal aortic aneurysms: from CT scan to silicone model.* J Biomech Eng, 2008. **130**(3): p. 034501.

49.   Corbett, T.J., et al., *Engineering silicone rubbers for in vitro studies: creating AAA models and ILT analogues with physiological properties.* J Biomech Eng, 2010. **132**(1): p. 011008.

50.   Xenos, E.S., et al., *Distribution of sac pressure in an experimental aneurysm model after endovascular repair: the effect of endoleak types I and II.* J Endovasc Ther, 2003. **10**(3): p. 516-23.

51.   Corbett, T.J., et al., *An improved methodology for investigating the parameters influencing migration resistance of abdominal aortic stent-grafts.* J Endovasc Ther, 2010. **17**(1): p. 95-107.

52.   Doyle, B.J., et al., *An experimental and numerical comparison of the rupture locations of an abdominal aortic aneurysm.* J Endovasc Ther, 2009. **16**(3): p. 322-35.

53.   Schurink, G.W., et al., *Stent attachment site-related endoleakage after stent graft treatment: An in vitro study of the effects of graft size, stent type, and atherosclerotic wall changes.* J Vasc Surg, 1999. **30**(4): p. 658-67.

54.   Finol, E.A. and C.H. Amon, *Blood flow in abdominal aortic aneurysms: pulsatile flow hemodynamics.* J Biomech Eng, 2001. **123**(5): p. 474-84.

55.   Raghavan, M.L., et al., *Wall stress distribution on three-dimensionally reconstructed models of human abdominal aortic aneurysm.* J Vasc Surg, 2000. **31**(4): p. 760-9.

56.   Vorp, D.A., M.L. Raghavan, and M.W. Webster, *Mechanical wall stress in abdominal aortic aneurysm: influence of diameter and asymmetry.* J Vasc Surg, 1998. **27**(4): p. 632-9.

57.   Hirsch, A.T., et al., *ACC/AHA Guidelines for the Management of Patients with Peripheral Arterial Disease (lower extremity, renal, mesenteric, and abdominal aortic): a collaborative report from the American Associations for Vascular Surgery/Society for Vascular Surgery, Society for Cardiovascular Angiography and Interventions, Society for Vascular Medicine and Biology, Society of Interventional Radiology, and the ACC/AHA Task Force on Practice Guidelines (writing committee to develop guidelines for the management of patients with peripheral arterial disease)--summary of recommendations.* J Vasc Interv Radiol, 2006. **17**(9): p. 1383-97; quiz 1398.

58.   Drangova, M., et al., *Elasticity and geometry measurements of vascular specimens using a high-resolution laboratory CT scanner.* Physiol Meas, 1993. **14**(3): p. 277-90.

59.   Erbel, R. and H. Eggebrecht, *Aortic dimensions and the risk of dissection.* Heart, 2006. **92**(1): p. 137-42.

60.   W.L. Gore & Associates, I., *Instructions for Use : Gore Excluder AAA Endoprosthesis.* 2011, W.L Gore & Associates, Inc.: Flagstaff. p. 48.